Nontrivial Spacetime Topology, Modified Dispersion Relations, and an $SO(3)$-Skyrme Model

Zur Erlangung des akademischen Grades eines
DOKTORS DER NATURWISSENSCHAFTEN
von der Fakultät für Physik des
Karlsruher Institutes für Technologie (KIT)

genehmigte

DISSERTATION

von

Dipl.-Phys. Markus Schwarz
aus Lahnstein, Rheinland-Pfalz

Tag der mündlichen Prüfung:	9. Juli 2010
Referent:	Prof. Dr. F.R. Klinkhamer (KIT)
Korreferent:	Prof. Dr. J. Polónyi (Université de Strasbourg)

Contents

Part I.

Introduction

General relativity and quantum mechanics both describe nature remarkably well. The two theories, however, cannot be unified thus far. In this thesis, we follow Wheeler, who argued that at scales comparable to the Planck length of approximately 1.6×10^{-35} m smooth spacetime becomes a spacetime foam instead. The idea is that quantum mechanical fluctuations in the curvature of spacetime are taking place constantly and, consequently, spacetime can no longer be considered to be smooth. If even the topology of spacetime fluctuates, regions with nontrivial topology (such as wormholes) could be constantly created and destroyed. Wheeler coined the word spacetime foam for this particular spacetime structure at the Planck scale.

We discuss some general aspects of spacetime foam in Part II. Chapter 1 presents Wheeler's argument [1] for the existence of a spacetime foam. Although a direct probing of physics at the Planck length seems impossible, in Chapter 2 we review how data on cosmic rays can be used to place tight bounds on spacetime foam parameters.

In Part III we discuss two types of spacetimes with nontrivial topology. In particular, we investigate if and how these spacetimes arise as solutions to Einstein's field equations. We start in Chapter 4 by reviewing spacetimes that contain wormholes. As was discovered by Morris and Thorne [2], the field equations of general relativity do indeed have wormhole solutions.

As a second type of nontrivial spacetime topology we consider spacetime defects. Such a defect "disturbs" the otherwise smooth spacetime, similar to a dislocation in an otherwise regular crystal. In the remainder of Part III, we focus on one particular defect, which is created from smooth Minkowski spacetime by a "surgery" procedure. The precise construction is given in Chapter 5. There, we also show that the resulting space has the same topological properties as $SO(3)$, the group of rotations in three dimensions. To obtain a spacetime with such a defect we are forced to introduce a matter field. Since the matter field must be compatible with the topology of the spacetime, we introduce an $SO(3)$-valued scalar field in Chapter 6. As the field's Lagrangian we choose that of a Skyrme model [3, 4]. We first solve the field equation for two kinds of fixed background metric in Chapter 7. We then present our numerical results for the complete Einstein-Skyrme equations in Chapter 8. It turns out that the spacetime obtained this way has a singular Ricci scalar curvature. Therefore, Chapter 9 reviews two singularity theorems by Gannon [5] and Friedman, Schleich, and Witt [6]. These theorems relate the singularity to the nontrivial spacetime topology and the matter energy density. The only way to circumvent these theorems is to allow for a negative energy density. We discuss how the model can be modified to achieve this.

In Part IV we discuss how microscopic spacetime defects modify the macroscopic dispersion relations of electromagnetic waves and Dirac fermions. Following the work of Bernadotte and Klinkhamer [7], in Chapter 11 we show that the presence of a microscopic defect leads to boundary conditions for electromagnetic waves and Dirac fermions. To satisfy these conditions correction fields have to be introduced. How the correction fields lead to a modified dispersion relation is discussed in Chapter 12. We apply this procedure for two spherical defect models in Chapters 13 and 14.

The last kind of defect, discussed in Chapter 15, is an example of a nonorientable spacetime.

Part V summarizes our results.

Part II.

General Aspects of Spacetime Foam

1. Motivation

The two major theories of the last century, quantum mechanics and general relativity, both describe nature remarkably well in their respective ranges of validity. Quantum mechanics successfully describes experiments from the molecular scale down to sub-proton distances. General relativity correctly describes phenomena from mm-scale laboratory experiments all the way up to cosmic distances. Even though the two theories generally work on such vastly different scales there are situations where both theories have to be taken into account. Such situations occur at the big bang and at the final state of the gravitational collapse of a star to a black hole. In these situations matter is compressed to such small volumes that quantum mechanics must ordinarily be taken into account. The mass of the amount of matter involved is so much that gravity cannot be ignored either, and a unified treatment of quantum mechanics and general relativity becomes necessary.

However, the unification of both theories has proven to be surprisingly difficult. The two most popular approaches, superstring theory and loop quantum gravity, have not yet yielded the desired result. One of the many problems that occur when one tries to merge quantum mechanics and general relativity is the following. When a physical system is confined in a small region, the uncertainty principle of quantum mechanics dictates a large uncertainty in momentum. This large momentum uncertainty translates into a large uncertainty in energy. An energy uncertainty causes an uncertainty in spacetime curvature via Einstein's equations of general relativity. Hence, the classical concept of spacetime is lost. But then one does not know what to define quantum field theory on. So far, neither superstring theory nor loop quantum gravity have found a generally accepted way out of this dilemma. It is a common belief that quantum mechanical fluctuations of spacetime become sizable at lengths comparable to the Planck length, $(G_N\hbar/c^3)^{1/2} \approx 1.6 \times 10^{-35}$ m, or at energies similar to the Planck energy, $(\hbar c^5/G_N)^{1/2} \approx 2.0 \times 10^9\text{J} \approx 1.2 \times 10^{19}\text{GeV}$.

Since a complete theory for quantized gravity does not yet exist, the answer to the question of what happens at the Planck length is not known. In this thesis, we follow Wheeler, who argued that at these length scales not only the geometry, but also the topology of spacetime fluctuates. The result of this would be that spacetime is no longer smooth but is made up of many regions with nontrivial topology. An illustration of such a spacetime foam is given in figure 1.1.

We now review Wheeler's argument [1] for the existence of a spacetime foam based on superspace[1]. The starting point is the observation [9] that it is possible to

[1]The superspace discussed here has nothing to do with the superspace occurring in supersymmetric field theories.

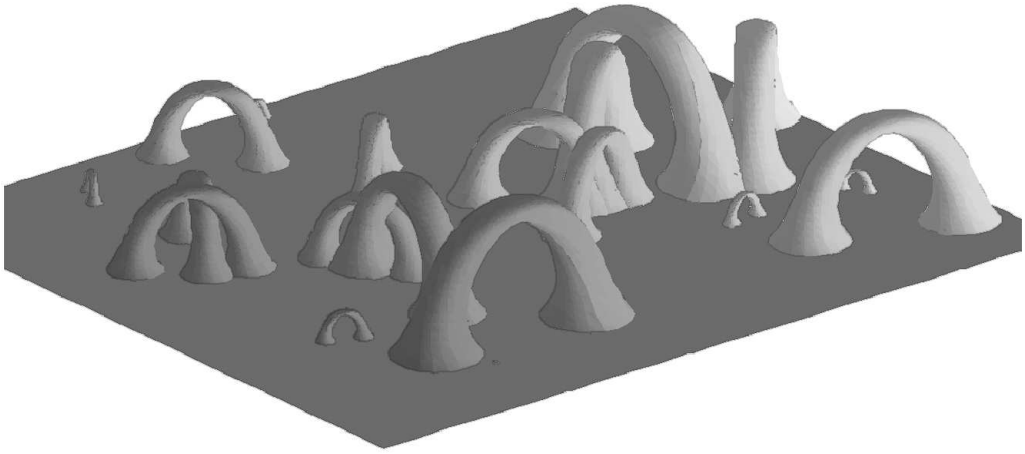

Figure 1.1.: An illustration of a classical spacetime foam at one instant of time. The otherwise flat spacetime contains wormholes of all microscopic scales. This figure is taken from [8].

reformulate Einstein's equations in such a way that they describe the time evolution of a three-dimensional hypersurface. This $3+1$ split is a change of point of view in general relativity, where one usually thinks of a four-dimensional spacetime, and is essential in the studies of initial value problems in general relativity. Very briefly, given a three-dimensional space with a spatial metric, a shift-vector, and a lapse function, which together must satisfy certain constraints, it is possible to describe the time evolution of that three-space. The resulting spacetime is then a solution to Einstein's equations. From this point of view, three-space is the analogue of a particle in classical mechanics. At each instant in time, space has a certain "shape" or geometry just as a classical particle has a certain position.

Wheeler defines superspace as the set of all three-geometries. The dynamical evolution of an initial three-space then traces out a path through superspace. Classically, only paths that extremize the Einstein-Hilbert action occur. Such a path is called a history and constitutes a four-dimensional spacetime that satisfies Einstein's equations of general relativity. Superspace is thus seen to play a similar role in general relativity as configuration space in classical mechanics.

If we could prescribe both the three-geometry and its rate of change with infinite precision we would obtain a path in superspace that is completely determined. But suppose that the uncertainty principle applies in this situation as well and does not allow this. Then the concept of a classical history in superspace would lose its meaning. Just as the concept of a particle's trajectory is replaced by a wave function, so should the history be replaced by a superposition of histories. As in Feynman's path integral approach to quantum mechanics, to obtain the probability of a transition from one three-geometry to another one should sum over all paths that connect the initial and final three-geometry. In the sum each path should

be weighted by its classical Einstein-Hilbert action. On scales much larger than the Planck length one could expect the probability of a transition from one three-geometry to another is sizable only for those geometries that are connected by paths that extremize the action. As mentioned above, such paths are spacetimes that are solutions to Einstein's field equations of general relativity. Hence, spacetime would appear classical on scales much larger than the Planck length.

At scales comparable to the Planck length paths that are not allowed classically could also become relevant. Two three-geometries might then be connected by paths that contain spaces of different topologies as well. If one took "snapshots" of three-space at different times, one would see spaces with different topologies. For instance, one would first find a space with one wormhole, then two, and then without a wormhole. Wheeler referred to this changing small scale structure as spacetime foam.

Similar to a quantum system that tunnels from one classical state into another, a spacetime obtained after tunneling could be long lived (compared to the Planck time) if it were again a classical solution of Einstein's field equations. The question is then what kind of spacetimes with nontrivial topology are allowed by Einstein's field equations. We will address this in Part III. In particular, we will investigate spacetimes that contain wormholes and topological defects. Assuming the existence of such a classical spacetime foam, we show in Part IV how it modifies the dispersion relations of electromagnetic waves and Dirac fermions that propagate through such a spacetime foam.

2. Experimental status

As discussed in the last chapter, quantum fluctuations in spacetime, if they indeed exist, are believed to occur on length scales similar to the Planck length of 1.6×10^{-35} m. This length corresponds to the Planck energy of approximately 1.2×10^{19}GeV. Current high energy colliders reach an energy of a few TeV, which is 16 orders of magnitude below the Planck energy. Using current technology, the radius of a particle collider that reaches the Planck energy would need to be approximately 375 light years. Clearly, a direct and conventional probing of physics at the Planck energy seems impossible.

However, there may be other effects through which physics at the Planck energy might be observable. The idea that we follow in this thesis is that Lorentz symmetry might no longer be valid at the Planck length. For example, the spacetime foam discussed in the previous chapter introduces a preferred frame and thereby breaks Lorentz invariance. The breakdown of Lorentz symmetry could manifest itself in either a direction dependence of the speed of light (vacuum birefringence), an energy dependence of the speed of light (dispersion), or vacuum-Cherenkov radiation of massive and electrically charged particles. We will discuss in detail how a spacetime foam leads to these kinds of effects in Part IV. Here, we just mention that, over large wavelengths, the spacetime foam effectively acts like an ordinary medium with an energy dependent index of refraction. Therefore, the dispersion relation of electromagnetic waves gets modified compared to their form in Minkowski spacetime and this allows for birefringence, dispersion, and Cherenkov radiation in vacuum. One can use data on ultra high-energy cosmic rays (UHECR) to place severe bounds on Lorentz symmetry breaking effects.

Amelino-Camelia *et al.* [10] presented the following idea to constrain modified photon dispersion relations. Here, a modified dispersion relation is assumed to yield an energy dependent speed of light. Consider a source that emits a flash of light in a certain energy interval. If the speed of light depends on energy, then photons of different energy would arrive at a detector at different times. Again, the nonobservation of such a time delay yields bounds on the parameters of the modified photon dispersion relation. Since the effect accumulates over distance traveled it is advantageous to look for cosmic sources. Furthermore, the flash should be as brief as possible to ensure that all photons really start at the same time. The energy range of the photons should be as large as possible as well. Gamma-ray bursts satisfy these conditions. They are outbursts of photons with energies up to several TeV that occur at distances of up to millions of light years and yet last only a few minutes. Since the classical spacetime foam models discussed in Part IV lead to an energy dependent speed of light, gamma-ray bursts were used by Bernadotte

and Klinkhamer [7] to place bounds on the spacetime foam parameters l and b (l denoting the average defect separation and b the typical defect size).

To place bounds on vacuum-Cherenkov radiation one can use the idea of Beall [11] (see also Coleman and Glashow [12]). We will show in Part IV that our spacetime foam models lead to a reduced speed of light, whereas the maximal attainable speed of fermions does not change. A fermion, a proton for instance, with very high energy could then have a speed exceeding the speed of light. Whenever such a situation occurs the proton emits Cherenkov radiation and thereby loses energy. It continues to do so until its energy is reduced to a threshold energy, where its speed is equal to the speed of light. Hence, the measurement of particles with ultra high energy can place tight bounds on this threshold energy.

The highest energy collisions on Earth do not happen in man-made colliders but occur in the upper regions of the atmosphere. These collisions take place between the atomic nuclei of air molecules and cosmic rays. Although cosmic rays were discovered about a hundred years ago their exact composition and origin are still not understood completely. Current understanding is that cosmic rays are ionized atomic nuclei that originate outside the solar system. Modern cosmic ray detectors, such as the Pierre Auger Observatory, have observed cosmic rays with energies up to 10^{11} GeV [13].

Given a particle with energy above the threshold energy, it turns out that it requires only nanoseconds for the particle's energy to drop to the threshold energy. Thus, the particle would lose its excess energy almost immediately and propagate only a few meters. The fact that particles with energies as high as 10^{11} GeV reach Earth then means that the threshold energy for vacuum Cherenkov radiation must be at least 10^{11} GeV. To translate the bound on the threshold energy into a bound on Lorentz symmetry breaking parameters requires a detailed calculation within the specific theory. For the Lorentz symmetry violating modified Maxwell theory this was done in [14, 15]. It is noteworthy that the bounds obtained by using UHECRs are tighter than laboratory bounds by ten orders of magnitude. For the classical spacetime foam models discussed in Part IV the calculations were done in [7]. The result is that the average distance l between the spacetime foam constituents (defects) must be larger than the typical defect size b by a factor of 10^7. This result then implies that spacetime appears to be rather smooth with only dilute defects.

Even though a direct probing of physics at the Planck length may be impossible, the above two examples show that it is possible to set tight bounds on Lorentz symmetry breaking and, thereby, constrain possible models of physics at the Planck scale.

Part III.

Topologically Nontrivial Solutions to Einstein's Equations

3. Introduction to Part III

Part III deals with solutions to Einstein's equations that have nontrivial topology. Having nontrivial topology means that these spacetimes contain closed curves that cannot be contracted to a point. As such, they belong to a different class of spacetimes than Minkowski spacetime. In Minkowski spacetime all closed curves are contractible and "turning on" gravity may bend spacetime but does not change its topological properties. The creation of spacetime with nontrivial topology may therefore be beyond the scope of general relativity. But if such a spacetime is created somehow (perhaps in a quantum-gravity phase) it is interesting to know if general relativity does admit it as a solution.

We first consider wormholes as an example of spacetimes with nontrivial topology. In brief, a wormhole connects asymptotically flat regions via a throat. Wormholes have been studied in general relativity for a long time and we review some results in Chapter 4. Usually, wormholes are unstable under small perturbations but recently a mechanism was found that could stabilize them. The idea is to introduce a scalar field with a suitable potential such that the Einstein-Klein-Gordon equation yields a wormhole spacetime and kink-like solution for the scalar. Since a kink is stable for topological reasons it could act as a "crutch" for the wormhole.

The remaining chapters deal with spacetimes that contain a topological defect. Similar to a defect in an ordinary crystal, a spacetime defect disturbs the otherwise trivial topology of the spacetime. Spacetime defects are defined by a "surgery" procedure. In particular, we will discuss a type I defect. It is constructed out of Minkowski spacetime by removing a spatial ball and identifying antipodal points on the would-be boundary. The radius of the cut-out ball will be referred to as the defect parameter. We give a detailed construction in Chapter 5. There, we will also investigate the topology of the resulting space and what it implies for the curvature.

These considerations lead us to introduce a particular kind of scalar field in Chapter 6. The Lagrangian of the field is taken to be that of the so-called Skyrme model and the solutions are called Skyrmions. We also discuss the principal mechanism through which this scalar field can again act as a "crutch" for the spacetime defect. Finally, we state the Einstein-Skyrme equations.

Before we solve the full Einstein-Skyrme equations, we consider two kinds of background metrics in Chapter 7. First, we take the background metric to be that of Minkowski spacetime and solve the field equation numerically. If the winding number of the Skyrmion is even, we reproduce the known results for Skyrmions. However, when the winding number is odd, we find that there exists a finite defect parameter that minimizes the energy. We then consider a background metric with constant curvature. In this case, the field equation can be solved analytically. Again

we find a finite defect parameter that minimizes the energy of the Skyrmion.

Finally, we attempt to solve the full Einstein-Skyrme equations in Chapter 8. Using a certain set of initial conditions we can reproduce the known results of gravitating Skyrmions, if the Skyrmion's winding number is even. For odd winding number we find that the mass is minimized by a finite defect parameter. However, a closer inspection reveals that the matter field does not account for all the mass present in the spacetime. We interpret this spurious mass as the energy needed to create this particular type of spherical defect. It is the work needed to "drill" a hole in spacetime and "sew" it up again.

However, we show in Chapter 9 that the spacetimes constructed in this way have a singular Ricci scalar curvature. This singularity can be accounted for by two singularity theorems. Essentially, these theorems say that an asymptotically flat spacetime with nontrivial topology and "normal" matter must have a singularity. Therefore, we discuss a modification of the matter Lagrangian to allow the matter field to have a negative energy density. So far, the resulting field equations could not be solved.

4. Wormholes

Before we discuss our attempt to find solutions to Einstein's field equations that contain a type I defect, we discuss another type of nontrivial spacetime topology, namely spacetimes that contain a "wormhole". This solution has been studied in the literature extensively, and we give a brief review in this chapter. A wormhole connects asymptotically flat regions of spacetime via a throat. Depending on whether the wormhole connects two different regions or the same asymptotic region, one speaks about *inter-* or *intra*-universe wormholes, see figure 4.1(a) and figure 4.1(b) respectively. The wormholes depicted in figure 1.1 are intra-universe wormholes as well.

In the context of this thesis, spacetimes with wormholes are of relevance because they contain noncontractible closed curves. The black curve shown in figure 4.1(b) passes through the wormhole and returns to its starting point. Unlike a closed curve in ordinary space $\mathbb{R}^n$, this closed curve cannot be contracted to a point. A manifold with such a property is called nonsimply connected. Simple connectivity is a topological property, meaning that it cannot be lost or changed by a continuous deformation of the manifold. For example, from the topological point of view a doughnut equals a coffee cup, because both have a "hole" and one can be transformed into the other continuously.

Historically, an early wormhole solution to general relativity was found by Einstein and Rosen in 1935 [16], where it was referred to as a "bridge". Later, the Einstein-Rosen bridge turned out be a spacelike hypersurface in the extended Schwarzschild solution [17]. Being spacelike, the bridge can never be crossed by particles because they travel along timelike geodesics. It took half a century until *traversible* wormholes were found by Morris and Thorne in 1988 [2]. Here, traversible refers to a number of requirements the spacetime must satisfy for an observer to pass through the wormhole. For example, the observer should not encounter any spacetime singularity and should reach the other end of the wormhole in a reasonable amount of time. Also tidal forces should not be too strong so that a human being, for example, is not ripped to pieces. But Morris and Thorne found that the matter needed to create the wormhole had to have *negative* energy density. They found out later[1] that matter must always have these peculiar effects. The reason is that, roughly, a spacetime with a nontrivial topology must have a singularity, unless matter has a negative energy density. We will review some of these singularity theorems later in Chapter 9.

Once a wormhole solution has been found, one may wonder if it is stable under

[1] See Chapter 14 of [18] for interesting details on this.

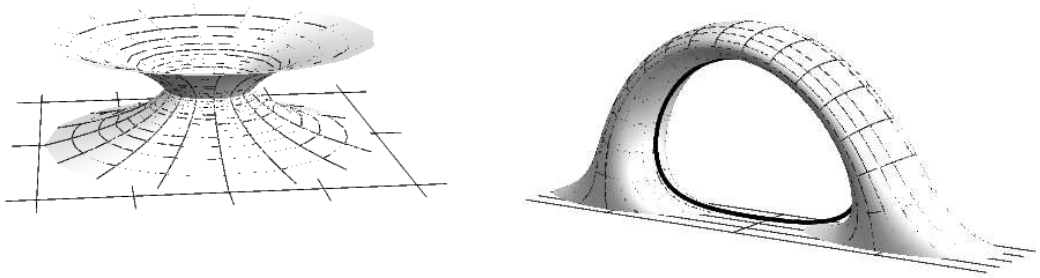

(a) (b)

Figure 4.1.: Illustration of an (a) inter-universe and (b) intra-universe wormhole. (a) is an embedding diagram of the Einstein-Rosen bridge. The black curve in (b) shows a noncontractible loop.

small perturbations. Usually, this requires a great deal of work. Sushkov and Kim found a wormhole solution that might be stabilized by an additional scalar field ϕ [19]. The trick is to add a suitable potential that has two different minima, ϕ_1 and ϕ_2. A finite energy configuration must then approach either of these minima at infinity. If the field approaches one minimum as $x \to -\infty$, say ϕ_1, and reaches ϕ_2 as $x \to \infty$, then it is not possible to deform the field continuously into one that is constant, say ϕ_2 [20]. Hence, the field is stable for topological reasons and is known as a *kink*. The idea is now that ϕ approaches the vacuum ϕ_1 in the asymptotic region on one side of the wormhole and ϕ_2 on the other side. Then the wormhole could be stabilized by such a kink-like scalar field.

After giving the definition of a traversible wormhole in the next section, we review the wormhole construction by Sushkov and Kim [19] in Section 4.2.

4.1. Traversible wormholes

The traversible wormholes were found by applying a "reverse engineering" approach. Rather than asking what geometry is created by a given matter content, Morris and Thorne [2] first specified the geometry of spacetime and then asked if general relativity allows for such a geometry. If this is the case, one can ask what kind of matter would be needed to create it. A spherically symmetric and static metric was assumed to make the calculations manageable. For a wormhole to be traversible, they made the following assumptions about the geometry

1. No singularities and horizons are present.

2. Tidal forces are small enough so that a traveler can pass through the wormhole.

3. The journey takes only a small amount of human lifetime, say, one year (both in proper time for the traveler and in coordinate time of a static observer).

The matter needed to create a traversible wormhole violates the weak energy condition, which means, roughly, that the energy density of matter must be negative in some regions of spacetime. We will discuss the interplay between nontrivial spacetime topology and matter in Chapter 9. Here, we just mention that, since the wormhole spacetime has no singularities (condition 1 above), Gannon's singularity theorem implies that the weak energy condition is violated. Furthermore, the traversability means that a particle can cross the wormhole and return. Its world line, projected onto the spatial hypersurface containing the wormhole, may then be a noncontractible path. To avoid the topological censorship theorem, which forbids such paths, matter must also violate the averaged null energy condition.

4.2. Wormholes supported by a kink

We review the wormhole construction of Sushkov and Kim in this section [19]. They succeeded in constructing a wormhole solution that is stabilized by a topologically nontrivial scalar field. For this reason their work is of relevance to this thesis.

Their action reads (in units with $c = G_N = 1$)

$$S = \int \left(\frac{1 - 8\pi\xi\phi^2}{8\pi} R - g^{\mu\nu}\partial_\mu\phi\partial_\nu\phi - 2V(\phi) \right) \sqrt{g}\, \mathrm{d}^4x \,. \tag{4.1}$$

Here, R is the Ricci scalar of the metric g and ϕ is a scalar field with potential V. The constant ξ is dimensionless.

The potential is chosen to have two minima at ϕ_1 and ϕ_2. A time-independent scalar field ϕ must then approach either of the two minima as x approaches $\pm\infty$, as otherwise the energy would not be finite. If the field approaches the same minimal value as $x \to \pm\infty$, say ϕ_1, the field can be deformed continuously into the constant field ϕ_1. However, it is known from field theory in flat spacetime that field configurations starting in one minimum at $x = -\infty$ and ending in the other at $x = \infty$ are topologically stable [20]. In this case the field cannot be continuously deformed into the constant solution, say ϕ_1. The idea of [19] was to use this effect to stabilize a wormhole. The field has minimal value ϕ_1 in one asymptotic region and ϕ_2 in the other. The field should vary from one to the other in the region of the wormhole throat.

The static and spherically symmetric *Ansatz* for the metric reads

$$\mathrm{d}s^2 = -A(\rho)\,\mathrm{d}t^2 + \frac{\mathrm{d}\rho^2}{A(\rho)} + r^2(\rho)\left(\mathrm{d}\theta^2 + \sin^2\theta\,\mathrm{d}\varphi^2\right) . \tag{4.2}$$

Here, ρ ranges from $-\infty$ to ∞ with roughly $\rho < 0$ on one side of the throat and $\rho > 0$ on the other. The area of a two-sphere is given by $4\pi r^2(\rho)$. The wormhole's

throat occurs where $r(\rho)$ has a minimum. The potential is chosen as

$$V(\phi) \equiv \frac{\lambda}{4}\left[(\phi-\bar{\phi})^2 - \frac{m^2}{\lambda}\right]^2 ,$$

where $\bar{\phi}$, $\lambda > 0$, and $m > 0$ are constants. The two minima of V are

$$\phi_1 \equiv \bar{\phi} - \tfrac{m}{\sqrt{\lambda}}, \quad \phi_2 \equiv \bar{\phi} + \tfrac{m}{\sqrt{\lambda}} .$$

The conditions on a traversible wormhole given in the previous section then translate into the following requirements

1. The function $A(\rho)$ must be positive everywhere, so that no horizons exist. Furthermore, no singularities must be present.

2. The radial function $r(\rho)$ must have a global minimum. This is then the wormhole throat radius.

3. Asymptotically, $r(\rho) \to |\rho|$, and $A(\rho) \to$ constant.

The last condition ensures that the coordinate radius $|\rho|$ agrees with the radius r, obtained by measuring the area of two-spheres. It also ensures that the metric becomes flat asymptotically on both sides of the wormhole. Since the idea is that the wormhole is stabilized by the kink-like scalar field ϕ, it must approach the vacuum value ϕ_1 on one side of the wormhole and ϕ_2 on the other.

The analysis of [19] shows that wormholes are possible only if

$$|\phi_1| < 1/\sqrt{8\pi\xi}, \quad |\phi_2| > 1/\sqrt{8\pi\xi} .$$

It is convenient to work with the following dimensionless quantities

$$\begin{array}{lll} x \equiv m\rho, & \tilde{r}(x) \equiv m r(\rho), & \eta(x) \equiv \phi(\rho), \quad \bar{\eta} = \frac{\bar{\phi}}{\kappa}, \\ \bar{\eta}_1 \equiv \bar{\eta} - 1, & \bar{\eta}_2 \equiv \bar{\eta} + 1, & \kappa \equiv \frac{m}{\sqrt{\lambda}} . \end{array}$$

The field equations derived from the action in equation (4.1) then read

$$2\frac{r''}{r} = -\frac{8\pi\kappa^2}{1-8\pi\xi\kappa^2\eta^2}[\eta'^2 - \xi(\eta^2)''] , \tag{4.3a}$$

$$A(r^2)'' - A''r^2 - 2 = -\frac{8\pi\kappa^2\xi(\eta^2)'}{1-8\pi\xi\kappa^2\eta^2} r^4 \left(\frac{A}{r^2}\right)' , \tag{4.3b}$$

$$(r^2 A\eta')' - \xi r^2 R(x)\eta - r^2(\eta-\bar{\eta})[(\eta-\bar{\eta})^2 - 1] = 0 . \tag{4.3c}$$

Here, and in the following, we wrote r instead of $\tilde{r}$ for notational convenience. A prime denotes differentiation with respect to x. Finally, the Ricci scalar reads

$$R(x) = -A'' - 4'\frac{r'}{r} - 4A\frac{r''}{r} - 2A\frac{r'^2}{r^2} + \frac{2}{r^2} .$$

Notice that the value x_0, where $\eta(x_0) = 1/\sqrt{8\pi\xi\kappa^2}$, is a singular point of equations (4.3a) and (4.3b). The point x_0 is taken to be zero. The field equations are regular at $x = 0$ if the following conditions are satisfied

$$\frac{r_0'}{r_0} = -\frac{A_0'}{2A_0}\,, \tag{4.4a}$$

$$\frac{r_0'}{r_0} = -\frac{\sqrt{8\pi}\kappa}{12\sqrt{\xi}\eta_0' A_0}\left[A_0\eta_0'^2 - \frac{1}{2}(\Delta\eta^2 - 1)^2\right]\,, \tag{4.4b}$$

where $r_0 \equiv r(0)$ and so on. Now, the fields can be expanded around $x = 0$

$$\begin{aligned} r(x) &= r_0 + r_0' x + \cdots\,, \\ A(x) &= A_0 + A_0' x + \cdots\,, \\ \eta(x) &= \frac{1}{\sqrt{8\pi\xi\kappa^2}} + \eta_0' x + \cdots\,. \end{aligned}$$

Only the three parameters, r_0, A_0, and η_0', are independent, with r_0' and A_0' already being determined by equations (4.4a) and (4.4b). The model parameters ξ, κ, and $\bar{\eta}$ are chosen as

$$\xi \equiv 1/6, \quad \kappa \equiv 1/\sqrt{8\pi}, \quad \bar{\eta} \equiv 1/\sqrt{8\pi\xi\kappa^2}\,,$$

and the boundary conditions are

$$r_0 \equiv 1, \quad \eta_0 \equiv 0.2, \quad A_0 \equiv 36.321\,278\,.$$

Here, the first two parameters are just fixed to some value. The remaining parameter (A_0) must, then, be tuned to give numerically a kink-like solution for the scalar field. Figure 4.2 shows the numerical solutions obtained for these parameters. First, notice that the radius r indeed has a minimum at $x \approx 3.5$. The throat radius is approximately 0.95. For large coordinate radii $|\rho|$, the radius r is seen to approach $|\rho|$. Second, the kink-like character of the scalar field η can be seen from Figs. (4.2(c)) and (4.2(d)). Namely, it approaches the vacuum values η_1 and η_2 on the left and right side, respectively. Third, the metric function A, depicted in Figs. (4.2(e)) and (4.2(f)), is smooth and positive everywhere. Finally, the asymmetry of the solutions is due to the different values of the potential V. Therefore, the spacetime is a wormhole supported by a kink-like scalar field configuration.

Figure 4.3 shows the energy density of the scalar field. It peaks at approximately $x \approx 6.6$ but is negative for some values as well. As mentioned in the introduction, negative energy density is a general property of spacetimes with nontrivial topology. We will elaborate on this point in chapter 9.

To summarize: Wormholes are spacetimes that contain asymptotic regions that are connected by a throat. They are topologically distinct from the usual Minkowski spacetime because they contain closed curves that cannot be contracted to a point. As was first shown by Morris and Thorne [2], it is possible to have wormhole spacetimes as smooth solutions of Einstein's equations [2]. Deciding whether wormholes

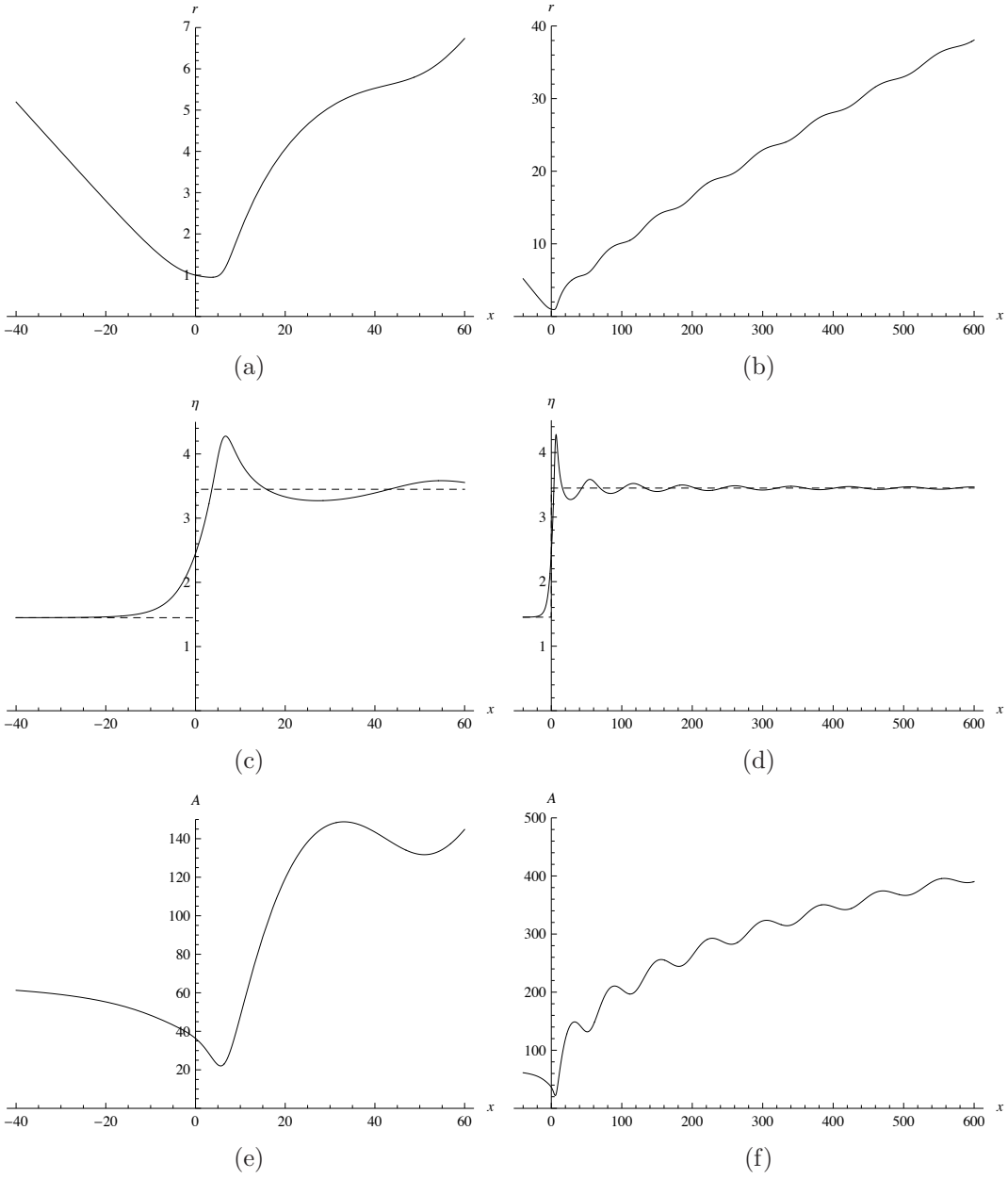

Figure 4.2.: The radius r, scalar field η and metric function A as functions of the dimensionless parameter $x \equiv m\rho$. The throat of the wormhole is located at $x \approx 3.5$, the minimal value of r. Therefore, points with $x \lesssim 3.5$ or $x \gtrsim 3.5$ are on opposite sides of the wormhole. The figures on the left and right show the "near" fields and "far" fields, respectively. Notice that η approaches its vacuum values $\eta_1 \equiv 1/\sqrt{8\pi\xi}\kappa - 1$ and $\eta_2 \equiv 1/\sqrt{8\pi\xi}\kappa + 1$ (dashed lines) on the left and right side of the wormhole, respectively. For details see text and [19].

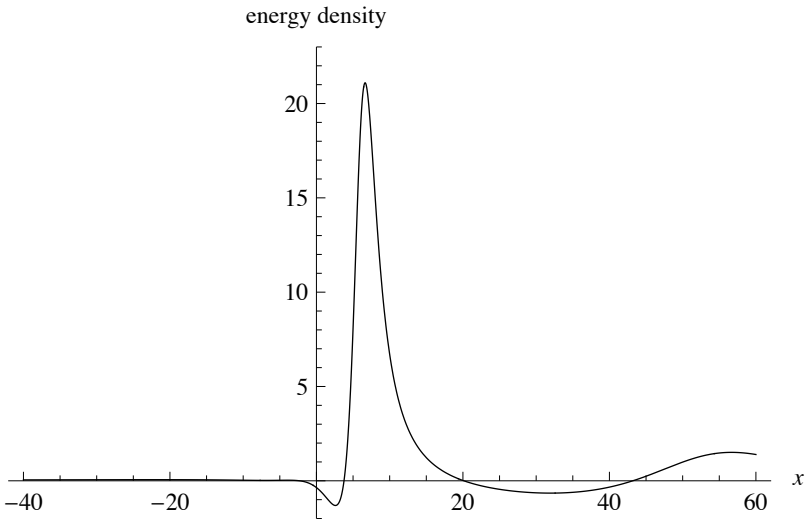

Figure 4.3.: The energy density as a function of $x \equiv m\rho$. Notice that it is negative at some values of x.

are stable under small perturbations is difficult. Nonetheless, Sushkov and Kim [19] constructed a wormhole that is supported by a scalar field configuration known as a kink. Since a kink is stable for topological reasons it cannot smoothly relax to the constant vacuum solution. This effect might stabilize the wormhole as well.

Since a wormhole is an example of a spacetime with nontrivial topology that is supported by a suitable scalar field, we try a similar approach for the spacetime with a type I defect. This will be the subject of the following chapters.

5. Topological properties of manifolds with a defect

In this chapter we will discuss what the existence of a defect implies for the topological properties of a space. Our goal is to study the topology of a space that contains a spherical defect of type I. Such a defect is created from three-dimensional Euclidean space by removing an open ball and identifying antipodal points on the would-be boundary. This construction is due to [7], where this type of defect was referred to as a $\tau = 1$ defect. Here, we will refer to it as a type I defect, to designate that this defect will become the basic building block of our spacetime foam model I, discussed in Chapter 13. We will denote the manifold that contains a type I defect by M_{I}.

Before discussing the three-dimensional case, we will introduce and illustrate the necessary concepts for a two-dimensional version in Section 5.1. The two-dimensional manifold that hosts this defect will be denoted by m_{I}. Although its purpose here is "pedagogical", it will also play a role when we discuss a spacetime foam of line defects in Chapter 15. Finally, we will discuss the spherical three-dimensional type I defect in Section 5.2.

5.1. Two-dimensional circular defect

In this section we discuss the properties of a two-dimensional manifold that contains a circular defect. The construction of this circular defect proceeds similarly to the three-dimensional counterpart. That is, we start from $\mathbb{R}^2$ and remove all points with a distance smaller than the "defect radius" b. Antipodal points on the resulting boundary circle are then identified.

5.1.1. Proof that m_{I} is a manifold

To prove that m_{I} is a two-dimensional manifold, we have to show that [21]:

1. m_{I} is a topological space,
2. m_{I} can be covered by charts, mapping open sets in m_{I} onto open sets in $\mathbb{R}^2$,
3. if two charts overlap, then the resulting map from $\mathbb{R}^2$ to $\mathbb{R}^2$ is infinitely differentiable.

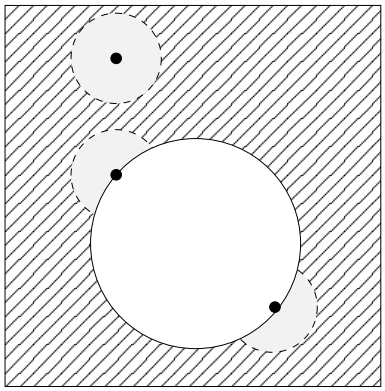

Figure 5.1.: Open regions of a point on the defect and far away from it. The same figure will also apply to the three-dimensional defect (where the third dimension is not shown).

We will also show that m_I is a Hausdorff space.

Simply put, defining a topology on a space is to define its open sets. We define the open sets of m_I by making reference to the topology of the original $\mathbb{R}^2$. An ϵ-neighborhood $U_{\epsilon,x}$ of a point $\boldsymbol{x} \in \mathbb{R}^2$ is defined by

$$U_{\epsilon,x} \equiv \{\boldsymbol{y} \in \mathbb{R}^2 : |\boldsymbol{x} - \boldsymbol{y}|_2 < \epsilon\}\,, \tag{5.1}$$

where the subscript '2' emphasizes that the usual metric of $\mathbb{R}^2$ is used. Thus, in the topology of m_I we include all $U_{\epsilon,x}$ for $|\boldsymbol{x}|_2 > b$ and $\epsilon < |\boldsymbol{x}|_2 - b$.

The ϵ-neighborhood of a point on the defect (that is, a point that originally belonged to the circle with radius b) is defined by using *two* neighborhoods in $\mathbb{R}^2$:

$$U_{\epsilon,1} \equiv \{\boldsymbol{y} \in \mathbb{R}^2 : |\boldsymbol{x} - \boldsymbol{y}|_2 < \epsilon\}\,,$$
$$U_{\epsilon,2} \equiv \{\boldsymbol{y} \in \mathbb{R}^2 : |\boldsymbol{x} + \boldsymbol{y}|_2 < \epsilon\}\,.$$

The first set consists of all points within a distance ϵ of the point $\boldsymbol{x}$, whereas the second set contains all points within ϵ-distance of the antipodal point $-\boldsymbol{x}$. We define the neighborhood for a point on the defect as the union of $U_{\epsilon,1}$ and $U_{\epsilon,2}$ but with all points with a radius of less than b removed (see figure 5.1):

$$U_{\epsilon,x} \equiv (U_{\epsilon,1} \cap U_{\epsilon,2}) \setminus \overset{\circ}{D}_b = \{\boldsymbol{y} \in \mathbb{R}^2 : (|\boldsymbol{x}-\boldsymbol{y}|_2 < \epsilon \vee |\boldsymbol{x}+\boldsymbol{y}|_2 < \epsilon) \wedge |\boldsymbol{y}|_2 \geq b\}\,, \tag{5.2}$$

where $\overset{\circ}{D}_b$ is the interior of a disc with radius b, i.e. all points with $|\boldsymbol{x}|_2 < b$. Notice that the set in (5.2) is not open with respect to the usual topology of $\mathbb{R}^2$, but we use it to *define* the open neighborhood of a point on the defect. The topology of m_I is then the union of all $U_{\epsilon,x}$ which are either of the form (5.1) or (5.2). To make m_I a topological space we formally add the empty set $\emptyset$ and m_I as a whole to the topology of m_I.

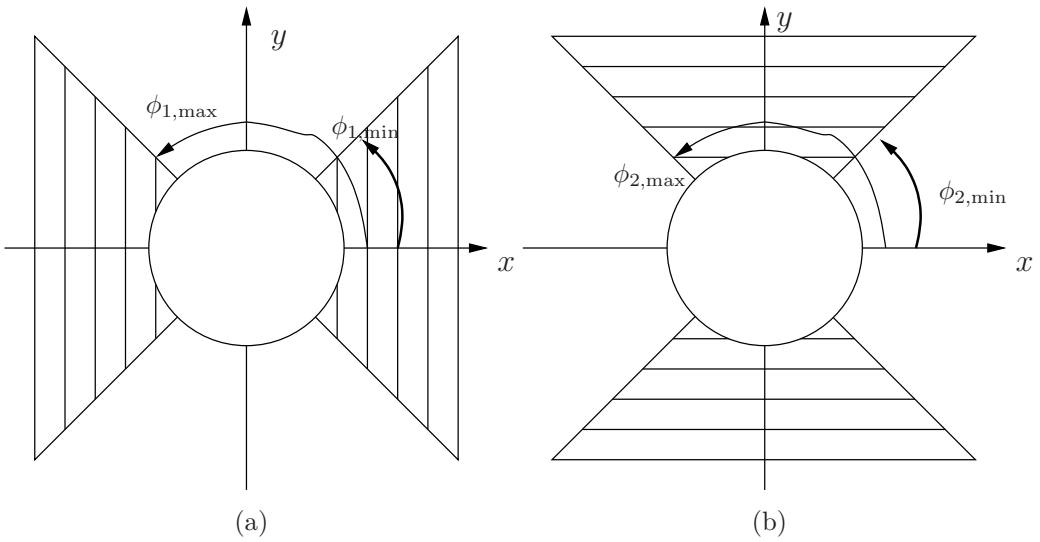

Figure 5.2.: The two regions that cover m_{I}. (a) The wedge-like regions that make up U_1. (b) The wedge-like regions that make up U_2. Both regions surround only one axis. Here, the maximal and minimal values of ϕ are equal for both patches but do not need to be in general.

Now that we have made m_{I} a topological space, we have to give appropriate charts. That is, we have to specify maps from open sets of m_{I} to open sets of $\mathbb{R}^2$.

To define these maps we cover all of m_{I} by two wedge-like regions, one including the x-axis and the other the y-axis, as shown in figure 5.2. All regions are defined by referring to polar coordinates (r, ϕ) in the original $\mathbb{R}^2$. The idea is to construct coordinates on these two "wedges" such that points on one side of the defect have a positive coordinate, while points on the other side have a negative coordinate. Finally, points on the defect have coordinate 0.

The "wedge" U_1 surrounding the x-axis is composed of two regions, see figure 5.2(a). Points to the left of the defect have angles ranging from $\phi_{1,\max}$ to $\phi_{1,\min} + \pi$, whereas points to the right have ϕ in the range $\phi_{1,\max} + \pi < \phi \leq 2\pi$ or $0 \leq \phi < \phi_{1,\min}$. Furthermore, the wedge must not intersect the y-axis, which means $\phi_{1,\min} < \pi/2$ and $\pi/2 < \phi_{1,\max} < \pi$. Explicitly, we have

$$U_1 \equiv \{x \in \mathbb{R}^2 : r \geq b \wedge \phi_{1,\max} < \phi < \phi_{1,\min} + \pi \\ \vee \ \phi_{1,\max} + \pi < \phi \leq 2\pi \ \vee \ 0 \leq \phi < \phi_{1,\min}\}\,.$$

On U_1 we introduce coordinates (X_1, Y_1) via

$$X_1(r,\phi) = \begin{cases} r-b, & 0 \le \cos\phi \\ b-r, & \cos\phi \le 0 \end{cases}, \qquad Y_1(\phi) = \begin{cases} \phi - \pi/2 & \cos\phi < 0 \\ \phi - 3\pi/2 & 3\pi/2 < \phi < 2\pi \\ \phi + \pi/2 & 0 \le \phi < \pi/2 \end{cases},$$
$$r(X_1) = \begin{cases} b + X_1, & X_1 \ge 0 \\ b - X_1, & X_1 < 0 \end{cases}, \quad \phi(X_1, Y_1) = \begin{cases} Y_1 + \pi/2 & X_1 < 0 \\ Y_1 + 3\pi/2 & X_1 > 0 \wedge Y_1 < \pi/2 \\ Y_1 - \pi/2 & X_1 > 0 \wedge Y_1 > \pi/2 \end{cases}. \tag{5.3}$$

Notice that $r(X_1) = b + |X_1|$ and that the ranges of these new coordinates are

$$\begin{aligned} -\infty < & X_1 < \infty\,, \\ 0 < Y_1(\phi_{1,\max}) < & Y_1 < Y_1(\phi_{1,\min}) < \pi\,. \end{aligned}$$

Hence, a negative value of X_1 means that the point with this coordinate is "to the left of the defect", while it is "to the right" if $X_1 > 0$. Finally, points that are on the defect have $X_1 = 0$.

Similarly, the "wedge" U_2 surrounding the y-axis is composed of points above and below the defect, see figure 5.2(b). Points "above" the defect have angles ranging from $\phi_{2,\min}$ to $\phi_{2,\max}$, while points "below" it have $\phi_{2,\min} + \pi < \phi < \phi_{2,\max} + \pi$. Since these "wedges" must not intersect the x-axis, we must have $0 < \phi_{2,\min}$ and $\phi_{2,\max} < \pi$. Thus, the region U_2 is defined by

$$\begin{aligned} U_2 \equiv \{x \in \mathbb{R}^2 : r \ge b \ \wedge\ & 0 < \phi_{2,\min} < \phi < \phi_{2,\max} < \pi \\ & \vee\ \pi < \phi_{2,\min} + \pi < \phi < \phi_{2,\max} + \pi < 2\pi\}\,. \end{aligned}$$

Coordinates (Y_2, X_2) on U_2 are defined by

$$X_2(\phi) = \begin{cases} \phi, & \phi < \pi \\ \phi - \pi, & \phi > \pi \end{cases}, \qquad r(Y_2) = \begin{cases} b + Y_2, & Y_2 \ge 0 \\ b - Y_2, & Y_2 < 0 \end{cases} = b + |Y_2|\,,$$
$$Y_2(r,\phi) = \begin{cases} r-b, & \phi < \pi \\ b-r, & \phi > \pi \end{cases}, \qquad \phi(Y_2, X_2) = \begin{cases} X_2, & Y_2 \ge 0 \\ X_2 + \pi, & Y_2 < 0 \end{cases}. \tag{5.4}$$

Here, $Y_2 < 0$ means that the point is "below" the defect, and "above" if $Y_2 > 0$. Points on the defect have $Y_2 = 0$. Now X_2 is the angular variable and the ranges of the coordinates are

$$\begin{aligned} -\infty < & Y_2 < \infty\,, \\ 0 < X_2(\phi_{2,\min}) < & X_2 < X_2(\phi_{2,\max}) < \pi\,. \end{aligned}$$

We use the notation (Y_2, X_2) in analogy to (r, ϕ) to make clear that Y_2 is the "radial", variable and that X_2 is the "angular" variable.

The next step in showing that m_{I} is a manifold is to demonstrate that the coordinates for U_1 and U_2 in overlapping regions are infinitely differentiable. Provided

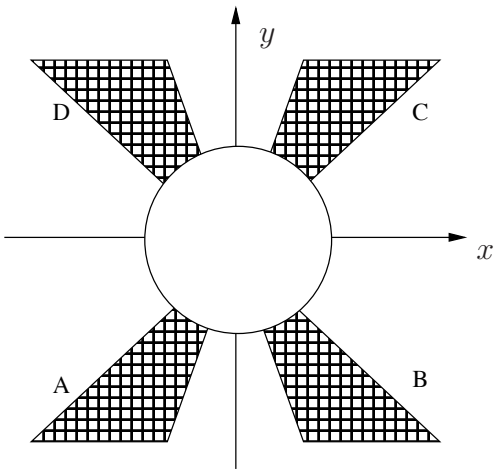

Figure 5.3.: The regions where the coordinate patches U_1 and U_2 overlap. Notice that the sets $A \cup C$ and $B \cup D$ are connected because of the antipodal identification at the circle.

that $\phi_{1,\min} < \phi_{2,\min}$ and $\phi_{1,\max} < \phi_{2,\max}$ the overlap between U_1 and U_2 is not empty and is shown in figure 5.3.

In the overlap regions, $A \cup C$ and $B \cup D$, the coordinate functions for U_1 and U_2 must be inverses of each other and infinitely differentiable. Using $Y_1(\phi(X_2, Y_2))$ etc. and the explicit relations in (5.3) and (5.4) we find

$$A \cup C: \quad X_1(Y_2) = Y_2, \quad Y_1(X_2) = X_2 + \pi/2\,, \tag{5.5a}$$

$$B \cup D: \quad X_1(Y_2) = -Y_2, \quad Y_1(X_2) = X_2 - \pi/2\,. \tag{5.5b}$$

From this one immediately sees that the coordinates are invertible functions of each other and infinitely differentiable.

In summary, we have equipped m_{I} with a topology and found coordinate charts for it. In the two overlapping regions the charts are maps from $\mathbb{R}^2$ to $\mathbb{R}^2$ which are invertible and infinitely differentiable. Thus, m_{I} is a two-dimensional manifold.

We now show that the manifold m_{I} also possesses the Hausdorff property, i.e. given two distinct points p and q of m_{I}, we show that there always exist open sets U (containing p) and V (containing q) such that $U \cap V = \emptyset$. For two points not on the defect we have, by definition, the usual topology of $\mathbb{R}^2$ and hence the Hausdorff property. When one point is on the defect ($r = b$) and the other is not ($r > b$), we can always take $\epsilon < (r - b)/2$ in (5.1) and (5.2) and then the two sets do not intersect. Finally, for two points (b, ϕ_1) and (b, ϕ_2) on the defect we can choose $\epsilon < |b(\phi_1 - \phi_2)|/2$.

Usually all manifolds encountered in physics have the Hausdorff property. An artificial example of a non-Hausdorff manifold can be found in figure 5 of [22]. However, since this example also involves a "cut-and-identify" procedure, it shows that identification of points can lead to non-Hausdorff manifolds. In the context of *hypothetical* time travel scenarios non-Hausdorff manifolds are also discussed in [23].

5.1.2. Properties of the manifold m_{I}

We continue the investigation of m_{I} by showing that m_{I} is a noncompact, nonorientable, and nonsimply connected manifold without boundary. Since we identified only points of a finite radius, m_{I} is still an unbounded space and hence not compact.

First, we show that m_{I} does not have a boundary. By looking at figure 5.1 one could think that points with $r = b$ constitute a boundary of m_{I}. But keep in mind that antipodal points are identified, which is not represented in figure 5.1. We have, therefore, to resort to the technical definition of a manifold with boundary [17, 21]: a two-dimensional manifold has a boundary if it is covered by a family of open sets which are homeomorphic to open sets of the "half plane" $\{(x, y) \in \mathbb{R}^2 : y \geq 0\}$. Then the boundary consists of points with $y = 0$.

To show that m_{I} does not have a boundary, we have to show that the coordinate ranges are not half open intervals of the form $[a, b)$. m_{I} would have a boundary if some coordinate would have values in a half open interval. For the (X_1, Y_1) coordinates defined in equation (5.3) we have that X_1 ranges from $-\infty$ to $+\infty$ and Y_1 lies in the open interval $(Y_1(\phi_{1,max}), Y_1(\phi_{1,min}))$. A similar results holds for the (X_2, Y_2) coordinates defined in equation (5.4). Since these two coordinate charts cover all of m_{I} and no coordinate value is mapped to an half open interval we conclude that m_{I} does not have boundary.

However, if we use the usual polar coordinates (r, ϕ) as coordinates for m_{I}, we have $r \in [b, \infty)$ and it appears that points with $r = b$ are boundary points. But this boundary is a boundary of the coordinate values rather than a boundary of the manifold. The reason is that the (r, ϕ) coordinates are not adapted to the topology of m_{I} at the defect. This can be seen from the fact that the identified points $\boldsymbol{x}$ and $-\boldsymbol{x}$ still have different coordinates (b, ϕ) and $(b, \pi + \phi)$. It is for this reason that the coordinates of equations (5.3) and (5.4) were introduced. In these coordinates $\boldsymbol{x}$ and $-\boldsymbol{x}$ have the same coordinate and the whole defect is mapped to an interior line. Therefore, when using polar coordinates we always have to take the coordinate boundary at $r = b$ into account. Such a coordinate boundary also occurs at the event horizon of a Schwarzschild black hole when the usual spherical polar coordinates are used. It must be taken into account when one uses the theorem of Gauß to convert a volume integral into an integral over the boundary of that volume.

Next, we consider the non-orientability of m_{I}. Here, we follow the definition of [21] and call a manifold orientable if the coordinates of *any* two overlapping charts U_1 and U_2 are related by a transformation whose Jacobian has positive determinant. In the overlap $A \cup C$, shown in figure 5.3, we see from equation (5.5a) that the Jacobian of the transformation from U_1 to U_2 has determinant $+1$. The coordinate transformation in the overlap $B \cup D$, on the other hand, is given by equation (5.5b) and has a Jacobian with determinant -1. Thus we see that m_{I} is not orientable.

Finally, we note that m_{I} is not simply connected. Loosely speaking, a manifold is simply connected if every closed loop can be shrunk continuously to a point. $\mathbb{R}^2$ is simply connected, while $\mathbb{R}^2 - \{\text{point}\}$ and a two-dimensional torus are examples of nonsimply connected manifolds. All closed curves that do not encircle the defect can

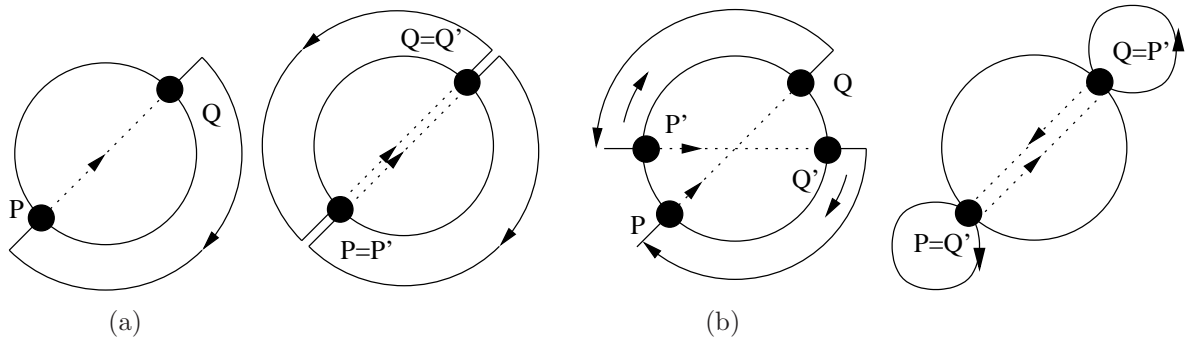

Figure 5.4.: (a) A noncontractible curve which is *closed* in m_{I} and passes through the defect once. (b) Another closed curve in m_{I} and which can be shrunk to a point.

be contracted to a point. Consider the curve of figure 5.4(a), which passes through the defect and is *closed* in m_{I} because the point P is identified with Q. If we tried to shrink the curve to a point by "sliding" Q over to P, P would also move because it is identical to Q. Hence the curve in figure 5.4(a) cannot be contracted to a point and m_{I} is not simply connected. The curve shown in figure 5.4(b), however, passes through the defect twice, and can be shrunk to a point by the shown sequence of curves. We thus find that curves which pass through the defect an even/odd number of times can/cannot be contracted to a point. Two classes of closed curves, therefore, exist on m_{I}.

5.1.3. Topology of m_{I}

In this section we show that m_{I} has the topology of the real projective plane. To see this, we perform an inflection at the circle with $r = b$ by introducing

$$\rho(r) \equiv b/r\,, \tag{5.6}$$

mapping m_{I} into the unit disc. Antipodal points on the (coordinate) boundary circle are still identified. Actually, the image of the coordinate transformation equation (5.6) is the unit disc with the origin removed. The unit disc with antipodal points on the boundary identified is but one of the definitions of the real projective plane $\mathbb{R}P^2$. Another way to define the real projective plane is to identify antipodal points on S^2. Since points on the southern hemisphere are identical to points on the northern hemisphere, it suffices to keep one hemisphere, say the northern one. Antipodal points on the equator are now identified. By projecting the hemisphere down to the equatorial plane we have arrived at the unit disc with antipodal points identified. We have thus shown that

$$m_{\mathrm{I}} \simeq \mathbb{R}P^2 - \{\text{point}\}\,. \tag{5.7}$$

Here, $\simeq$ means "homeomorphic to".

The result that m_{I} is topologically $\mathbb{R}P^2 - \{\text{point}\}$ agrees with all results of the last section. First, because the origin is not included the unit disc is not closed and

hence not compact. When considering fields on m_{I} we usually require that they approach some constant value as r approaches ∞. If this is the case we can add a point $\{\infty\}$ to m_{I} which then gets mapped to the origin by equation (5.6). In this way we have done a one-point compactification of m_{I}. Unless (non-)compactness is of importance we will work with the compactified space which is then homeomorphic to $\mathbb{R}P^2$.

Second, it is known that $\mathbb{R}P^2$ is not orientable and nonsimply connected. This last property can be seen from equation (5.4(b)) once one inflects all the curves at the circle. Finally, the fundamental group π_1 of the real projective plane is isomorphic to $\mathbb{Z}_2$, the group of integers modulo 2,

$$\pi_1(\mathbb{R}P^2) \simeq \mathbb{Z}_2 \,.$$

This statement means that there are exactly two classes of closed curves, namely those that can or cannot be contracted to a point.

5.1.4. Transformation of vectors at the defect

As an application of the results above, we derive the transformation properties of vectors. They will be used later in Part IV. The idea is to look at a curve that passes through the defect. In the coordinates (Y_2, X_2), defined in equation (5.4), this simply means that the curve C intersects the line $Y_2 \equiv 0$. Since we will work only in one coordinate patch we drop the index '2' from now on. The map $(Y, X) \to (r, \phi)$, given in equation (5.4), and C induce a curve c in $\mathbb{R}^2$. The point where C intersects the line $Y \equiv 0$ has the *two* points (b, ϕ) and $(b, \pi + \phi)$ as preimages in $\mathbb{R}^2$. This awkwardness again results from the two points not being identified in $\mathbb{R}^2$. In the same way, the tangent vector of C at $(0, X)$ corresponds to *two* tangent vectors of c in $\mathbb{R}^2$. One is the tangent vector of c evaluated at (b, ϕ) and the other is the vector at $(b, \pi + \phi)$. We will show that these two vectors then automatically satisfy the boundary conditions used in Chapter 13. Furthermore, although the curve c does not *look* smooth in $\mathbb{R}^2$ we use an immersion of $\mathbb{R}P^2$ into $\mathbb{R}^3$ where $\boldsymbol{x}$ and $-\boldsymbol{x}$ are identified and the curve is indeed seen to be smooth.

We start with a curve defined in (Y, X)-coordinates by

$$C(\lambda) \equiv (Y_0 + \lambda(Y_1 - Y_0), X_0 + \lambda(X_1 - X_0)) \,, \tag{5.8}$$

which is a straight line starting at $C(0) = (Y_0, X_0)$ and ending at $C(1) = (Y_1, X_1)$. It is supposed to start below the Y-axis and intersect the Y-axis at $\lambda = 1/2$. The tangent vector $\boldsymbol{V}$ of C as defined by equation (5.8) is given by

$$\boldsymbol{V} = (Y_1 - Y_0)\partial_Y + (X_1 - X_0)\partial_X \,.$$

As a specific example we consider the curve

$$C_{\mathrm{ex}}(\lambda) = (2\,\lambda - 1, \pi/4 + \lambda\,\pi/2) \,, \tag{5.9}$$

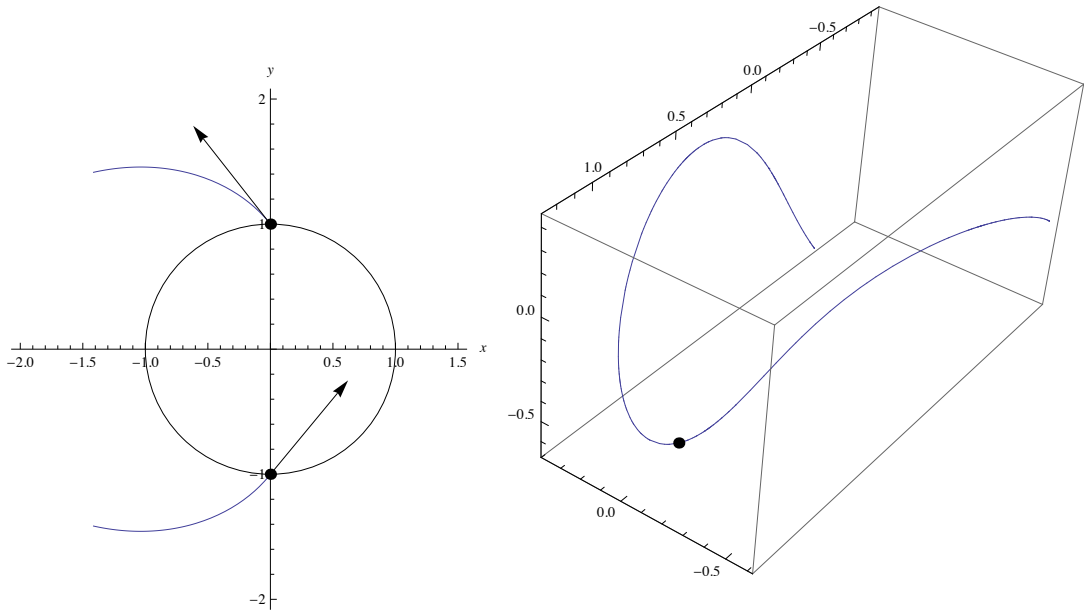

(a) (b)

Figure 5.5.: (a) Graph of the curve c_{ex}. The two (normalized) tangent vectors at $\boldsymbol{x}$ and $-\boldsymbol{x}$ are also shown. Notice that the graph does not look smooth at the defect, but the tangent vectors satisfy equations (5.13a) and (5.13b). (b) The same curve, but now the points belong to Boy's surface, which is an immersion of the real projective plane in $\mathbb{R}^3$. Now the curve looks smooth, but the points where c_{ex} passes through the defect are mapped to a point where the surface intersects itself. For clarity, the surface itself is not shown.

which intersects the Y-axis at $\lambda = 1/2$. Next, we define the induced curve $c(\lambda)$ in the (r, ϕ)-coordinates $\mathbb{R}^2$ by

$$c(\lambda) \equiv (r(Y(\lambda)), \phi(Y(\lambda), X(\lambda))) \,,$$

where $Y(\lambda)$ and $X(\lambda)$ can be read off equation (5.8) and are explicitly given by

$$r(\lambda) \equiv b + |Y(\lambda)| = b + |Y_0 + (Y_1 - Y_0)\lambda| \,, \tag{5.10a}$$

$$\phi(\lambda) \equiv \begin{cases} \pi + X_0 + (X_1 - X_0)\lambda, & \lambda < 1/2 \\ X_0 + (X_1 - X_0)\lambda, & \lambda > 1/2 \end{cases} \,. \tag{5.10b}$$

Figure 5.5(a) shows the induced curve c_{ex} of C_{ex}. Now, as c approaches the defect from above, that is $\lambda \geq 1/2$, we have

$$\boldsymbol{v}(\boldsymbol{x}) \equiv \lim_{\lambda \to 1/2^+} \frac{\mathrm{d}c}{\mathrm{d}\lambda} = \frac{\partial r}{\partial \lambda}\partial_r(\boldsymbol{x}) + \frac{\partial \phi}{\partial \lambda}\partial_\phi(\boldsymbol{x}) = (Y_1 - Y_0)\partial_r(\boldsymbol{x}) + (X_1 - X_0)\partial_\phi(\boldsymbol{x}) \,, \tag{5.11}$$

while on the opposite side, meaning $\lambda \leq 1/2$, we obtain

$$\boldsymbol{v}(-\boldsymbol{x}) \equiv \lim_{\lambda \to 1/2^-} \frac{\mathrm{d}c}{\mathrm{d}\lambda} = \frac{\partial r}{\partial \lambda}\partial_r(\boldsymbol{x}) + \frac{\partial \phi}{\partial \lambda}\partial_\phi(\boldsymbol{x}) = -(Y_1 - Y_0)\partial_r(-\boldsymbol{x}) + (X_1 - X_0)\partial_\phi(-\boldsymbol{x})\,. \tag{5.12}$$

Due to the identification of $\boldsymbol{x}$ and $-\boldsymbol{x}$, however, the vectors in equations (5.11) and (5.12) are identical. Therefore, the components satisfy

$$v^r(\boldsymbol{x}) = -v^r(-\boldsymbol{x})\,, \tag{5.13a}$$

$$v^\phi(\boldsymbol{x}) = v^\phi(-\boldsymbol{x})\,. \tag{5.13b}$$

Equations (5.13a) and (5.13b) are the boundary conditions we will use in Part IV. Physically speaking, equation (5.13a) means that if a particle enters the defect on one side, it leaves on the other side. Equation (5.13b) implies that if a vector points to another point on the defect, then the identified vector points to the identified point. The induced curve in figure 5.5(a) *looks* discontinuous in the usual topology of $\mathbb{R}^2$, but actually satisfies the boundary conditions of equations (5.13a) and (5.13b).

That equations (5.13a) and (5.13b) are indeed the boundary conditions for a tangent vector of a smooth curve can also be seen by using an immersion of $\mathbb{R}P^2$ into $\mathbb{R}^3$. Out of the many immersions we use Boy's surface, in the parametrization given by [24]. If the complex number $\rho = r\mathrm{e}^{i\phi}$ of maximal absolute value 1 represents a point of the unit disc, then the following yields a parametrization of Boy's surface

$$x(\rho) = g_x(\rho)/g(\rho)\,, \tag{5.14a}$$

$$y(\rho) = g_y(\rho)/g(\rho)\,, \tag{5.14b}$$

$$z(\rho) = g_z(\rho)/g(\rho)\,, \tag{5.14c}$$

with

$$\begin{aligned} g_x(\rho) &\equiv -\frac{3}{2}\mathrm{Im}\left(\frac{\rho(1-\rho^4)}{\rho^6 + \sqrt{5}\rho^3 - 1}\right)\,, \\ g_y(\rho) &\equiv -\frac{3}{2}\mathrm{Re}\left(\frac{\rho(1+\rho^4)}{\rho^6 + \sqrt{5}\rho^3 - 1}\right)\,, \\ g_z(\rho) &\equiv \mathrm{Im}\left(\frac{1+\rho^6}{\rho^6 + \sqrt{5}\rho^3 - 1}\right) - \frac{1}{2}\,, \\ g(\rho) &\equiv g_x^2(\rho) + g_y^2(\rho) + g_z^2(\rho)\,. \end{aligned}$$

To find the graph of C on Boy's surface we first use equation (5.4) to obtain the curve c in $\mathbb{R}^2$. Second, we apply the coordinate transformation equation (5.6), mapping c into the unit disc. Here, we finally use equations (5.14a)–(5.14c) to obtain the graph on Boy's surface. For the curve defined in equation (5.9) the result is shown in figure 5.5(b) and is seen to be a smooth curve in $\mathbb{R}^3$ on Boy's surface. For clarity, Boy's surface itself is not shown because it is a non-orientable and self-intersecting surface. The marked point is the image of the two points where c passes through the defect and is a point where Boy's surface intersects itself.

5.1.5. Curvature of m_I

In this section we discuss the problems that arise when one tries to equip m_I with the standard Euclidean metric.

We start by equipping the original m_I with the standard Euclidean metric

$$\mathrm{d}s^2 = \mathrm{d}r^2 + r^2\mathrm{d}\phi^2 \,. \tag{5.15}$$

As discussed in Section 5.1.2, the polar coordinates (r, ϕ) are not well suited to investigate properties at the defect. Hence, we use the coordinates (Y, X) defined in equation (5.4). Expressed in these coordinates the metric in equation (5.15) reads

$$\mathrm{d}s^2 = \mathrm{d}Y^2 + (b + |Y|)^2\mathrm{d}X^2 \,. \tag{5.16}$$

Notice the dependence on the absolute value of Y. Using $\mathrm{abs}''(x) = 2\delta(x)$ the Ricci curvature is given by

$$R = \frac{-4}{b + |Y|}\delta(Y) = -\frac{4}{b}\delta(Y) \,, \tag{5.17}$$

which is zero everywhere expect at the line $Y = 0$ representing the defect. Thus, by imposing the standard Euclidean metric on m_I the Ricci-scalar develops a δ-singularity at the defect.

To better understand the occurrence of the curvature singularity we use the link between a manifold's geometry and its topology provided by the Gauß-Bonnet theorem. If m is a two-dimensional compact manifold with boundary ∂m, then the Euler characteristic of m, denoted $\chi(m)$, is related to the Gauß curvature K by

$$2\pi\chi(m) = \int_m K\mathrm{d}A + \oint_{\partial m} \kappa\mathrm{d}s \,. \tag{5.18}$$

For a two-dimensional Riemannian manifold the Gauß curvature K is related to the Ricci scalar R via

$$R = 2K \,.$$

The geodesic curvature vector $\boldsymbol{\kappa}$ of a curve is the covariant derivative of the tangent vector $\boldsymbol{T}$, that is

$$\boldsymbol{\kappa} \equiv \nabla_{\boldsymbol{T}}\boldsymbol{T} \,, \tag{5.19}$$

and the geodesic curvature κ is the magnitude of $\boldsymbol{\kappa}$. The right hand side of equation (5.18) involves only quantities depending on the geometry of the manifold. The left hand side is a multiple of the Euler characteristic and is a topological invariant, i.e. it is independent of the metric. Hence, we can use equation (5.18) as a tool to test whether a manifold with known topology admits a given metric. We now show that the singularity in equation (5.17) ensures that the Gauß-Bonnet theorem is satisfied when the standard Euclidean metric is used on m_I.

To apply equation (5.18) we must have a compact manifold. As shown in Section 5.1.2 the manifold m_I is not compact. Therefore, we construct a compact submanifold of m_I. For this we use polar coordinates (r, ϕ) and consider a "ring" consisting

of all points with $b \leq r \leq R$. Since this manifold is compact, with the circle of radius R as its boundary (the points with $r = b$ are just a coordinate boundary, see Section 5.1.2), we can apply equation (5.18). After using equation (5.6) this "ring" consists of all points with $\rho_0 \leq \rho \leq 1$, where

$$\rho_0 \equiv b/R > 0\,.$$

This compact two-dimensional submanifold is actually the Möbius strip [25], and its Euler characteristic is known to be

$$\chi(\text{Mö}) = 0\,.$$

The Gauß-Bonnet theorem, equation (5.18), then implies that an admissible metric for $\mathbb{R}P^2$ must have a Gauß curvature such that its integral over the Möbius strip cancels the contribution from the boundary.

After the inflection given by equation (5.6) the Euclidean metric in equation (5.15) is given by

$$\mathrm{d}s^2 = \frac{b^2}{\rho^4}\mathrm{d}\rho^2 + \frac{b^2}{\rho^2}\mathrm{d}\phi^2\,. \tag{5.20}$$

The boundary circle with radius ρ_0, parametrized by arc length $s \in [0, 2\pi\, b/\rho_0]$, is given by

$$\begin{aligned}\rho(s) &= \rho_0\,,\\ \phi(s) &= 2\pi - \frac{\rho_0}{b}\,s\,.\end{aligned}$$

Using this parametrization and the metric in equation (5.20) one obtains for the curvature vector

$$\boldsymbol{\kappa} = \rho_0^3/b^2\,\partial_\rho\,,$$

and for its magnitude

$$\kappa = \frac{\rho_0}{b}\,.$$

With this we obtain

$$\oint_{\partial\text{Mö}} \kappa \mathrm{d}s = \frac{\rho_0}{b}\int_0^{2\pi\, b/\rho_0} \mathrm{d}s = 2\pi\,. \tag{5.21}$$

If the metric in equation (5.20) were flat everywhere, we would have

$$\int_{\text{Mö}} K\mathrm{d}A = 0\,. \tag{5.22}$$

Combining equations (5.22) and (5.21) would give

$$\int_{\text{Mö}} K\mathrm{d}A + \oint_{\partial\text{Mö}} \kappa\mathrm{d}s = 2\pi \neq 2\pi\,\chi(\text{Mö}) = 0\,.$$

Clearly, the Gauß-Bonnet theorem is violated and we arrive at the conclusion that *it is not possible to equip the manifold m_I with the Euclidean metric that is flat everywhere.*

Using the (Y, X) coordinates, the Möbius strip consists of a box with $-Y_0 \leq Y \leq Y_0$ and $0 \leq X \leq \pi$.[1] If we now use the Ricci scalar in equation (5.17) we obtain

$$\int_{\text{Mö}} K \mathrm{d}A = \int_0^{\pi} \int_{-Y_0}^{Y_0} -2\frac{(b+|Y|)}{b}\delta(Y)\mathrm{d}Y\,\mathrm{d}X = -2\pi\,. \tag{5.23}$$

The two lines

$$\begin{aligned} Y(s) &= \pm Y_0\,, \\ X(s) &= \pi - \frac{s}{1+Y_0}\,, \end{aligned}$$

constitute the boundary, and the arc length s runs from 0 to $\pi(b + Y_0)$. On both lines the magnitude κ of the curvature vector equals $1/(1 + Y_0)$ and we obtain

$$\oint_{\partial\text{Mö}} \kappa \mathrm{d}s = 2\int_0^{\pi(b+Y_0)} \frac{1}{b+Y_0}\mathrm{d}s = +2\pi\,. \tag{5.24}$$

Now combining equations (5.23) and (5.24) gives the correct result

$$\int_{\text{Mö}} K\mathrm{d}A + \oint_{\partial\text{Mö}} \kappa \mathrm{d}s = -2\pi + 2\pi = 2\pi\chi(\text{Mö}) = 0\,.$$

Thus, by imposing the standard Euclidean metric, which is flat almost everywhere, the nontrivial topology of m_I forced the Ricci scalar to develop a δ-singularity at the defect. It is this singularity that, when integrated over, cancels the boundary term and gives the correct Euler characteristic of the Möbius strip. Ultimately, we are interested in finding solutions to Einstein's equations that have nontrivial topology but are free of singularities. Thus it is of interest to see what metrics on m_I are admissible and devoid of singularities. We now show that a metric with constant, nonzero, curvature satisfies the Gauß-Bonnet theorem and has no singularities.

A metric for m_I with Gauß curvature of $1/3b^2$, in the coordinates (ρ, ϕ), reads

$$\mathrm{d}s^2 = \frac{3b^2}{1-\rho^2}\mathrm{d}\rho^2 + 3b^2\,\rho^2\mathrm{d}\phi^2\,.$$

Again, the boundary circle with radius ρ_0 of Möbius strip is parametrized in terms of arc length s as

$$\begin{aligned} \rho(s) &= \rho_0\,, \\ \phi(s) &= \frac{s}{\sqrt{3}\,b\,\rho_0}\,, \end{aligned}$$

[1] Technically, points where either $X = 0$ or $X = \pi$ are not in the coordinate patch (5.4) and we would have to use the second patch, (5.3), as well. Since all quantities of interest are finite on the x-axis (where $X = 0$ or $X = \pi$), however, it yields no contribution to the integrals. This is the same as using spherical coordinates (r, θ, ϕ) on the z-axis when all quantities are finite there.

with s ranging from 0 to $2\pi\sqrt{3}\,b\,\rho_0$. The norm κ of the curvature vector evaluates to

$$\kappa = \frac{\sqrt{1-\rho_0^2}}{\sqrt{3}\,b\,\rho_0}\,,$$

and we obtain

$$\oint_{\partial \mathrm{M\ddot{o}}} \kappa \mathrm{d}s = 2\pi\sqrt{1-\rho_0^2}\,. \tag{5.25}$$

The integral of the Gauß curvature evaluates to

$$\int_{\mathrm{M\ddot{o}}} K \mathrm{d}A = 2\pi \int_1^{\rho_0} \frac{\rho}{\sqrt{1-\rho^2}} \mathrm{d}\rho = -2\pi\sqrt{1-\rho_0^2}\,. \tag{5.26}$$

Equations (5.25) and (5.26) add up to zero, which is the correct result. Hence, we have shown that by choosing a metric with *nonvanishing* curvature it is possible to satisfy the Gauß-Bonnet theorem without a singularity in the curvature.

To summarize: We constructed a two-dimensional circular defect, m_I by removing the interior of a disc of radius b and then identified antipodal points on the would-be boundary circle. It was shown in Section 5.1.1 that m_I is indeed a manifold. By finding appropriate coordinates we derived the transformation properties of vectors at the defect. Furthermore, we showed in Section 5.1.3 that m_I is homeomorphic to the real projective plane $\mathbb{R}P^2$ (up to a one-point compactification). From this we saw that m_I is nonorientable and nonsimply connected. Finally, we discussed in Section 5.1.5 that m_I cannot be equipped with the standard Euclidean metric, because the Ricci scalar curvature contains a singularity. Most of the techniques employed to analyze m_I will be used in the next section, where we consider the three-dimensional defect.

5.2. Three-dimensional spherical defect

In this section we investigate the three-dimensional space M_I containing a type I defect. It will become a spatial hypersurface in a four-dimensional spacetime in the following chapter. The construction is similar to its two-dimensional counterpart m_I. The starting point is $\mathbb{R}^3$ from which we remove the interior of a ball of radius b. Now points on the sphere with radius b constitute a boundary. By identifying antipodal points on this sphere the boundary is removed. This is the same construction used in [7] to create a $\tau = 1$ defect. As in the last section we first prove in Section 5.2.1 that M_I is a three-dimensional manifold. In Section 5.2.2 we show that it is orientable and nonsimply connected. For completeness, we also derive the boundary conditions for tangent vectors at the defect. Finally, in Section 5.2.3, we investigate the topology and whether or not M_I admits a smooth Euclidean metric.

5.2.1. Proof that M_I is a manifold

The proof that M_I is a manifold proceeds along similar lines to the m_I case. After defining the topology we give the coordinate charts and show that they are infinitely differentiable in the regions of overlap.

We again start to define a topology on M_I by making reference to the defining $\mathbb{R}^3$. Similarly to equation (5.1), an ϵ-neighborhood $U_{\epsilon,x}$ of a point $\boldsymbol{x} \in \mathbb{R}^3$ not on the defect is defined by

$$U_{\epsilon,x} \equiv \{\boldsymbol{y} \in \mathbb{R}^3 : |\boldsymbol{x} - \boldsymbol{y}|_3 < \epsilon\}\,, \tag{5.27}$$

where the subscript '3' indicates that the usual metric of $\mathbb{R}^3$ is used. Again we include all $U_{\epsilon,x}$ in the topology of M_I with $|\boldsymbol{x}|_3 > b$ and $\epsilon < |\boldsymbol{x}|_3 - b$. Two open sets in $\mathbb{R}^3$ are also required to define the open sets for points on the defect:

$$\begin{aligned} U_{\epsilon,1} &\equiv \{\boldsymbol{y} \in \mathbb{R}^3 : |\boldsymbol{x} - \boldsymbol{y}|_3 < \epsilon\}\,, \\ U_{\epsilon,2} &\equiv \{\boldsymbol{y} \in \mathbb{R}^3 : |\boldsymbol{x} + \boldsymbol{y}|_3 < \epsilon\}\,. \end{aligned}$$

The first set is a ball of radius ϵ centered at $\boldsymbol{x}$ while the second is a ball centered around $-\boldsymbol{x}$. Thus we define an open set for a point on the defect by

$$U_{\epsilon,x} \equiv (U_{\epsilon,1} \cap U_{\epsilon,2}) \setminus \mathring{B}_b = \{\boldsymbol{y} \in \mathbb{R}^3 : (|\boldsymbol{x}-\boldsymbol{y}|_3 < \epsilon \vee |\boldsymbol{x}+\boldsymbol{y}|_3 < \epsilon) \wedge |\boldsymbol{y}|_3 \geq b\}\,, \tag{5.28}$$

where the interior of a ball of radius b is subtracted this time. $U_{\epsilon,x}$ in (5.28) is a straightforward generalization of (5.2). Again (5.28) is not an open set in the defining $\mathbb{R}^3$. As for the m_I case, M_I is the union of all these $U_{\epsilon,x}$. To make M_I a topological space we formally add the empty set $\emptyset$ to the topology of M_I.

To define the coordinate maps of M_I we need three "wedges", one around each axis but not intersecting the other two axes, as shown in figure 5.6. We introduce coordinate charts on each "wedge" as in the m_I case. On each chart, one coordinate ranges from $-\infty$ to $+\infty$ and corresponds to the radius, where the sign encodes whether a point is "left" or "right" of the defect. Points with coordinate 0 are on the defect. For the "wedge" surrounding the z-axis we have to introduce another set of spherical coordinates, as the usual spherical coordinates (r, θ, ϕ) are ill defined along the z-axis. We define the other set of coordinates (r, ϑ, φ), which are well defined on the z-axis, by

$$\begin{aligned} x &= r \sin\vartheta \, \sin\varphi, \\ y &= r \cos\vartheta, \\ z &= r \sin\vartheta \, \cos\varphi. \end{aligned}$$

With the definition that regions 1, 2, and 3 cover the x-, y-, and z-axes respectively,

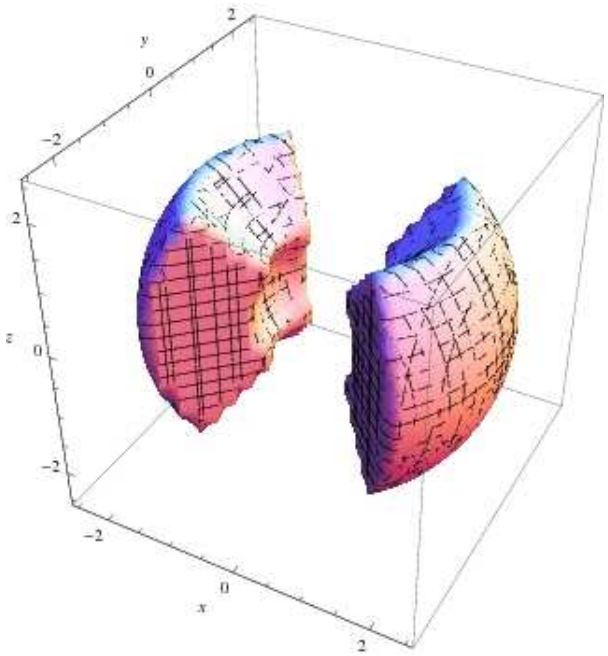

Figure 5.6.: One of the three "wedges" that are used to cover M_{I}. The one shown here surrounds the x-axis but does not intersect the other axes. The other two "wedges" are obtained from this one by a 90° rotation.

we obtain the coordinate maps

$$X_1(r,\phi) = \begin{cases} r-b, & \cos\phi \geq 0 \\ b-r, & \cos\phi < 0 \end{cases}, \qquad r(X_1) = \begin{cases} b+X_1, & X_1 \geq 0 \\ b-X_1, & X_1 < 0 \end{cases}$$

$$Y_1(\phi) = \begin{cases} \phi - \pi/2, & \cos\phi < 0 \\ \phi - 3\pi/2, & 3\pi/2 < \phi < 2\pi \\ \phi + \pi/2, & 0 \leq \phi < \pi/2 \end{cases}, \qquad \theta(X_1,Z_1) = \begin{cases} Z_1, & X_1 \geq 0 \\ \pi - Z_1, & X_1 < 0 \end{cases}$$

$$\phi(X_1,Y_1) = \begin{cases} Y_1 + \pi/2, & X_1 < 0 \\ Y_1 + 3\pi/2, & X_1 > 0 \wedge Y_1 < \pi/2 \\ Y_1 - \pi/2, & X_1 > 0 \wedge Y_1 > \pi/2 \end{cases} \qquad Z_1(\theta,\phi) = \begin{cases} \theta, & \cos\phi \geq 0 \\ \pi - \theta, & \cos\phi < 0 \end{cases} \tag{5.29}$$

$$X_2(\phi) = \begin{cases} \phi, & \phi < \pi \\ \phi - \pi, & \phi > \pi \end{cases}, \qquad r(Y_2) = \begin{cases} b+Y_2, & Y_2 \geq 0 \\ b-Y_2, & Y_2 < 0 \end{cases},$$

$$Y_2(r,\phi) = \begin{cases} r-b, & \phi < \pi \\ b-r, & \phi > \pi \end{cases}, \qquad \theta(Y_2,Z_2) = \begin{cases} Z_2, & Y_2 \geq 0 \\ \pi - Z_2, & Y_2 < 0 \end{cases},$$

$$Z_2(\theta,\phi) = \begin{cases} \theta, & 0 < \phi < \pi \\ \pi - \theta, & \phi > \pi \end{cases}, \qquad \phi(X_2,Y_2) = \begin{cases} X_2, & Y_2 \geq 0 \\ X_2 + \pi, & Y_2 < 0 \end{cases}, \tag{5.30}$$

$$
X_3(\varphi) = \begin{cases} \varphi - \pi/2, & \cos\varphi < 0 \\ \varphi - 3\pi/2, & 3\pi/2\varphi < 2\pi \\ \varphi + \pi/2, & 0 < \varphi < \pi/2 \end{cases}
\qquad
r(Z_3) = \begin{cases} b + Z_3, & Z \geq 0 \\ b - Z_3, & Z < 0 \end{cases}
$$

$$
Y_3(\vartheta, \varphi) = \begin{cases} \vartheta, & \cos\varphi > 0 \\ \pi - \vartheta, & \cos\varphi < 0 \end{cases}
\qquad
\vartheta(Y_3, Z_3) = \begin{cases} Y_3, & Z_3 \geq 0 \\ \pi - Y_3, & Z_3 < 0 \end{cases}
$$

$$
\varphi(X_3, Z_3) = \begin{cases} X_3 + \pi/2, & Z_3 \leq 0 \\ X_3 + 3\pi/2, & Z > 0 \wedge X_3 < \pi/2 \\ X_3 - \pi/2, & Z > 0 \wedge X_3 > \pi/2 \end{cases}
\qquad
Z_3(r, \varphi) = \begin{cases} r - b, & \cos\varphi \geq 0 \\ b - r, & \cos\varphi < 0 \end{cases}
\tag{5.31}
$$

Notice that the coordinate patches in equations (5.29) and (5.30) are the two-dimensional coordinates of equations (5.3) and (5.4) amended by the third coordinate Z. We continue the practice of Section 5.1.1 and write for example (Z, Y, X) to indicate that Z is the "radial" coordinate and Y and X are the "inclination" and "azimuthal" angles, respectively. Points on the defect have "radial" coordinate 0, for example $Y_2 = 0$ in equation (5.30). The ranges of the coordinates defined by equation (5.29) are

$$
\begin{aligned}
-\infty < & X_1 < \infty\,, \\
0 < & Y_1 < \pi\,, \\
0 < & Z_1 < \pi\,,
\end{aligned}
$$

and similarly for the other two. $X_1 < 0$ or $X_1 > 0$ in equation (5.29) means that the point in question is to the "left" or to the "right" of the defect, respectively.

As the last part of the proof we have to check that the coordinates in Eqs.(5.29)–(5.30) are inverses of each other and infinitely differentiable on the region where the "wedges" overlap. For regions 1 and 2 the check is similar to the m_{I} manifold, now amended by a third Z coordinate. The result is

$$
A \cup C : X_1(Y_2) = Y_2, \quad Y_1(X_2) = X_2 + \pi/2, \quad Z_1 = Z_2\,, \tag{5.32a}
$$

$$
B \cup D : X_1(Y_2) = -Y_2, \quad Y_1(X_2) = X_2 - \pi/2, \quad Z_1 = \pi - Z_2\,, \tag{5.32b}
$$

where A is the three-dimensional analog of the region A in figure 5.3, and similarly for the other ones. From equation (5.32) we see that the two coordinates are inverses of each other and smooth functions of each other. Due to the use of two spherical coordinates the relations between the coordinates on the overlaps of region 3 with region 1 and 2 are less trivial. For example, in the overlap region of 2 and 3 given by

$$
\begin{aligned}
0 < X_2 < \pi, \quad & 0 < X_3 < \pi/2\,, \\
0 < Z_2 < \pi/2, \quad & 0 < Y_3 < \pi/2\,,
\end{aligned}
\tag{5.33}
$$

we find,

$$
\begin{aligned}
X_3(X_2, Z_2) &= \pi/2 + \arctan(\tan Z_2 \, \cos X_2)\,, \\
Y_3(X_2, Z_2) &= \arctan\left(\frac{\sqrt{1 - \sin^2 Z_2 \, \sin^2 X_2}}{\sin Z_2 \, \sin X_2}\right), \qquad Z_3(Y_2) = Y_2\,, \\
X_2(X_3, Y_3) &= \operatorname{arccot}(-\tan Y_3 \, \cos X_3)\,, \\
Z_2(X_3, Y_3) &= \arctan\left(\frac{\sqrt{1 - \sin^2 Y_3 \, \sin^2 X_3}}{\sin Y_3 \, \sin X_3}\right). \qquad (5.34)
\end{aligned}
$$

However, neither function has a pole in the coordinate specified by (5.33) and is infinitely differentiable. Also, using standard trigonometric identities one can show that these functions are inverse to each other. Similar relations hold for the other overlap regions, thus showing that the coordinate charts are infinitely differentiable on the overlaps. Thus all charts are invertible smooth maps in the regions of overlap, and hence M_{I} is a manifold.

That M_{I} has the Hausdorff property is shown in the same way as for m_{I}. The only difference is that for two points (b, θ_1, ϕ_1) and (b, θ_2, ϕ_2) on the defect we have to take ϵ to be the minimum of either $|b(\phi_1 - \phi_2)|/2$ or $|b(\theta_1 - \theta_2)|/2$.

5.2.2. Properties of M_{I}

We now show that M_{I} is a noncompact, orientable and nonsimply connected manifold without boundary. The arguments for each of these properties are similar to those discussed for m_{I} in Section 5.1.2.

The fictitious coordinate boundary at $r = b$ again results from the spherical polar coordinates not being suited to describe the defect. In the usual topology of $\mathbb{R}^3$ these points are boundary points, but in the topology of M_{I}, defined in equation (5.28), they are not. Also, in the coordinate patches adapted to the topology of M_{I}, as defined by Eqs .(5.29)–(5.29), points on the defect are mapped into the interior of the coordinate "box".

Again, noncompactness follows from the fact that we identified only points at a finite radius and M_{I} is still unbounded. That M_{I} is not simply connected can also be seen from figure 5.4, which applies to M_{I} as well, if we think of it as a two-dimensional slice through M_{I}. Closed curves in M_{I} therefore fall into two distinct classes: those which can or cannot be contracted to a point.

Finally, we find that M_{I} is orientable as opposed to the nonorientable m_{I}. When calculating the Jacobian of the transformation in equation (5.32b) the third equation yields an additional minus sign, as compared to equation (5.5b), and the resulting determinant is +1. A lengthy, but straightforward, calculation reveals that the Jacobians of the transformations in equation (5.34) also have Jacobians with positive determinants.

We close this section by deriving the transformation properties of tangent vectors at the defect. The idea is exactly the same as in Section 5.1.4. In the (Y, Z, X)

coordinate patch we consider the straight line C

$$C(\lambda) \equiv (Y_0 + \lambda(Y_1 - Y_0), Z_0 + \lambda(Z_1 - Z_0), X_0 + \lambda(X_1 - X_0)) \,, \tag{5.35}$$

with $\lambda \in [0, 1]$ and which is supposed to pass through the $Y = 0$ plane at, say, $\lambda = 1/2$. Writing ΔY for $Y_1 - Y_0$ (and similarly for $Z_1 - Z_0$ and $X_1 - X_0$), the tangent vector V of C reads

$$V = \Delta Y \partial_Y + \Delta Z \partial_Z + \Delta X \partial_X \,.$$

Now we use equation (5.30) to obtain the image c of C in $\mathbb{R}^3$

$$r(\lambda) = b + |Y_0 + \Delta Y \lambda| \,, \tag{5.36a}$$

$$\theta(\lambda) = \begin{cases} Z_0 + \Delta Z \lambda, & \lambda \geq 1/2 \\ \pi - Z_0 - \Delta Z \lambda, & \lambda \leq 1/2 \end{cases} \,, \tag{5.36b}$$

$$\phi(\lambda) = \begin{cases} X_0 + \Delta X \lambda, & \lambda \geq 1/2 \\ \pi + X_0 + \Delta X \lambda, & \lambda \leq 1/2 \end{cases} \,. \tag{5.36c}$$

As λ approaches $1/2$ the two tangent vectors v of c at $\boldsymbol{x}$ and $-\boldsymbol{x}$ read

$$\boldsymbol{v}(\boldsymbol{x}) \equiv \lim_{\lambda \to 1/2^+} \frac{\mathrm{d}c}{\mathrm{d}\lambda} = \Delta Y \partial_r(\boldsymbol{x}) + \Delta Z \partial_\theta(\boldsymbol{x}) + \Delta X \partial_\phi(\boldsymbol{x}) \,, \tag{5.37a}$$

$$\boldsymbol{v}(-\boldsymbol{x}) \equiv \lim_{\lambda \to 1/2^-} \frac{\mathrm{d}c}{\mathrm{d}\lambda} = -\Delta Y \partial_r(-\boldsymbol{x}) - \Delta Z \partial_\theta(-\boldsymbol{x}) + \Delta X \partial_\phi(-\boldsymbol{x}) \,. \tag{5.37b}$$

Since spherical coordinates are not adapted to the topology of M_{I}, the tangent vector of c at the defect appears as the two vectors in equation (5.37). Therefore, when we identify the two vectors, we obtain the following for the components

$$v^r(\boldsymbol{x}) = -v^r(-\boldsymbol{x}) \,, \tag{5.38a}$$

$$v^\theta(\boldsymbol{x}) = -v^\theta(-\boldsymbol{x}) \,, \tag{5.38b}$$

$$v^\phi(\boldsymbol{x}) = +v^\phi(-\boldsymbol{x}) \,. \tag{5.38c}$$

Equations (5.38a)–(5.38c) are the boundary conditions for a type I defect that will be used in Chapter 13 (equations (13.6a)–(13.6c)). In the next section it will be shown that M_{I} is homeomorphic to $\mathbb{R}P^3$. Unfortunately, there exists no way to represent $\mathbb{R}P^3$ as a subset of $\mathbb{R}^3$.

5.2.3. Topology and curvature of M_{I}

The proof that

$$M_{\mathrm{I}} \simeq \mathbb{R}P^3 - \{\text{point}\}$$

proceeds along similar lines to those in Section 5.1.3. We work in spherical polar coordinates and perform an inflection at the sphere of radius b, see equation (5.6). In this way, M_{I} is mapped into the unit ball with antipodal points on the boundary

identified. Again the origin of the ball is not included, making the space non-compact. Provided that all fields defined on M_{I} have a well-defined limit as $r \to \infty$ we can add a point $\{\infty\}$ to M_{I} and obtain a compact space. This extra point is then mapped to the origin by the inflection. The unit ball with antipodal points identified is, however, just one definition of the real projective space $\mathbb{R}P^3$ [21]. This concludes the proof that $M_{\mathrm{I}} \simeq \mathbb{R}P^3 - \{\text{point}\}$.

This result is consistent with the properties of M_{I} stated in the previous section. Namely, $\mathbb{R}P^3$ is a three-dimensional, orientable, nonsimply connected manifold without boundary.

To see what happens when we equip M_{I} with a flat Euclidean metric we employ the coordinates (Y, Z, X) defined in equation (5.30). However, we start with the metric given in spherical polar coordinates as

$$\mathrm{d}s^2 = \mathrm{d}r^2 + r^2\mathrm{d}\theta^2 + r^2\sin^2\theta\mathrm{d}\phi^2\,,$$

which in the (Y, Z, X) coordinates reads

$$\mathrm{d}s^2 = \mathrm{d}Y^2 + (b + |Y|)^2\mathrm{d}Z^2 + (b + |Y|)^2\sin^2 Z\mathrm{d}X^2\,.$$

The Ricci scalar R can now be calculated as

$$R = -2\frac{\mathrm{abs}'(Y)^2 - 1 + 2(b + \mathrm{abs}(Y))\mathrm{abs}''(Y)}{(b + \mathrm{abs}(Y))^2}\,. \tag{5.39}$$

After using

$$\begin{aligned}\mathrm{abs}'(x)^2 &= 1\,,\\ \mathrm{abs}''(x) &= 2\delta(x)\,,\end{aligned}$$

equation (5.39) turns out to be

$$R = -8\frac{\delta(Y)}{b + \mathrm{abs}(Y)} = -8\frac{\delta(r - b)}{r}\,. \tag{5.40}$$

Equation (5.40) shows that by forcing M_{I} to have the Euclidean metric almost everywhere, a δ-function in the Ricci scalar is created at the defect. Since there is no Gauß-Bonnet theorem in three dimensions we cannot interpret the magnitude of this singularity. Its existence is tied to the antipodal identification at the defect.

To see what happens if we use a metric with constant curvature instead, it is useful to start by giving the metric in the inflected coordinates (ρ, θ, ϕ). By rescaling ρ we can always ensure that ρ is in the range from 0 to π. We choose the following metric

$$\mathrm{d}s^2 = \mathrm{d}\rho^2 + 4\sin^2(\rho/2)\,\mathrm{d}\theta^2 + 4\sin^2(\rho/2)\sin^2\theta\,\mathrm{d}\phi^2\,.$$

After the transformation $\rho \to \pi/r$ and then using coordinates (Y, Z, X) the metric transforms into

$$\mathrm{d}s^2 = \frac{\pi^2}{(1 + |Y|)^4}\mathrm{d}Y^2 + 4\sin^2\left(\frac{\pi}{2(1 + |Y|)}\right)\mathrm{d}Z^2 + 4\sin^2\left(\frac{\pi}{2(1 + |Y|)}\right)\sin^2 Z\,\mathrm{d}X^2\,.$$

From this we obtain the following for the Ricci scalar

$$R = \frac{3}{2} + 4\frac{(1+|Y|)^2}{\pi}\,\cot\left(\frac{\pi}{2(1+|Y|)}\right)\,\delta(Y) = \frac{3}{2}\,. \tag{5.41}$$

Unlike the Ricci scalar in equation (5.40) the term in front of the δ-function evaluates to zero and R is constant and smooth everywhere.

We conclude this section by one further property of $\mathbb{R}P^3$ which is also shared by M_{I}. As in the previous paragraph we perform a rescaling of $\mathbb{R}P^3$ such that we obtain a ball with radius π and antipodal points with $\rho = \pi$ are identified. This ball is identical to $SO(3)$, the group of rotations in three-dimensional Euclidean space. Such a rotation can always be parametrized by giving the axis of rotation and the magnitude of the rotation. The axis of rotation is specified by a unit vector $\hat{n}$, which in turn is specified once the usual angles θ and ϕ are given. The rotation around $\hat{n}$ with rotation angle ω is then carried out in the usual right handed sense. ω is thus restricted to be in the interval $[0, \pi]$ (for a rotation of more than 180° we have to rotate around $-\hat{n}$ in the right handed sense). The group of rotations is parametrized by points in the ball of radius π. Finally, note that a rotation of 180° around $\hat{n}$ gives the same result as a 180° rotation around -$\hat{n}$. Thus, antipodal points on the boundary have to be identified and $SO(3)$ is identical to a ball of radius π with antipodal points on the boundary identified. To summarize, we have the following relations between M_{I}, $\mathbb{R}P^3$, and $SO(3)$

$$M_{\mathrm{I}} \simeq \mathbb{R}P^3 - \text{point} \simeq SO(3) - \text{point}\,.$$

The result that M_{I} is homeomorphic to $SO(3)$ is crucial for the following chapters. Ultimately, we want to find solutions to Einstein's equations that have the spatial topology of M_{I}. Matter fields then have to be compatible with this topology as well. Since M_{I} is $SO(3)$ topologically, we will see that an $SO(3)$-valued scalar field naturally fits on this spacetime.

6. An SO(3)-Skyrme model

6.1. General considerations

In the last chapter we showed that the space M_{I} of a defect obtained from $\mathbb{R}^3$ by removing a ball of radius b and antipodal identification is a three-dimensional manifold and has the topology of $SO(3)$. Now, we investigate if and how M_{I} can be a spatial hypersurface of a four-dimensional spacetime. This spacetime would then have the topology $\mathbb{R} \times SO(3)$. As regards to Part IV we also want the spacetime to be Minkowskian far away from the defect, which requires spacetime to become flat asymptotically. The results of Chapter 5 indicate that the nontrivial topology of M_{I} will not allow the flat Minkowski metric to be smooth everywhere. Rather, a metric with constant curvature seems to be preferred. Thus, to obtain a metric that is at least flat asymptotically, we require some matter field which, via Einstein's equations, "irons out" the curvature at infinity. If this turns out to be the case, then the defect can be considered as an isolated region for which a mass can be defined. As an additional feature we would like the defect to be stable in the sense that there exists some finite defect parameter b which minimizes the mass of the defect. If the defect were to shrink to zero its mass would become infinite. Such a shrinking can only be discussed within the full time-dependent Einstein equations, if at all. To discuss what happens in this limit probably requires quantum gravity as well. To avoid all these difficulties we constrain our investigations to the time-independent case and treat b as an additional parameter of our model. We then compare how quantities such as the mass of a defect depend on b.

6.2. The Skyrme field

For the reasons stated in the last section, we want a matter field that is compatible with the topology of the spatial hypersurface. On the one hand, we want the matter field to have a sufficiently rich structure to give nontrivial effects. On the other hand, we want it to be simple enough so that the equations of motion do not become too complicated. The result of these considerations is that we take an $SO(3)$-valued scalar field Ω as our matter field

$$\Omega : \mathbb{R} \times M_{\mathrm{I}} \simeq \mathbb{R} \times SO(3) - \{\text{point}\} \to SO(3)\,. \tag{6.1}$$

This matter field is simple in the sense that it is a scalar field, and is rich because of its nontrivial internal group structure. We are only looking for static solutions

to Einstein's equations, and hence we take Ω to be time-independent. Furthermore, we make a hedgehog *Ansatz* for Ω

$$\Omega(\boldsymbol{x}) \equiv R_{\hat{x}}(F(r))\,. \tag{6.2}$$

In equation (6.2), $\boldsymbol{x}$ is a point of the spatial hypersurface M_{I} with coordinates (r, θ, ϕ), $r \geq b$. On the right hand side, $R_{\hat{n}}(\omega)$ denotes the usual rotation matrix in $\mathbb{R}^3$ around an axis specified by the unit vector $\hat{n}$ with a rotation angle ω. The name "hedgehog" for these kinds of field was introduced by [26] and refers to the property that the direction in space given by $\boldsymbol{x}$ is in the same direction $\hat{n}$ in the internal space. Finally, $F(r)$ is the profile function. It is this function which is to be determined by the field equations. A general rotation around $\hat{x}$ with angle ω is given by

$$R_{\hat{n}}(\omega) = \cos\omega\,\mathbb{1} + \sin\omega\,\hat{n}\cdot\boldsymbol{X} + (1-\cos\omega)\hat{n}\otimes\hat{n}\,, \tag{6.3}$$

where $\boldsymbol{X}$ stands for the three generators of SO(3) around the x-, y-, and z-axes

$$X_x = \begin{pmatrix} 0 & 0 & 0 \\ 0 & 0 & -1 \\ 0 & 1 & 0 \end{pmatrix},\; X_y = \begin{pmatrix} 0 & 0 & 1 \\ 0 & 0 & 0 \\ -1 & 0 & 0 \end{pmatrix},\; X_z = \begin{pmatrix} 0 & -1 & 0 \\ 1 & 0 & 0 \\ 0 & 0 & 0 \end{pmatrix}. \tag{6.4}$$

The hedgehog *Ansatz* equation (6.2) then reads explicitly

$$\Omega(\boldsymbol{x}) = \cos F(r)\,\mathbb{1} + \sin F(r)\,\hat{x}\cdot\boldsymbol{X} + [1-\cos F(r)]\hat{x}\otimes\hat{x}\,. \tag{6.5}$$

As mentioned in Section 5.2.3 on page 45, we parametrize an element of $SO(3)$ by three angles $(\vartheta, \alpha, \beta)$, with both ϑ and α ranging from 0 to π and $\beta \in [0, 2\pi]$. The pair (α, β) defines the axis of rotation and ϑ is the angle of rotation. Now using spherical polar coordinates (r, θ, ϕ) for the base space M_{I} and the hedgehog *Ansatz* for Ω we obtain

$$\vartheta(\boldsymbol{x}) = F(r)\,, \tag{6.6a}$$
$$\alpha(\boldsymbol{x}) = \theta\,, \tag{6.6b}$$
$$\beta(\boldsymbol{x}) = \phi\,. \tag{6.6c}$$

The first condition which the nontrivial topology of M_{I} demands of Ω is that it must be equal at identified points

$$\Omega(\boldsymbol{x}\big|_{r=b}) = \Omega(-\boldsymbol{x}\big|_{r=b})\,. \tag{6.7}$$

Since $\hat{n}(\boldsymbol{x}) = -\hat{n}(-\boldsymbol{x})$, a comparison with equation (6.3) shows that equation (6.7) requires

$$\sin F(b)\,\hat{n}(\boldsymbol{x})\cdot\boldsymbol{X} = \sin F(b)\,\hat{n}(-\boldsymbol{x})\cdot\boldsymbol{X} = -\sin F(b)\,\hat{n}(\boldsymbol{x})\cdot\boldsymbol{X}\,,$$

which can only be satisfied if

$$F(b) = n\,\pi,\; n \in \mathbb{Z}\,. \tag{6.8}$$

We show in Appendix A.1 that, with this boundary condition, the gradient $\nabla\Omega$ automatically satisfies the boundary conditions for a vector at the defect.

6.3. The Skyrme Lagrangian

We now introduce the Lagrangian L for our model. We include the Hilbert Lagrangian for the metric. Besides a kinetic term the Lagrangian for Ω is also supposed to include terms that are fourth order in the field derivatives. The first term is the usual Skyrme term [3, 4], while the additional second term is the kinetic term squared [27]. Thus the model Lagrangian takes the form

$$L \equiv \int_{M_\mathrm{I}} \mathcal{L}\, \mathrm{d}^3x \equiv \int_{M_\mathrm{I}} \left(\mathcal{L}_\mathrm{grav} + \mathcal{L}_\mathrm{kin} + \mathcal{L}_\mathrm{Skyrme} + \mathcal{L}_\mathrm{add}\right) \mathrm{d}^3x\,, \tag{6.9}$$

where the Hilbert-, kinetic-, and Skyrme Lagrange densities are given by

$$\mathcal{L}_\mathrm{grav} \equiv \frac{1}{16\pi G_N} R\sqrt{-g}\,, \tag{6.10a}$$

$$\mathcal{L}_\mathrm{kin} \equiv \frac{f^2}{4} \mathrm{Tr}\left(\omega_\mu\, \omega^\mu\right) \sqrt{-g}\,, \tag{6.10b}$$

$$\mathcal{L}_\mathrm{Skyrme} \equiv \frac{1}{16e^2} \mathrm{Tr}\left(\left[\omega_\mu, \omega_\nu\right] \left[\omega^\mu, \omega^\nu\right]\right) \sqrt{-g}\,, \tag{6.10c}$$

$$\mathcal{L}_\mathrm{add} \equiv \frac{\gamma}{48e^2} \left[\mathrm{Tr}(\omega_\mu\, \omega^\mu)\right]^2 \sqrt{-g}\,. \tag{6.10d}$$

Here, R denotes the Ricci curvature of the metric g with signature $(-,+,+,+)$ and G_N is Newton's constant. In units with $c = 1$, the quantities f^2 and $1/e^2$ have the dimensions of mass over length and mass times length respectively, while γ is dimensionless and assumed to be positive. The field $\omega_\mu \equiv \Omega^{-1}\partial_\mu\Omega$ takes values in the Lie-algebra $so(3)$. We use the following notational conventions. Lower case Greek letters denote spacetime coordinates while lower case Roman letters denote the coordinates of the spatial M_I. Capital Roman letters denote the internal $SO(3)$ or $so(3)$ coordinates and run from 1 to 3. For example, we write

$$\omega_\mu = \omega_\mu^L X_L\,,$$

for the Lie-algebra valued one-form ω_μ, with the basis vectors X_L of $so(3)$ defined in equation (6.4). While the spacetime indices are raised and lowered with the spacetime metric, the placement of the Lie-algebra indices solely follows notational convenience. Einstein's summation convention is understood for all kinds of repeated indices, unless stated otherwise.

Equation (6.10a) is the usual Hilbert Lagrange density of general relativity and the remaining three terms make up the matter Lagrangian for the scalar field. The first of these terms, equation (6.10b), gives the kinetic energy of Ω. Equation (6.10c) is originally due to Skyrme [3, 4]. Together, equations (6.10b) and (6.10c) constitute the Lagrangian of the so-called Skyrme model. Instead of our $SO(3)$-valued field Ω Skyrme's field is $SU(2)$-valued. The motivation to study this model comes from the fact that it has stable solutions that are characterized by a topological quantum number. These solutions, called Skyrmions, are interpreted as baryons and

small perturbations around these solutions correspond to mesons. The Skyrmion's topological quantum number is identified with the baryon number B. Witten has shown [28] that the $SU(2)$-Skyrme model can be regarded as a low energy effective field theory for quantum chromodynamics. Furthermore, the Skyrme model becomes exact in the limit where the number of colors becomes large. Today, quantized Skyrmions of higher topological quantum numbers are used as models for light nuclei [29]. When gravity is included in the model, that is the terms in Eqs. (6.10a)–(6.10c) comprise the action, one speaks of a gravitating Skyrme model. Solutions to this theory that also have a topological quantum number were found in [30] and are called gravitating Skyrmions. Due to the close relation between $SO(3)$ and $SU(2)$, on which we comment in depth in Chapter 7, we can reproduce all of the results of the $SU(2)$-Skyrme model. Finally, the additional fourth order term, equation (6.10d), was not present in the original work of Skyrme. In the form used here it is due to [27]. Its main effect is that it gives a *negative* contribution to the energy density (for $\gamma > 0$), as we will show in Section 6.4. We will ignore this term in the following chapters, that is we set $\gamma \equiv 0$, but will consider it later in Chapter 9, where we will also discuss the physical reason for its inclusion in the model.

Finiteness of the action requires finiteness of the Lagrangian in equation (6.9), which in turn implies that the matter field Ω must approach the constant $\mathbb{1}$ sufficiently fast. For the hedgehog *Ansatz* in equation (6.5) this means that the profile function must approach 0 as r approaches ∞. In summary, the nontrivial topology created by the defect and finiteness of the action demand the following two boundary conditions for the profile function of the hedgehog *Ansatz*

$$F(b) = n\,\pi,\ n \in \mathbb{Z}\,, \tag{6.11a}$$

$$F(\infty) = 0\,. \tag{6.11b}$$

The first important aspect of the boundary conditions in equations (6.11a) and (6.11b) is that they allow for a one-point compactification of M_{I}. As described in Chapter 5 this means that we amend M_{I} by a point $\{\infty\}$ where the profile function is supposed to take the value 0. Therefore, we have, at fixed times, that Ω is topologically a map

$$\Omega : SO(3) \to SO(3)\,. \tag{6.12}$$

It is argued in [31] that maps from $SO(3)$ to $SO(3)$ fall into distinct homotopy classes. The meaning of this is that maps from $SO(3)$ to $SO(3)$ that cannot be deformed into each other continuously belong to different classes. In this language the closed loops in $SO(3)$ considered in Chapter 5 are maps from the circle S^1 to $SO(3)$ and fall into two distinct classes. According to [31] the homotopy classes of maps from $SO(3)$ to $SO(3)$ are related to the homotopy classes from S^3 to $SO(3)$. It is well known [21] that the latter can be equipped with a group structure, called the homotopy group. One has [21]

$$\pi_3(SO(3)) \simeq \mathbb{Z}\,, \tag{6.13}$$

where $\pi_3(SO(3))$ denotes the homotopy group of maps from S^3 to $SO(3)$. The integer occurring in equation (6.13) is called the topological degree or winding number and counts, loosely speaking, how many times a given map "winds around" $SO(3)$. An important property of the winding number is that it is a topological invariant: if a map is deformed continuously its winding number does not change. In the $SU(2)$-Skyrme model one considers maps from S^3 to $SU(2) \simeq S^3$ and the homotopy group of these maps is also $\mathbb{Z}$. The winding number is then interpreted as the baryon number.

Instead of maps from S^3 to $SO(3)$ we consider a matter field Ω that is a map from $SO(3)$ to $SO(3)$. It is argued in [31] that the corresponding homotopy classes can also be categorized by an integer, and hence that the winding number is a topological invariant. We show in Appendix A.2 that the integer n occurring in the boundary condition equation (6.11a) is actually the winding number of Ω.

6.4. The field equations

The field equations for Ω in terms of the three coordinates θ^K are the Euler-Lagrange equations

$$\frac{\mathrm{d}}{\mathrm{d}x^\mu}\frac{\partial \mathcal{L}_\mathrm{M}}{\partial \partial_\mu \theta^K} - \frac{\partial \mathcal{L}_\mathrm{M}}{\partial \theta^K} = 0\,, \tag{6.14}$$

where the Lagrange density of matter $\mathcal{L}_\mathrm{M}$ is the sum of $\mathcal{L}_\mathrm{kin}$, $\mathcal{L}_\mathrm{Skyrme}$, and $\mathcal{L}_\mathrm{add}$. Writing

$$\omega_\mu = \Omega^{-1}\partial_\mu \Omega = \Omega^{-1}\frac{\partial \Omega}{\partial \theta^L}\frac{\partial \theta^L}{\partial x^\mu} \equiv \omega_L \partial_\mu \theta^L\,, \tag{6.15}$$

and using

$$\begin{aligned} -\frac{1}{2}\mathrm{Tr}(\omega_L\,\omega_M) &= H_{LM}\,, \\ -\frac{1}{2}\mathrm{Tr}\left([\omega_L,\omega_M][\omega_O,\omega_P]\right) &= H_{LO}H_{MP} - H_{LP}H_{MO}\,, \end{aligned}$$

where H_{LM} are the components of the metric of $SO(3)$, explicitly given by

$$H = \mathrm{d}\vartheta^2 + 4\sin^2(\vartheta/2)\,\mathrm{d}\alpha^2 + 4\sin^2(\vartheta/2)\sin^2\alpha\,\mathrm{d}\beta^2\,, \tag{6.16}$$

we obtain

$$\begin{aligned} \mathcal{L}_\mathrm{kin} &= -\frac{f^2}{2}H_{LM}\partial_\mu\theta^L\partial_\nu\theta^M g^{\mu\nu}\sqrt{g}\,, \\ \mathcal{L}_\mathrm{Skyrme} &= -\frac{1}{8e^2}\left(H_{LO}H_{MP} - H_{LP}H_{MO}\right)\partial_\mu\theta^L\partial_\nu\theta^M\partial_\kappa\theta^O\partial_\lambda\theta^P g^{\mu\kappa}g^{\nu\lambda}\sqrt{g}\,, \\ \mathcal{L}_\mathrm{add} &= \frac{\gamma}{12e^2}H_{LM}\partial_\mu\theta^L\partial_\nu\theta^M g^{\mu\nu}H_{OP}\partial_\kappa\theta^O\partial_\lambda\theta^P g^{\kappa\lambda}\sqrt{g}\,. \end{aligned}$$

The energy-momentum tensor $T_{\mu\nu}$ of the Skyrme field Ω is defined by

$$T_{\mu\nu} \equiv -2\frac{\partial L_\mathrm{mat}}{\partial g^{\mu\nu}} + g_{\mu\nu}L_\mathrm{mat}\,, \tag{6.17}$$

with $L_{\text{mat}} \equiv \mathcal{L}_{\text{mat}}/\sqrt{-g}$ and $\mathcal{L}_{\text{mat}} \equiv \mathcal{L}_{\text{kin}} + \mathcal{L}_{\text{Skyrme}} + \mathcal{L}_{\text{add}}$. Finally, the Euler-Lagrange equations are complemented by Einstein's field equations

$$R_{\mu\nu} - \frac{1}{2} g_{\mu\nu} R = 8\pi G_N \, T_{\mu\nu} \,,$$

where $R_{\mu\nu}$ and R denote the Ricci tensor and scalar of the metric g, respectively.

We now derive the Einstein-Skyrme field equations used in later chapters. The *Ansatz* for the static, spherically symmetric spacetime metric g in spherical polar coordinates (t, r, θ, ϕ) is

$$ds^2 = -\mathrm{e}^{2\nu(r)} \mathrm{d}\, t^2 + \mathrm{e}^{2\lambda(r)} \mathrm{d}\, r^2 + r^2 \mathrm{d}\theta^2 + r^2 \sin^2(\theta) \mathrm{d}\phi^2 \,, \tag{6.18}$$

with two functions $\nu(r)$ and $\lambda(r)$. From now on we work with the dimensionless radial coordinate

$$x \equiv f \, e \, r \,, \tag{6.19a}$$

$$x_{\text{def}} \equiv f \, e \, b \,. \tag{6.19b}$$

In the following we will suppress the x dependence of $\nu(x)$, $\lambda(x)$, and $F(x)$ and write a prime for $\mathrm{d}/\mathrm{d}\, x$. To obtain an asymptotically flat metric the functions ν and λ must satisfy

$$\nu(\infty) = 0 \,, \tag{6.20a}$$

$$\lambda(\infty) = 0 \,. \tag{6.20b}$$

Using the hedgehog *Ansatz* given in equation (6.5) for the matter field and equation (6.18) for the metric, Einstein's equations in the form $x^2 \, G^\mu_\nu = 8\pi G_N \, x^2 \, T^\mu_\nu$ become

$$\begin{aligned} \mathrm{e}^{-2\lambda} \left(1 + 2x\nu'\right) - 1 = 8\pi\,\eta \Bigg\{ & \frac{\mathrm{e}^{-2\lambda}}{2} \left[x^2 + 4\sin^2\left(F/2\right)\left(1 - 2\gamma/3\right)\right] F'^2 \\ & - 4\sin^2(F/2) \left[1 + \frac{\sin^2\left(\theta/2\right)}{x^2} \left(1 - 4\gamma/3\right)\right] \\ & - \frac{\gamma}{4} \mathrm{e}^{-4\lambda} x^2 F'^4 \Bigg\} \,, \end{aligned} \tag{6.21a}$$

$$2x\left(\nu' + \lambda'\right) = 8\pi\,\eta \left[\left(x^2 + 4\sin^2\left(F/2\right)\left(1 - 2\gamma/3\right)\right) F'^2 - \frac{\gamma}{3} \mathrm{e}^{-2\lambda} x^2 F'^4\right] \,, \tag{6.21b}$$

$$\begin{aligned} \mathrm{e}^{-2\lambda} x \left[(\nu' - \lambda')(1 + x\nu') + x\nu''\right] = 2\pi\eta \Bigg[& 16(1 - 4\gamma/3) \frac{\sin^4(F/2)}{x^2} \\ & - \mathrm{e}^{-2\lambda} x^2 F'^2 (2 - \gamma \mathrm{e}^{-2\lambda} F'^2/3) \Bigg] \,, \end{aligned} \tag{6.21c}$$

where the first, second, and third equations follow from the (t,t), (x,x), and (θ,θ) component of Einstein's equations, respectively. The dimensionless quantity η is defined by

$$\eta \equiv G_N f^2 \,, \tag{6.22}$$

and gives the relative strength between Newton's constant G_N and the Skyrme constant f. Due to the spherical symmetry, the (ϕ,ϕ)-component equals the (θ,θ)-component in equation (6.21c). To obtain the explicit form of the Euler-Lagrange equations for the three components (ϑ,α,β) from equation (6.14) with the spacetime metric g given in equation (6.18) and the internal metric H in equation (6.16) is tedious but straightforward. Inserting the hedgehog *Ansatz* in the result shows that the functions α and β given in equations (6.6b) and (6.6c) satisfy the Euler-Lagrange equations automatically. The only nontrivial equation is that for the profile function

$$\begin{aligned}
0 = &- \left[\left(1-\gamma \mathrm{e}^{-2\lambda} F'^2\right) x^2 + 4\sin^2(F/2)\,(1-2\gamma/3)\right] F'' \\
&- 2\sin F \left[\frac{1}{2}\,(1-2\gamma/3)\,F'^2 - \mathrm{e}^{2\lambda}\left(1+2\frac{\sin^2(F/2)}{x^2}\,(1-4\gamma/3)\right)\right] \\
&- \left[2x + \left(x^2 + 4\sin^2(F/2)\,(1-2\gamma/3)\right)(\nu'-\lambda')\right] F' \\
&+ \frac{\gamma}{3}\mathrm{e}^{-2\lambda}\left(2x + x^2\,(\nu'-3\lambda')\right) F'^3 \,.
\end{aligned} \tag{6.23}$$

Notice that ν' can be eliminated from equations (6.21b) and (6.23) by use of equation (6.21a). After doing this we obtain

$$\begin{aligned}
0 = &- \left[(1-\gamma \mathrm{e}^{-2\lambda} F'^2)x^2 + 4(1-2\gamma/3)\sin^2(F/2)\right] F'' \\
&+ 2\mathrm{e}^{2\lambda}\left[1+2(1-4\gamma/3)\frac{\sin^2(F/2)}{x^2}\right]\sin F \\
&+ \frac{F'}{x}\left(\left[4(1-2\gamma/3)\frac{\sin^2(F/2)}{x^2}-1\right]x^2 + x^2\mathrm{e}^{2\lambda}\left[1+4(1-2\gamma/3)\frac{\sin^2(F/2)}{x^2}\right]\right. \\
&\qquad \left.\times\left\{32\pi\eta\sin^2(F/2)\left[1+(1-4\gamma/3)\frac{\sin^2(F/2)}{x^2}\right]-1\right\}\right) \\
&- (1-2\gamma/3)\sin(F)F'^2 - \frac{2\pi\gamma\eta}{3}x^3\mathrm{e}^{-2\lambda}\left[1+4(1-2\gamma/3)\frac{\sin^2(F/2)}{x^2}\right]F'^5 \\
&- \frac{2\gamma}{3}x\left[32\pi\eta\sin^2(F/2)\left(1+(1-4\gamma/3)\frac{\sin^2(F/2)}{x^2}\right)-1\right]F'^3 \,,
\end{aligned} \tag{6.24a}$$

$$\begin{aligned}
2x\lambda' = &\,\mathrm{e}^{2\lambda}\left\{32\pi\,\eta\sin^2(F/2)\left[1+(1-4\gamma/3)\frac{\sin^2(F/2)}{x^2}\right]-1\right\} - \frac{2\pi\,\eta\,\gamma}{3}\mathrm{e}^{-2\lambda}x^2F'^4 \\
&+1+4\pi\,\eta x^2\left[1+4(1-2\gamma/3)\frac{\sin^2(F/2)}{x^2}\right]F'^2 \,,
\end{aligned} \tag{6.24b}$$

$$2x\nu' = \mathrm{e}^{2\lambda} - 1 + 8\pi\eta\left(\frac{x^2}{2}\left[1 - \frac{\gamma}{2}\mathrm{e}^{-2\lambda}F'^2\right]F'^2 + 2\sin^2(F/2)\right.$$
$$\left.\times\left\{(1-2\gamma/3)F'^2 - 2\mathrm{e}^{2\lambda}\left[1 + (1-4\gamma/3)\frac{\sin^2(F/2)}{x^2}\right]\right\}\right). \tag{6.25}$$

Equations (6.24) and (6.25) are the Einstein-Skyrme equations that we want to solve subject to the boundary conditions in equations (6.11) and (6.20) and which we repeat here in dimensionless units for completeness

$$\begin{aligned} F(x_{\mathrm{def}}) &= n\,\pi, \quad F(\infty) = 0\,, \\ \nu(\infty) &= 0, \qquad \lambda(\infty) = 0\,, \end{aligned}$$

where x_{def} is defined in equation (6.19b) and $n \in \mathbb{Z}$ is the winding number of the Skyrme field (see discussion on page 51).

Before we solve these field equations, we mention some of their properties. First, notice that the equations for the metric components (equations (6.24b) and (6.25)) are first order equations, while the equation for the profile function(equation (6.24a)) is of second order. Differentiating equation (6.25) with respect to x and inserting the result together with equations (6.24) and (6.25) into equation (6.21c) we find that it is satisfied identically. Therefore, it suffices to consider the first order equations for the metric.

A second property of equations (6.24) and (6.25) is the asymptotic behavior of the metric and the profile function. To obtain this behavior we rewrite the equations in terms of $\xi \equiv 1/x$ and expand around $\xi = 0$. The result of this straightforward but tedious calculation is

$$F_{\mathrm{asympt}}(x) = \frac{F_\infty}{x^2} + \mathcal{O}\left(\frac{1}{x^3}\right), \tag{6.26a}$$

$$\lambda_{\mathrm{asympt}}(x) = \frac{\lambda_\infty}{x} + \mathcal{O}\left(\frac{1}{x^2}\right), \tag{6.26b}$$

$$\nu_{\mathrm{asympt}}(x) = -\lambda_{\mathrm{asympt}}(x)\,. \tag{6.26c}$$

Here, F_∞ and λ_∞ are constants. The result of equation (6.26c) enables us to use the following strategy in solving the ordinary differential equations (ODEs) in equations (6.24) and (6.25). First, we try to solve equations (6.24a) and (6.24b) numerically from x_{def} to some $x_{\max}$. Provided we have a solution for F and λ we use equation (6.26c) to obtain the value of ν at $x_{\max}$ which serves as our initial condition for equation (6.25).

We conclude this section by giving the explicit expression for the energy density. With the Lagrangian given by equation (6.9) we evaluate equation (6.17) using the hedgehog *Ansatz* (equation (6.6)) for the matter field and the *Ansatz* in equation (6.18) for the metric. The energy density of the matter field is then given by

the T_{00} component and reads

$$\begin{aligned} T_{00}\frac{1}{e^2\, f^4} =& 4\mathrm{e}^{2\nu}\frac{\sin^2(F/2)}{x^2}\left[1+(1-4\gamma/3)\frac{\sin^2(F/2)}{x^2}\right] \\ &+\frac{1}{2}\mathrm{e}^{2(\nu-\lambda)}\left[1+4(1-2\gamma/3)\frac{\sin^2(F/2)}{x^2}\right]F'^2-\frac{\gamma}{12}\mathrm{e}^{2(\nu-2\lambda)}F'^4\,, \end{aligned} \tag{6.27}$$

where $e^2\, f^4$ has units of mass per length cubed. Terms proportional to γ originate from the additional Lagrangian L_{add} in equation (6.9). As can be seen from equation (6.27) these terms always lower the energy density. Without them the energy density is strictly positive.

7. Nongravitating $SO(3)$-Skyrmions

Before we consider gravity, we first investigate solutions to the Skyrme model on a fixed background. First, we take (an almost) flat background metric and, then, one with constant curvature. In the latter case the field equations can be solved analytically. Throughout this section we relate our findings to known results of the $SU(2)$-Skyrme model. Furthermore, we only consider the kinetic- and Skyrme-term in this chapter that is, the Lagrangian is given by

$$L \equiv \int_{M_\mathrm{I}} \mathcal{L}\, \mathrm{d}^3x \equiv \int_{M_\mathrm{I}} (\mathcal{L}_\mathrm{kin} + \mathcal{L}_\mathrm{Skyrme})\, \mathrm{d}^3x\,. \tag{7.1}$$

It can be obtained from equation (6.9) by setting $\gamma \equiv 0$ and ignoring the Hilbert-Lagrangian $\mathcal{L}_\mathrm{grav}$.

7.1. Flat background metric

In this section we equip the M_I spacetime with the usual Minkowski metric. As mentioned in Section 5.2.3, this metric is flat almost everywhere - that is, its Ricci scalar is a δ-function centered at the defect. Despite this shortcoming we consider the Minkowski background metric as a "benchmark" scenario. It will be shown later in this section that our $SO(3)$-Skyrme model reduces to the usual $SU(2)$-Skyrme model in the appropriate limit. The latter model does have solutions on Minkowski spacetime.

We work in the usual spherical polar coordinates (t, r, θ, ϕ) for Minkowski spacetime, and the metric takes the form

$$ds^2 = -\mathrm{d}\,t^2 + \mathrm{d}\,r^2 + r^2\mathrm{d}\theta^2 + r^2\,\sin^2(\theta)\mathrm{d}\phi^2\,. \tag{7.2}$$

Compared to the *Ansatz* in equation (6.18) we now have

$$\nu(r) \equiv 0\,, \tag{7.3a}$$
$$\lambda(r) \equiv 0\,. \tag{7.3b}$$

For the $SO(3)$-valued matter field Ω we keep using the hedgehog *Ansatz* given in equation (6.5) on page 48, which we repeat here for completeness

$$\Omega(\boldsymbol{x}) = \cos F(r)\,\mathbb{1} + \sin F(r)\,\hat{x}\cdot\boldsymbol{X} + (1-\cos F(r))\hat{x}\otimes\hat{x}\,.$$

In terms of the coordinates $(\vartheta, \alpha, \beta)$ for $SO(3)$ the hedgehog *Ansatz* reads

$$\begin{aligned}\vartheta(\boldsymbol{x}) &= F(r)\,,\\ \alpha(\boldsymbol{x}) &= \theta\,,\\ \beta(\boldsymbol{x}) &= \phi\,.\end{aligned}$$

As mentioned in Section 6.4, these *Ansätze* for α and β automatically satisfy the Euler-Lagrange equations for generic metric functions ν and λ. This result, therefore, holds true for the situation considered here, with both ν and λ vanishing. The only field equation not already satisfied is the one for the profile function F, which reads

$$\left(x^2 + 4\sin^2(F/2)\right) F'' + 2x\,F' + 2\sin F\left(\frac{1}{2}F'^2 - 1 - 2\frac{\sin^2(F/2)}{x^2}\right) = 0\,. \tag{7.4}$$

Recall that we are using the dimensionless quantity $x \equiv f\,e\,r$. Notice that equation (7.4) is just equation (6.24a) without gravity ($G_N \equiv 0$ leading to $\eta \equiv 0$), γ set to 0, and using equation (7.3). The boundary conditions for F in this flat metric scenario are the same as the ones in curved spacetime, because Ω must still respect the nontrivial topology of M_I and should have a finite energy. Again, for completeness, we repeat the boundary conditions here

$$F(x_\mathrm{def}) = n\,\pi,\ n \in \mathbb{Z}\,, \tag{7.5a}$$

$$F(\infty) = 0\,, \tag{7.5b}$$

where $x_\mathrm{def} \equiv f\,e\,b$, and the integer n is the winding number of Ω. Our task is to solve equation (7.4) for various values of the parameter x_def, subject to the boundary conditions in equation (7.5).

Before we do this, however, we give the energy density of Ω. Using the simplifications mentioned above, the energy density, equation (6.27), turns into

$$T_{00}\frac{1}{e^2\,f^4} = \frac{1}{2}F'^2 + 4\frac{\sin^2(F/2)}{x^2}\left[\frac{1}{2}F'^2 + 1 + \frac{\sin^2(F/2)}{x^2}\right]. \tag{7.6}$$

The total field energy E is thus given by

$$E(x_\mathrm{def})\frac{e}{f} = \int_{M_\mathrm{I}} T_{00}\,\mathrm{d}^3x = 4\pi\int_{x_\mathrm{def}}^{\infty}\frac{1}{2}F'^2 + 4\frac{\sin^2(F/2)}{x^2}\left[\frac{1}{2}F'^2 + 1 + \frac{\sin^2(F/2)}{x^2}\right]\mathrm{d}x. \tag{7.7}$$

Notice that the energy depends on the defect parameter x_def through the lower limit of integration. An important property of the energy, as given in equation (7.7), is that it can be rewritten in terms of the winding number n. To see this, we complete the square in equation (7.7) and obtain, after some algebra,

$$\begin{aligned}E(x_\mathrm{def})\frac{e}{4\pi\,f} = \int_{x_\mathrm{def}}^{\infty} x^2\left(\frac{F'}{\sqrt{2}} + 2\frac{\sin(F/2)^2}{x^2}\right)^2 + 2\sin(F/2)^2(F' + \sqrt{2})^2\\ - 3\sqrt{2}\pi\left(\frac{2}{\pi}\sin^2(F/2)F'\right)\mathrm{d}x\,.\end{aligned}$$

Comparing with equation (A.6) on page 139, we see that the integral over the last term is just a multiple of the winding number n of the field. Therefore, we obtain the following relation between the field energy and the winding number

$$E(x_{\text{def}})\frac{e}{4\pi f} = 3\sqrt{2}\,\pi\, n + \int_{x_{\text{def}}}^{\infty} x^2 \left(\frac{F'}{\sqrt{2}} + 2\frac{\sin(F/2)^2}{x^2}\right)^2 + 2\sin(F/2)^2(F'+\sqrt{2})^2 \mathrm{d}x\,. \tag{7.8}$$

Since the integrand in equation (7.8) is a sum of two squares, its contribution to the energy is always positive. Thus, within a topological sector, where all field configurations have the same winding number n, the energy is bounded from below by

$$E_{\text{Bogo}} \equiv 12\sqrt{2}\,\pi^2\, nf/e \leq E(x_{\text{def}}). \tag{7.9}$$

A similar bound, with n replaced in equation (7.9) by $-n$, holds when $n < 0$. This topological bound on the energy is named after Bogomolnyi, who discovered that topological solitons in many theories have energies bounded by the topological degree [32]. The Bogomolnyi bound can be achieved iff both squares in equation (7.8) vanish identically, and this condition leads to the following two *first* order equations for F

$$F' = -\sqrt{2}\,, \tag{7.10a}$$

$$F' = -\sqrt{8}\frac{\sin(F/2)^2}{x^2}\,. \tag{7.10b}$$

Since the first equation requires F' to be constant while the second demands F' to vary, we see that they cannot both be satisfied. Indeed, we will see later that the energy exceeds the Bogomolnyi bound by at least 23%.

7.1.1. Solutions with even winding number

Instead of starting with the investigation of Skyrme fields with winding number 1, we will first investigate fields that have an even winding number. As we will see, such fields correspond to the well studied $SU(2)$-Skyrme fields, and we reproduce various results known in the literature.

Specifically, we will take the winding number to equal 2, and equation (7.5a) reads

$$F(x_{\text{def}}) = 2\pi\,.$$

Unfortunately, an analytic solution to equation (7.4) is not known, and we have to revert to numerical methods. Since the problem is a boundary value problem, we use the so-called shooting method. With this method, one starts at one end of the interval (here x_{def}), where the function satisfies the boundary condition (here $F(x_{\text{def}}) = n\pi$, with $n = 2$). Then one "guesses" the remaining unknown derivative (here $F'(x_{\text{def}})$), and "shoots" by evolving the ODEs (here just one) to the other boundary. Usually, the numerical solution obtained in this way will not satisfy the boundary conditions at the second end point. One then goes back and adjusts

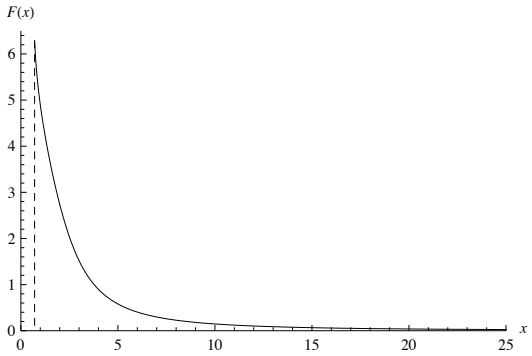

Figure 7.1.: The profile function $F(x)$ for $n = 2$ and $x_{\text{def}} = 1/\sqrt{2}$ (indicated by the dashed line).

the unknown derivative at the starting point (here $F'(x_{\text{def}})$) until the numerical solution satisfies all boundary conditions. Since our second end point is ∞, an exact implementation of the shooting algorithm is not possible. To obtain numerical solutions with high accuracy in this case one would have to substitute $x \to \xi \equiv 1/x$ and start from $\xi = 0$. Finally, one shoots from both x_{def} and $\xi = 0$ to some intermediate point until one obtains a smooth function there. Here, we follow a slightly less accurate, but much easier, method. Namely, we start at x_{def} and, after "guessing" a value for $F'(x_{\text{def}})$, solve the ODEs to some maximal x_{max}. We end the shooting if the profile function is sufficiently small at x_{max} and physical quantities, such as the energy, do not change under variation of x_{max}. When comparable results exist in the literature, we are always in agreement, within numerical uncertainty.

Figure 7.1 shows the profile function $F(x)$ for the particular value $x_{\text{def}} = 1/\sqrt{2}$. More interesting than the profile function is the dependence of the field energy on x_{def}. Figure 7.2 depicts the ratio of the field energy and the topological lower bound as a function of x_{def}. The energy always exceeds its lower bound by at least 23%. This is in agreement with the discussion following equations (7.10a) and (7.10b), where we showed that the lower bound cannot be achieved. As x_{def} approaches zero, the energy remains finite and is larger than E_{Bogo} by approximately 23%.

It is not a coincidence that the $SU(2)$-Skyrme model also has a hedgehog solution with winding number 1 that exceeds the Bogomolnyi bound by 23%. The reason for this is that, in the situation considered here, Ω is a map with winding number 2, and, hence, covers $SO(3)$ twice. But a map that covers $SO(3)$ *twice* is equivalent to a map that covers $SU(2)$ *once*, because $SU(2)$ is the double cover of $SO(3)$ [21]. Therefore, our $SO(3)$-Skyrmion with $n = 2$ is equivalent to an $SU(2)$-Skyrmion with $B = 1$. Explicitly, we have

$$\Omega(\boldsymbol{x}) = R_{\hat{x}}(F(r)) \backsimeq U(\boldsymbol{x}) \equiv \mathrm{e}^{\mathrm{i}\chi(r)\hat{x}\cdot\boldsymbol{\sigma}}\,,$$

where $\boldsymbol{\sigma}$ denotes the three Pauli matrices, and $\chi(r) = F(r)/2$. Indeed, we can recover the field equations of the $SU(2)$-Skyrme model as follows. To compare

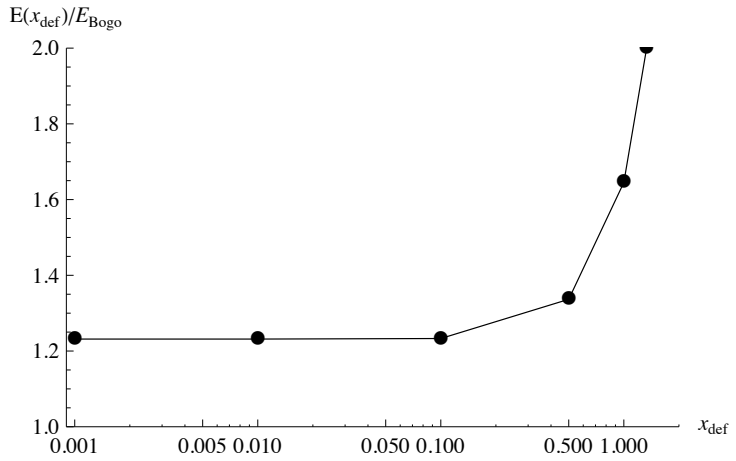

Figure 7.2.: Ratio of the field energy $E(x_{\rm def})$ and the Bogomolnyi bound $E_{\rm Bogo}$ as a function of the defect parameter $x_{\rm def} = e\,f\,b$ with winding number $n = 2$. Here, $E_{\rm Bogo}$ is the lower bound on the energy, see equation (7.8). The ratio increases as $x_{\rm def}$ increases, but approaches the finite value ~ 1.23 in the limit of vanishing $x_{\rm def}$.

our equations with those of the $SU(2)$-Skyrme model, as given in [20], we have to substitute

$$F \to 2\chi\,, \tag{7.11}$$

and rescale the dimensional quantities f and e as

$$f \to f/2\,, \tag{7.12a}$$

$$e \to \sqrt{8}g\,. \tag{7.12b}$$

From equation (7.11) we see that our boundary condition, $F(0) = 2\pi$, transforms into $\chi(0) = \pi$, which is the correct boundary condition for $U(\boldsymbol{x})$ at the origin. Finally, to compare our dimensionless radius, $x = f\,e\,r$, to the one used by [20], $\tilde{x} \equiv f\,g\,r$, we use equation (7.12) and obtain

$$x \to \sqrt{2}\tilde{x}\,.$$

When expressed in these rescaled quantities, our field equation, equation (7.4), becomes

$$(\tilde{x}^2 + 2\sin^2\chi)\chi'' + 2\tilde{x}\chi' + \sin(2\chi)\left[\chi'^2 - 1 - \frac{\sin^2\chi}{\tilde{x}^2}\right] = 0\,,$$

which equals equation (9.21) in [20] (our $\chi(\tilde{x})$ corresponds to their $f(r)$). In the limit of vanishing defect parameter our energy, $E(0) \sim 1.23E_{\rm Bogo}$, agrees with the energy obtained in [30], once equation (7.9) is used for $E_{\rm Bogo}$ and our parameters are rescaled according to equation (7.12). Explicitly, we find that the limiting energy $E(0) = 1.23 \times E_{\rm Bogo} = 1.23 \times 12\sqrt{2}\pi^2 \times 2 \approx 412 f/e$ has the value ≈ 72.8 when the rescaled units of equation (7.12) are used. This value can also be read from figure (1) in [30].

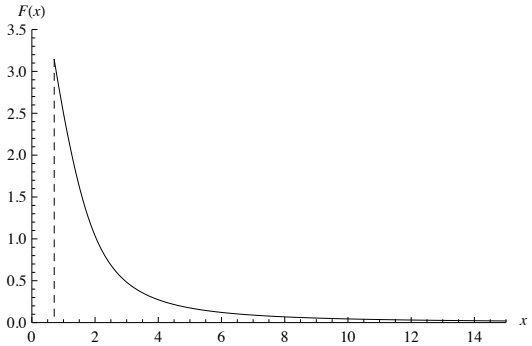

Figure 7.3.: The profile function $F(x)$ for $n = 1$ and $x_{\text{def}} = 1/\sqrt{2}$ (indicated by the dashed line).

We now comment on finiteness of the energy in the limit $x_{\text{def}} \to 0$. With $F(x_{\text{def}}) = 2\pi$ at the defect, the field Ω reads

$$\Omega(\boldsymbol{x}_{\text{def}}) = R_{\hat{x}}(2\pi) = \mathbb{1}\,.$$

Since Ω is just a constant at the defect, it is well defined even when $x_{\text{def}} = 0$. As a result, the field energy remains finite for vanishing defect parameter.

7.1.2. Solutions with odd winding number

Although the method to obtain numerical solutions to the field equation, equation (7.4), when n is odd, is the same as discussed in the last subsection, the properties of the solution are quite different.

Here, we concentrate on $n = 1$, and our boundary condition at the defect is given by

$$F(x_{\text{def}}) = \pi\,.$$

Numerically solving equation (7.4), subject to this boundary condition, yields profile functions such as the one shown in figure 7.3 for $x_{\text{def}} = 1/\sqrt{2}$. A comparison with the profile function for the case $n = 2$ in figure 7.1 does not show qualitative differences.

This changes when we consider the energy. Figure 7.4 shows the ratio of the field energy and the Bogomolnyi bound E_{Bogo} for $n = 1$. The energy exceeds E_{Bogo} for all x_{def} by at least 22%, and the minimal energy is reached when $x_{\text{def}} \approx 1/\sqrt{2}$. Since E_{Bogo} is linear in n, this minimal energy equals half of the energy of the solution with $n = 2$. For $x_{\text{def}} > 1/\sqrt{2}$ the energy grows linearly, whereas it diverges like $1/x_{\text{def}}$ when x_{def} approaches zero. This contrasts with the case when $n = 2$, where the ratio does not diverge as $x_{\text{def}} \to 0$, but approaches 1.23 instead. The reason for this dependence on the winding number can be understood as follows.

For n odd, Ω reads, at the defect,

$$\Omega(\boldsymbol{x}_{\text{def}}) = R_{\hat{x}}(\pi) = -\mathbb{1} + 2\hat{x} \otimes \hat{x}\,. \tag{7.13}$$

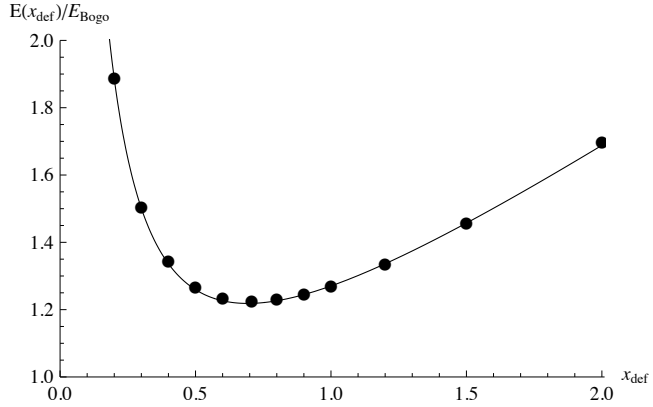

Figure 7.4.: Ratio of the field energy $E(x_{\mathrm{def}})$ and the Bogomolnyi bound E_{Bogo} as a function of $x_{\mathrm{def}} \equiv f\,e\,b$ for $n = 1$. The minimum occurs at $x_{\mathrm{def}} \approx 1/\sqrt{2}$, where the energy exceeds the Bogomolnyi bound by approximately 22%. The curve $a/\mathrm{x}_{\mathrm{def}} + b\,\mathrm{x}_{\mathrm{def}} + c$ is fitted to the points with $a \approx 0.264$, $b \approx 0.55$, and $c \approx 0.457$.

The field now contains a term proportional to $\hat{n} \otimes \hat{n}$, which is not well-defined at the origin and is not present for even n. On the usual Euclidean space, where the origin is not removed, this property would disqualify Ω from being a smooth field everywhere, and we would be forced to consider fields with even winding number only. Here, however, the origin is removed and antipodal points at $r = b$ are identified, leading to the requirement that Ω must satisfy $\Omega(\boldsymbol{x}) = \Omega(-\boldsymbol{x})$ there. As can be seen from equation (7.13), the $SO(3)$-valued field Ω can satisfy this without being a constant, and this distinguishes it from an $SU(2)$-valued field. It is this richer structure, together with the Skyrme term in equation (7.1), that causes the $1/x_{\mathrm{def}}$-dependence of the energy.

To conclude, we can see that the field energy has a minimum at a finite defect parameter $x_{\mathrm{def}} \sim 1/\sqrt{2}$ if the winding number of Ω is odd. When Ω has an even winding number, it is equivalent to an $SU(2)$-Skyrme field, and as such has a finite energy even when $x_{\mathrm{def}} \to 0$. In the following chapter, these results will be seen to carry over to the gravitating case as well.

7.2. Background metric with constant curvature

Since the flat background metric has a singular Ricci scalar, in this section we consider a metric for M_{I} that is free of any singularity. As shown in Section 5.2.3, a metric with constant curvature is such a metric. Since M_{I} is $SO(3)$ topologically we will use the metric of $SO(3)$ as the metric for M_{I}. Besides being singularity free, this metric has constant curvature.

It turns out to be convenient to work with the coordinate

$$\xi(r) \equiv \frac{\pi b^2}{r}\,.$$

Notice that because $r \in [b, \infty)$ we have $\xi \in (0, \pi b]$. So, in the coordinates (ξ, θ, ϕ) the space M_{I} is seen to be a ball of radius πb with antipodal boundary points identified. The metric of $SO(3)$, given in equation (6.16), then reads in these coordinates

$$ds^2 = \mathrm{d}\xi^2 + 4b^2 \sin^2(\xi/2b) \left[\mathrm{d}\theta^2 + \sin^2\theta \, \mathrm{d}\phi^2\right] .$$

Taking it as the spatial metric, we use the following for the spacetime metric

$$ds^2 = -\mathrm{d}t^2 + \mathrm{d}\xi^2 + 4b^2 \sin^2(\xi/2b) \left[\mathrm{d}\theta^2 + \sin^2\theta \, \mathrm{d}\phi^2\right] . \tag{7.14}$$

We introduce dimensionless coordinates as

$$\varrho \equiv e f \, \xi$$

with $\varrho_{\mathrm{def}} \equiv e f \, b$, so that ϱ is in the range $(0, \pi \varrho_{\mathrm{def}}]$. Again, after making a hedgehog *Ansatz*

$$\begin{aligned} \vartheta(\boldsymbol{x}) &= F(\varrho) \,, \\ \alpha(\boldsymbol{x}) &= \theta \,, \\ \beta(\boldsymbol{x}) &= \phi \,, \end{aligned}$$

we find that the only Euler-Lagrange equation not already satisfied is the one for the profile function, which reads

$$\begin{aligned} 4\varrho_{\mathrm{def}}^2 \left[\varrho_{\mathrm{def}}^2 \sin^2(\varrho/2\varrho_{\mathrm{def}}) + \sin^2(F/2)\right] F'' = {} & \frac{\left[2\varrho_{\mathrm{def}}^2 \sin^2(\varrho/2\varrho_{\mathrm{def}}) + \sin^2(F/2)\right] \sin F}{\sin^2(\varrho/2\varrho_{\mathrm{def}})} \\ & - \varrho_{\mathrm{def}}^2 \left[2\varrho_{\mathrm{def}} \sin(\varrho/\varrho_{\mathrm{def}}) + F' \sin F\right] F' . \end{aligned} \tag{7.15}$$

The boundary conditions for a field with winding number $n = 1$ are

$$F(\pi \varrho_{\mathrm{def}}) = \pi \,, \tag{7.16a}$$

$$F(0) = 0 \,. \tag{7.16b}$$

A solution of equation (7.15) that satisfies these boundary conditions is

$$F(\varrho) = \varrho/\varrho_{\mathrm{def}} \,. \tag{7.17}$$

Notice that with this profile function the field Ω becomes the identity map between $M_{\mathrm{I}} \simeq SO(3)$ and the target $SO(3)$. The energy of the field, in terms of the Bogomolnyi bound $12\sqrt{2}\pi^2$, turns out to be

$$\begin{aligned} E(\varrho_{\mathrm{def}}) \frac{e}{f} = 12\sqrt{2}\pi^2 + 4\pi \int_0^{\pi\varrho_{\mathrm{def}}} & 2\sin^2(F/2) \left[F' - \sqrt{2}\right]^2 \\ & + \varrho_{\mathrm{def}}^2 \sin^2(\varrho/2\varrho_{\mathrm{def}}) \left[\sqrt{2}F' - \frac{\sin^2(F/2)}{\varrho_{\mathrm{def}}^2 \sin^2(\varrho/2\varrho_{\mathrm{def}})}\right]^2 \mathrm{d}\varrho \,, \end{aligned} \tag{7.18}$$

and inserting the solution equation (7.17) yields

$$E(\varrho_{\text{def}})\frac{e}{f} = 6\pi^2\left(\frac{1}{\varrho_{\text{def}}} + 2\varrho_{\text{def}}\right) .$$

The minimum energy is thus seen to occur at $\varrho_{\text{def}} = 1/\sqrt{2}$ and is, in fact, the Bogomolnyi bound. So, unlike for the flat background metric used in the last section, the Bogomolnyi bound can be achieved.

From the analytic point of view, this can be seen by looking at the two first order ODEs arising from minimizing equation (7.18)

$$F' = \sqrt{2}\,, \tag{7.19a}$$

$$\sqrt{2}F' = \frac{\sin^2(F/2)}{\varrho_{\text{def}}^2 \sin^2(\varrho/2\varrho_{\text{def}})}\,. \tag{7.19b}$$

As in equation (7.10a) on page 59, we see from the first equation that F must be a linear function of ϱ.[1] Due to the $\sin^2$-term in the denominator of equation (7.19b), instead of the x^2 in equation (7.10b), the ϱ-dependent numerator and denominator cancel, provided F is of the form $\varrho/\varrho_{\text{def}}$. As a result, the right hand side of equation (7.19b) is now a constant. Finally, equation (7.19b) is compatible with equation (7.19a) iff $\varrho_{\text{def}} = 1/\sqrt{2}$. Ultimately, the x^2- or $\sin^2$-denominator trace back to the use of the flat or curved background metric, equation (7.2) or equation (7.14), respectively.

There is also a geometric reason why the Bogomolnyi bound can be achieved for the curved metric in equation (7.14), but not for the flat one in equation (7.2). We argued in the last chapter that our boundary conditions allow a point ∞ to be adjoined to M_{I}. As a result, M_{I} becomes compact and *topologically* equivalent to $SO(3)$. Whether it is also *isometric* to $SO(3)$ depends, of course, on what metric we prescribe on M_{I}. Since Ω is a map from M_{I} to $SO(3)$ we can use it to pull back the metric on $SO(3)$ to M_{I}. Now, it was shown in [33] that the energy of a Skyrme field is a measure of how well it preserves the metric. The Bogomolnyi bound can only be obtained if the Skyrme field is an isometry – that is, if it preserves lengths and angles. Since $SO(3)$ is a space of constant curvature, Ω cannot be an isometry if we equip M_{I} with a flat background metric. Hence, the Bogomolnyi bound can never be achieved. But when the metric equation (7.14) is used on M_{I}, the Skyrme field can be an isometry. In the units used here, this happens when $\varrho_{\text{def}} = 1/\sqrt{2}$.

7.3. Summary

In this chapter, we investigated the $SO(3)$-Skyrme model on M_{I} for two fixed background metrics. The first of these two metrics was taken to be the (almost) flat

[1] The sign in equation (7.10a) is opposite to the one in equation (7.19a), because, here, F *increases* from 0 to $\pi\varrho_{\text{def}}$ for increasing ϱ.

Minkowski metric. We then solved the resulting Euler-Lagrange equations numerically. It turned out that we recovered the well studied $SU(2)$-Skyrme model when the winding number of the Skyrme field was even. For this reason, the field energy remained finite even in the limit of vanishing defect parameter. However, when the winding number is odd, we found that a finite defect parameter exists, for which the energy is minimized. In either case, the energy always exceeds its topological lower bound.

When M_{I} is equipped with the natural metric of $SO(3)$ the resulting Euler-Lagrange equation was solved analytically. Again, the energy had a minimal value for a finite defect parameter. Unlike the previous case, this minimal value equaled the topological lower bound. The geometric reason for this is that the Skyrme field is an isometry in this special case.

We will study the gravitating Skyrme model in the next chapter, and will see that the qualitative features of the solutions are the same as in this chapter.

8. Gravitating $SO(3)$-Skyrmions

We now consider gravitating $SO(3)$-Skyrmions. Throughout this chapter we will work with the Lagrangian

$$L \equiv \int_{M_{\mathrm{I}}} \mathcal{L}\, \mathrm{d}^3x \equiv \int_{M_{\mathrm{I}}} \left(\mathcal{L}_{\mathrm{grav}} + \mathcal{L}_{\mathrm{kin}} + \mathcal{L}_{\mathrm{Skyrme}}\right)\, \mathrm{d}^3x\,. \tag{8.1}$$

The *Ansatz* for the metric is

$$ds^2 = -\mathrm{e}^{2\nu(r)}\mathrm{d}\,t^2 + \mathrm{e}^{2\lambda(r)}\mathrm{d}\,r^2 + r^2\mathrm{d}\theta^2 + r^2\,\sin^2(\theta)\mathrm{d}\phi^2\,, \tag{8.2}$$

and we make a hedgehog *Ansatz* for the $SO(3)$-valued scalar field Ω, with the profile function $F(r)$ to be determined from the field equations. Hence, the field equations for the metric and the Skyrme field are the ones given in Eqs.(6.24)–(6.25), still with $\gamma \equiv 0$. Before we present our numerical results in Sections 8.3.1 and 8.3.2, we comment on different ways to obtain the mass of the curved spacetime. The first method "weighs" the spacetime by looking at the orbits of massive test particles and applying Kepler's third law. This method is used, in fact, by astronomers to measure a mass of a black hole. By observing the orbits of stars close to the center of the Milky Way, they inferred the central mass to be about 4.3 million solar masses [34]. The second method uses Komar's definition for the mass [35]. It is useful for us, since it allows for a decomposition into three different components: the energy density, the gravitational energy density, and what we call the defect mass. We interpret the latter contribution as the energy needed to create the type I defect. The two methods yield the same mass.

As for the nongravitating case, we find that the mass of an $SO(3)$-Skyrmion with even winding number approaches a finite value for vanishing defect parameter. In this limit the mass equals that of the gravitating $SU(2)$-Skyrmion. For $SO(3)$-Skyrmions with odd winding number, the mass has a minimal value for a finite defect parameter. Unlike the flat case, the mass does not diverge for vanishing defect parameter. Instead, an event horizon begins to form, once the defect parameter drops below a critical value.

8.1. Defect mass via Kepler's 3rd law

In this section we "weigh" the defect by considering a massive test particle on a stable circular orbit far away from the defect. An observer at r_0 sends out a test particle on a stable circular orbit, and then measures the time T at which the particle

returns. The mass contained within the radius r_0, causing the particle to move on a circular path, can then be calculated via Kepler's 3rd law as

$$M_{\text{Kepler}}(r_0)\, G_N \equiv \left(\frac{2\pi}{T}\right)^2 r_0^3\,, \tag{8.3}$$

where the major half axis is r_0 in this case. We now express M_{Kepler} in terms of the metric by solving the geodesic equation for the test particle.

The four-velocity of the particle reads

$$(u^\mu) \equiv (\dot{t}, \dot{r}, \dot{\theta}, \dot{\phi}) \equiv dx^\mu/d\tau\,,$$

and is normalized to -1, i.e. $u_\mu u^\mu = -1$. Here, τ is the proper time. In the following, we assume that the particle is in the equatorial plane, where $\theta = \pi/2$. The geodesic equation $\nabla_u u = 0$ then reads explicitly

$$\ddot{t} = -2\dot{t}\dot{r}^2\nu'\,, \tag{8.4a}$$
$$\ddot{x} = -\dot{r}^2\lambda' - \mathrm{e}^{-2(\lambda-\nu)}\dot{t}^2\nu' + \mathrm{e}^{-2\lambda} r\dot{\phi}^2\,, \tag{8.4b}$$
$$\ddot{\phi} = -2\dot{\phi}\frac{\dot{r}}{r}\,, \tag{8.4c}$$

where a prime denotes $\mathrm{d}/\mathrm{d}x$. The spacetime described by the metric in equation (8.2) admits a time-like Killing field $(\xi^\mu) = (1,0,0,0)$, and a space-like Killing field $(\psi^\mu) = (0,0,0,1)$. Therefore, the following two quantities are conserved on the particle's geodesic

$$E \equiv -g_{\mu\nu}\xi^\mu u^\nu = \mathrm{e}^{2\nu}\dot{t}\,, \tag{8.5a}$$
$$L \equiv g_{\mu\nu}\psi^\mu u^\nu = r^2\dot{\sigma}\,. \tag{8.5b}$$

Here, E is the particle's energy, in units of its rest mass, as seen by a static observer – that is, an observer whose four-velocity equals $(\xi^\mu) = (1,0,0,0)$ and who is at rest at infinity. In a similar way, the quantity L can be interpreted as the particle's angular momentum divided by its rest mass.

For a circular orbit we have $r(\tau) = r_0$ and $\dot{r} = 0$ as well as $\ddot{r} = 0$. The two geodesic equations for t and ϕ, equations (8.4a) and (8.4c), then simplify to $\ddot{t} = 0$ and $\ddot{\sigma} = 0$. Starting the experiment at time $t = 0$ at an angle $\sigma = 0$ and using equations (8.5a) and (8.5b) the solutions to equations (8.4a) and (8.4c) are

$$t(\tau) = \mathrm{e}^{-2\nu(r_0)}\, E\,\tau\,,$$
$$\sigma(\tau) = \frac{L}{r_0^2}\,\tau\,.$$

The particle has completed a full period in a proper time τ_P if $\phi(\tau_P) = 2\pi$. Therefore, the observer measures a period T of

$$T = t(\tau_P) = 2\pi\, r_0^2\, \mathrm{e}^{-2\nu(r_0)}\frac{E}{L}\,.$$

Hence, the observer determines the mass within the orbit to be

$$M_{\text{Kepler}}(r_0)\, G_N = \frac{\mathrm{e}^{4\nu(r_0)}}{r_0}\,\frac{L^2}{E^2}\,. \tag{8.6}$$

To eliminate E and L from equation (8.6), notice that equation (8.4b) can be written as

$$\ddot{r} = \mathrm{e}^{-2\lambda}\left(\frac{L^2}{r^3} - \mathrm{e}^{-2\nu}E^2\nu'\right)\,.$$

For a circular orbit $\ddot{r}$ must vanish, which leads to

$$\mathrm{e}^{-2\nu(r_0)}E^2\nu'(r_0) = \mathrm{e}^{-2\lambda}L^2/r_0^3\,. \tag{8.7}$$

With this result we can eliminate both L and E in equation (8.6), and the Kepler mass reads

$$M_{\text{Kepler}}(r_0)G_N = \mathrm{e}^{2\nu(r_0)}\, r_0^2\,\nu'(r_0)\,. \tag{8.8}$$

Finally, we use $x \equiv f e\, r$ and obtain

$$M_{\text{Kepler}}e/f = \mathrm{e}^{2\nu(x_0)}\, x_0^2\,\nu'(x_0)/\eta\,, \tag{8.9}$$

where $x_0 \equiv efr_0$, $\eta \equiv G_N f^2$, and e/f has the unit of one over mass.

At the end of Section 6.4 we showed that ν becomes $-\lambda_\infty/x$ asymptotically. Thus, we see that the constant λ_∞ must be positive, as otherwise the mass in equation (8.8) would neither be finite nor positive. Explicitly, we have

$$\widehat{M}_{\text{Kepler}} \equiv \lim_{x_0\to\infty} M_{\text{Kepler}}(x_0)e/f = \lim_{x_0\to\infty} \mathrm{e}^{-2\lambda_\infty/x_0}\,\frac{x_0^2}{\eta}\,\frac{\lambda_\infty}{x_0^2} = \lambda_\infty/\eta\,,$$

and the physical interpretation of the free parameter λ_∞ is that it gives the mass of the spacetime.

We conclude with two brief remarks. The first is that equation (8.8) yields the mass M appearing in the Schwarzschild-metric. This can be seen directly by using $\nu = \ln(1-2M/r)/2$ in equation (8.9). The second remark concerns the normalization of the four-velocity (u^μ). Using equations (8.5a) and (8.5b) we find $u_\mu u^\mu = L^2/r^2 - \mathrm{e}^{-2\nu}E^2 = -1$, and solving for E^2 we find

$$E^2 = \mathrm{e}^{2\nu}\left(1 + L^2/r^2\right)\,.$$

Equating this with the other equation for E^2 (equation (8.7)), and solving for L^2 we find

$$L^2 = r^3\nu'/1 - r\nu' > 0\,.$$

Since we know that $\nu' > 0$ holds at least asymptotically, we find that the condition for the existence of circular orbits is

$$r_0\nu'(r_0) < 1\,.$$

8.2. Komar mass of the defect

Besides the mass obtained via Kepler's law, there is another way to define the mass of a gravitating system. It is useful, because it allows us to see how much each field energy contributes to the total mass. The definition is due to Komar [35], and can be applied whenever the spacetime is static, asymptotically flat, and which is vacuum in the neighborhood of infinity [17]. All of these requirements hold for the spacetime under consideration. Furthermore, the spacetime must have a timelike Killing vector field ξ^μ with $\xi^\mu\xi_\mu \to -1$ as $r \to \infty$. The timelike vector field given in the last section has such a normalization, because $\xi^\mu\xi_\mu = -\exp(2\nu) \to -1$.

Working directly in dimensionless quantities, the Komar mass within a radius x_0 is then defined by [17]

$$M_{\text{Komar}}(x_0)\frac{e}{f} \equiv -\frac{1}{8\pi\eta}\oint_S \alpha\,, \tag{8.10}$$

Here, S is a spatial two-Sphere of radius x_0. The two-form α is obtained by acting with the natural volume form $\epsilon = \sqrt{|g|}\,\mathrm{d}x\wedge\mathrm{d}\theta\wedge\mathrm{d}\phi$ on the tensor field $(\nabla^\mu\xi^\nu)\partial_\mu\otimes\partial_\nu$. The result of this operation is

$$\alpha = -2\mathrm{e}^{\nu-\lambda}x^2\nu'\,\sin\theta\,\mathrm{d}\theta\wedge\mathrm{d}\phi\,. \tag{8.11}$$

Equation (8.10) then yields

$$M_{\text{Komar}}(x_0)e/f = \mathrm{e}^{\nu(x_0)-\lambda(x_0)}\,x_0^2\,\nu'(x_0)/\eta\,. \tag{8.12}$$

At first glance, equation (8.12) is similar to, but not quite the same as, equation (8.8). However, asymptotically $\nu_{\text{asympt}}(x_0) = -\lambda_{\text{asympt}}(x_0) = \lambda_\infty/x_0$, and then the exponent in equation (8.12) equals that in equation (8.8). Thus we find

$$\widehat{M}_{\text{Komar}} \equiv \lim_{x_0\to\infty} M_{\text{Komar}}(x_0)e/f = \lim_{x_0\to\infty}\mathrm{e}^{-2\lambda_\infty/x_0}\,\frac{x_0^2}{\eta}\,\frac{\lambda_\infty}{x_0^2} = \lambda_\infty/\eta\,,$$

which agrees with the asymptotic value of the Kepler mass.

As for M_{Kepler}, equation (8.12) yields the mass M of a Schwarzschild spacetime, once the appropriate expressions for the metric functions ν and λ are substituted.

We now rewrite the surface integral occurring in the definition of the Komar mass as a volume integral. This will allow us to see the contribution of the Skyrme field energy and the "gravitational field energy" separately. Since the spatial hypersurface is topologically $SO(3)$ and, hence, orientable, we can use Stokes's theorem to convert the surface integral in equation (8.10) into a volume integral. For a two-form ω Stokes's theorem reads

$$\int_M \mathrm{d}\,\omega = \oint_{\partial M}\omega\,,$$

where M is the manifold and ∂M its boundary. In our case, and with the coordinates used so far, the volume Σ is enclosed by the sphere at x_0 and the defect at x_{def}. As mentioned in Chapter 5, the latter sphere constitutes a "coordinate boundary" only,

because the x-coordinate is bounded from below by $\mathrm{x}_{\mathrm{def}}$. We therefore find that the boundary $\partial\Sigma$ consists of the two disjointed sets S_{x_0} and $S_{\mathrm{x}_{\mathrm{def}}}$. Using Stokes's theorem we find

$$-\frac{1}{8\pi\eta}\oint_{S_{x_0}}\alpha+\frac{1}{8\pi\eta}\oint_{S_{\mathrm{x}_{\mathrm{def}}}}\alpha=\frac{1}{\eta}\int_{\Sigma}\mathrm{d}\alpha\,. \tag{8.13}$$

The plus sign on the left hand side is due to the opposite orientation of $S_{\mathrm{x}_{\mathrm{def}}}$. On the right hand side the three-form $\mathrm{d}\alpha$ can be expressed in terms of the Ricci tensor $R_{\mu\nu}$ as [17]

$$\mathrm{d}\alpha=-2R_{\mu\nu}n^{\mu}\xi^{\nu}\mathrm{d}V\,.$$

Here

$$\begin{aligned}(n^{\mu})&\equiv(\mathrm{e}^{-\nu},0,0,0)\,,\\ \mathrm{d}V&\equiv\mathrm{e}^{\lambda}x^{2}\sin\theta\,\mathrm{d}x\,\mathrm{d}\theta\,\mathrm{d}\phi\,,\end{aligned}$$

denote the unit future pointing normal to Σ, and the natural volume form on Σ, respectively. The relevant component of the Ricci tensor reads

$$R_{00}=\mathrm{e}^{2(\nu-\lambda)}\left[(2-x\lambda')\nu'+x\nu'^{2}+x\,\nu''\right]/x\,.$$

Notice that $\mathrm{d}\alpha=-2R_{00}\xi^{0}n^{0}\mathrm{d}V$ can be simplified using

$$R_{00}\xi^{0}n^{0}\mathrm{d}V=\partial_{x}\left(\mathrm{e}^{\nu-\lambda}x^{2}\nu'\right)\sin\theta\,\mathrm{d}x\wedge\mathrm{d}\theta\wedge\mathrm{d}\phi\,.$$

Putting all of this together, the Komar mass is given by

$$M_{\mathrm{Komar}}(x_0)e/f=-\frac{1}{8\pi\eta}\oint_{S_{x_0}}\alpha=\frac{1}{4\pi\eta}\int_{\Sigma}R_{\mu\nu}n^{\mu}\xi^{\nu}\mathrm{d}V-\frac{1}{8\pi\eta}\oint_{S_{\mathrm{x}_{\mathrm{def}}}}\alpha\,. \tag{8.14}$$

Now, we use Einstein's equations, $R_{\mu\nu}=8\pi G_N\left(T_{\mu\nu}-1/2Tg_{\mu\nu}\right)$, to obtain an expression for the Komar mass in terms of the energy momentum tensor. We find that the Komar mass can be written as a sum of three terms

$$M_{\mathrm{Komar}}(x_0)e/f=M_{\mathrm{mat}}(x_0)e/f+M_{\mathrm{grav}}(x_0)e/f+M_{\mathrm{def}}e/f \tag{8.15}$$

where

$$M_{\mathrm{mat}}(x_0)\frac{e}{f}\equiv\int_{\Sigma}T_{00}\mathrm{e}^{\lambda(x)-\nu(x)}\,x^{2}\,\sin\theta\,\mathrm{d}x\,\mathrm{d}\theta\,\mathrm{d}\phi\,, \tag{8.16a}$$

$$M_{\mathrm{grav}}(x_0)\frac{e}{f}\equiv\int_{\Sigma}\left(T_{00}-Tg_{00}\right)\mathrm{e}^{\lambda(x)-\nu(x)}\,x^{2}\,\sin\theta\,\mathrm{d}x\,\mathrm{d}\theta\,\mathrm{d}\phi\,, \tag{8.16b}$$

$$M_{\mathrm{def}}e/f\equiv-\frac{1}{8\pi\,\eta}\oint_{S_{\mathrm{x}_{\mathrm{def}}}}\alpha=\frac{1}{\eta}\,\mathrm{e}^{\nu(\mathrm{x}_{\mathrm{def}})-\lambda(\mathrm{x}_{\mathrm{def}})}\,{\mathrm{x}_{\mathrm{def}}}^{2}\,\nu'(\mathrm{x}_{\mathrm{def}})\,. \tag{8.16c}$$

Notice that the mass is no longer given by an integral over just the energy density T_{00}. However, when spacetime is flat, equation (8.16a) reduces to the usual expression for the energy, see equation (7.7). The second contribution, equation (8.16b), contains

the gravitational energy within the volume. The integrand cannot, however, be understood as the local energy density of the gravitational field. The physical reason for this is that one can always find a local Minkowskian coordinate system where the effects of gravitational forces are absent, and, hence, the local gravitational field energy vanishes as well [36]. As a result, the concept of "local gravitational energy density" becomes a coordinate dependent one. Hence, various expressions for the "local energy density" exist, but they are only pseudo-tensors in the sense that they depend on the coordinate system used. For example, both the Einstein- and Landau-Lifshitz pseudo-tensors are valid in Cartesian coordinates only. The form of the pseudo-tensor used here is due to Møller [37] (see also [38]). Despite the coordinate arbitrariness of the integrands, the volume integral in equation (8.16b) *is* independent of the coordinates used, because it arises from a surface integral. Hence, we emphasize that the total energy within a sphere is well defined by the first surface integral in equation (8.14).

The last contribution, M_{def}, requires some special considerations. In the form given in equation (8.16c), it is due to the coordinate boundary at x_{def}. To see what happens to M_{def} in a coordinate system that does not have this boundary, we use the (Y, Z, X)-coordinates, introduced in equation (5.30) in Section 5.2.1. Recall that, in these coordinates points have coordinate $Y = 0$ on the defect, with $Y \in (-\infty, \infty)$, and that there is thus no coordinate boundary.

The sphere at x_0 is mapped to the two planes $Y = Y_+ \equiv x_0 - \mathrm{x}_{\text{def}} > 0$ and $Y = Y_- \equiv \mathrm{x}_{\text{def}} - x_0 < 0$. Hence, equation (8.14) becomes

$$M_{\text{Komar}}(Y_0)e/f = -\frac{1}{8\pi\eta}\oint_{Y=Y_+}\alpha - \frac{1}{8\pi\eta}\oint_{Y=Y_-}\alpha = \frac{1}{4\pi\eta}\int_\Sigma R_{\mu\nu}n^\mu\xi^\nu \mathrm{d}V\,. \tag{8.17}$$

Furthermore, the metric transforms into

$$\mathrm{d}s^2(ef)^2 = -\mathrm{e}^{\nu(\mathrm{x}_{\text{def}}+|Y|)}\mathrm{d}T^2 + \mathrm{e}^{\lambda(\mathrm{x}_{\text{def}}+|Y|)}\mathrm{d}Y^2 + (\mathrm{x}_{\text{def}}+|Y|)^2\left(\mathrm{d}Z^2 + \sin^2 Z\,\mathrm{d}Y^2\right)\,,$$

where, in a slight misuse of notation, the time and radial coordinates, T and Y, are dimensionless. To calculate the Ricci tensor $R_{\mu\nu}$ we again use $[\mathrm{abs}'(x)]^2 = 1$ as well as $\mathrm{abs}''(x) = 2\delta(x)$. We obtain

$$\begin{aligned} R_{TT} =& 2\,\mathrm{e}^{2[\nu(\mathrm{x}_{\text{def}}+|Y|)-\lambda(\mathrm{x}_{\text{def}}+|Y|)]}\,\nu'(\mathrm{x}_{\text{def}}+|Y|)\,\delta(Y) + \mathrm{e}^{2[\nu(\mathrm{x}_{\text{def}}+|Y|)-\lambda(\mathrm{x}_{\text{def}}+|Y|)]} \\ &\times\left\{\left[\nu'(\mathrm{x}_{\text{def}}+|Y|) - \lambda'(\mathrm{x}_{\text{def}}+|Y|) + \frac{2}{\mathrm{x}_{\text{def}}+|Y|}\right]\nu'(\mathrm{x}_{\text{def}}+|Y|)\right. \\ &\left. + \nu''(\mathrm{x}_{\text{def}}+|Y|)\right\}. \end{aligned} \tag{8.18}$$

Hence, the price for the disappearance of the boundary at x_{def} is the occurrence of a δ-function centered at $Y = 0$. The volume integral in equation (8.17) is then

explicitly given by

$$\begin{aligned}\int_\Sigma R_{\mu\nu}n^\mu\xi^\nu \mathrm{d}V = \int_{Y_-}^{Y_+}\int_0^\pi\int_0^\pi \Big\{ & 2\,\mathrm{e}^{\nu(\mathrm{x}_{\mathrm{def}}+|Y|)-\lambda(\mathrm{x}_{\mathrm{def}}+|Y|)}(\mathrm{x}_{\mathrm{def}}+|Y|)^2\nu'(\mathrm{x}_{\mathrm{def}}+|Y|)\,\delta(Y) \\ & + \mathrm{e}^{\nu(\mathrm{x}_{\mathrm{def}}+|Y|)-\lambda(\mathrm{x}_{\mathrm{def}}+|Y|)}\,(\mathrm{x}_{\mathrm{def}}+|Y|)^2\Big[\nu''(\mathrm{x}_{\mathrm{def}}+|Y|) \\ & + \left(\nu'(\mathrm{x}_{\mathrm{def}}+|Y|)-\lambda'(\mathrm{x}_{\mathrm{def}}+|Y|)+\frac{2}{\mathrm{x}_{\mathrm{def}}+|Y|}\right)\nu'(\mathrm{x}_{\mathrm{def}}+|Y|)\Big]\Big\} \\ & \times \sin Z\,\mathrm{d}X\,\mathrm{d}Z\,\mathrm{d}Y\,.\end{aligned}$$

The integrals over X, Z and the δ-function are trivial. To evaluate the remaining integral over Y, we split the integration region as follows

$$\int_{Y_-}^{Y_+}\mathrm{d}Y = \int_{Y_-}^{0}\mathrm{d}Y + \int_0^{Y_+}\mathrm{d}Y\,,$$

and substitute $u \equiv \mathrm{x}_{\mathrm{def}} - Y$ and $u \equiv \mathrm{x}_{\mathrm{def}} + Y$ in the first and second integral on the right hand side, respectively. Finally, we use

$$\mathrm{e}^{\nu(u)-\lambda(u)}u\,(\{2+u[\nu'(u)-\lambda'(u)]\}\nu'(u)+\nu''(u)u) = \frac{\mathrm{d}}{\mathrm{d}u}\mathrm{e}^{\nu(u)-\lambda(u)}u^2\nu'(u) \equiv \frac{\mathrm{d}}{\mathrm{d}u}g(u)\,,$$

to obtain

$$\begin{aligned}\frac{1}{4\pi\eta}\int_\Sigma R_{\mu\nu}n^\mu\xi^\nu\mathrm{d}V &= \mathrm{e}^{\nu(\mathrm{x}_{\mathrm{def}})-\lambda(\mathrm{x}_{\mathrm{def}})}{\mathrm{x}_{\mathrm{def}}}^2\nu'(\mathrm{x}_{\mathrm{def}})/\eta \\ &\quad + \frac{1}{2\eta}\left[-g(\mathrm{x}_{\mathrm{def}})+g(x_0)+g(x_0)-g(\mathrm{x}_{\mathrm{def}})\right] \\ &= \mathrm{e}^{\nu(x_0)-\lambda(x_0)}x_0^2\nu'(x_0)/\eta\,,\end{aligned}$$

which equals the result obtained in equation (8.12).

To learn more about the origin of the δ-function in equation (8.18) we use Einstein's equations,

$$R_{00} = 8\pi\eta\left(T_{00}-\frac{1}{2}Tg_{00}\right)\,.$$

The right hand side turns out to be

$$\begin{aligned}\left(T_{00}-\frac{1}{2}Tg_{00}\right) = & \frac{\mathrm{e}^{2\nu(\mathrm{x}_{\mathrm{def}}+|Y|)}}{(\mathrm{x}_{\mathrm{def}}+|Y|)^2}\Big[4(1-4\gamma/3)\frac{\sin^4(F(\mathrm{x}_{\mathrm{def}}+|Y|)/2)}{(\mathrm{x}_{\mathrm{def}}+|Y|)^2} \\ & + 2\mathrm{e}^{-2\lambda(\mathrm{x}_{\mathrm{def}}-|Y|)}(1-2\gamma/3)\sin^2(F(\mathrm{x}_{\mathrm{def}}+|Y|)/2)F'(\mathrm{x}_{\mathrm{def}}+|Y|)^2 \\ & - \frac{1}{12}\gamma(\mathrm{x}_{\mathrm{def}}+|Y|)^4\mathrm{e}^{-4\lambda(\mathrm{x}_{\mathrm{def}}+|Y|)}F'(\mathrm{x}_{\mathrm{def}}+|Y|)^4\Big]\end{aligned} \tag{8.19}$$

Notice that equation (8.19) does not contain a δ-function! Thus, the left hand side of Einstein's equation is singular at the defect, whereas the right hand side is not.

Or, phrased in another way, the singularity in $R_{\mu\nu}$ is not sourced by the matter field. Indeed, looking back at equation (8.14), we see that the singularity shows up as the surface integral of a geometric quantity that is not directly related to matter. If matter is not the source of M_{def}, what could be? Here, we interpret M_{def} as the energy needed to create the type I defect out of the original Minkowski spacetime. Loosely speaking, M_{def} measures the work needed to "drill" a hole in spacetime and "twist" the boundary before "sewing" it up again. To prove that this is really the case, one would need to have a theory where it is possible to describe these changes in topology dynamically. Common belief is that a theory of quantum gravity is needed for this. From this point of view, it is understandable that our classical matter field Ω cannot create such a transition. It can, however, prevent the defect from "collapsing" or "shrinking", as we will show in the next section.

To summarize: Within the framework of general relativity, the mass is defined primarily not through a volume integral of an energy density, but by geometric quantities in the asymptotically flat region of spacetime. Here, we have used two definitions that are equivalent in our scenario. In the first definition one "weighs" the defect by looking at closed orbits of test particles and then applying Kepler's third law. The second definition is due to Komar [35]. It is useful, because it allows the mass to be decomposed into three contributions. The first contribution is just the volume integral of the energy density, similar to flat spacetime. The second part represents the gravitational energy of the system. Finally, the third contribution does not arise from the matter field, and we interpret it as the energy required to create a type I defect out of Minkowski spacetime.

8.3. Numerical results

Here, we present numerical solutions to the Einstein-Skyrme equations (6.24) and (6.25) in Section 6.4. The boundary conditions are

$$\begin{aligned} F(x_{\text{def}}) &= n\,\pi, \quad F(\infty) = 0\,, \\ \nu(\infty) &= 0, \qquad \lambda(\infty) = 0\,. \end{aligned} \tag{8.20}$$

The method used to obtain these results is the same as in the nongravitating case, see Section 7.1.1. That is, we give initial conditions for F and λ at x_{def}, and evolve the functions numerically up to some sufficiently large x. Using the fact that, asymptotically, $\nu = -\lambda$, we obtain the initial condition for ν and evolve back to x_{def}.

Since the ODE for F is of second order and equation (8.20) yields only one condition at x_{def}, we have $F'(\mathrm{x}_{\text{def}})$ as an unknown parameter. Furthermore, equation (8.20) does not yield any condition for $\lambda(\mathrm{x}_{\text{def}})$, so this constitutes another unknown parameter. These two parameters need to be determined, such that the boundary conditions at infinity are satisfied. In the usual $SU(2)$-Skyrme model, regularity of the field equations at the origin leads to an additional relation between $F(x_{\min})$ and $\lambda(x_{\min})$. The relation can be used to express the latter in terms of the former [30, 39]. Then there is only one free parameter which needs to be adjusted.

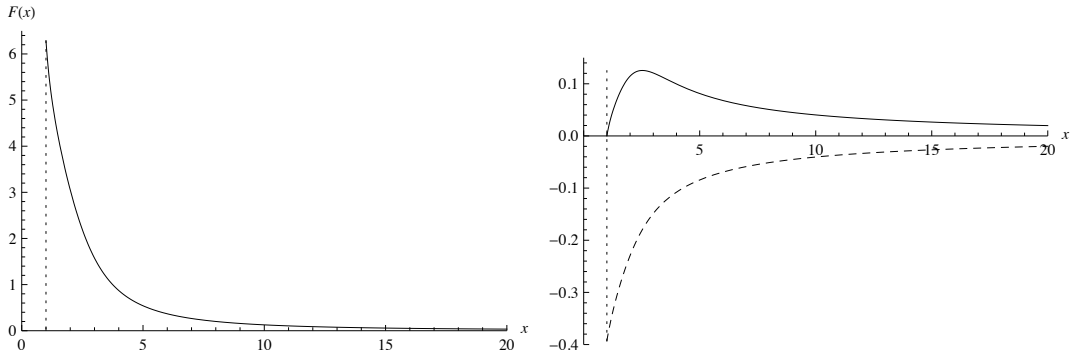

(a) (b)

Figure 8.1.: Numerical solutions of the Einstein-Skyrme equations as functions of the dimensionless radius $x \equiv ef\,r$. (a) Profile function F. (b) Metric functions λ (continuous) and ν (dashed). The solutions were obtained with $G_N f^2 = 1/400\pi$ and $\mathrm{x_{def}} = 1$ (dotted vertical line). The winding number of the Skyrme field was 2.

Since we explicitly removed the origin, regularity at the origin is not an issue here. Alternatively, we could use the asymptotic expansions for F and λ, equations (6.26a) and (6.26b). Again, however, two unknown parameters, F_∞ and λ_∞, are required.

In this chapter, we decide to use

$$\lambda(\mathrm{x_{def}}) = 0\,,$$

for two reasons. First, when $G_N \to 0$, our results approach that of the nongravitating case. Second, when $\mathrm{x_{def}} = 0$ and our $SO(3)$-Skyrme field has an even winding number, our results agree with the results of the gravitating $SU(2)$-Skyrme model [30, 39].

8.3.1. Results for even winding number

For the nongravitating case, we start by investigating $SO(3)$-Skyrmions with even winding number. Specifically, we choose

$$F(\mathrm{x_{def}}) = 2\pi\,.$$

With this boundary condition, our $SO(3)$-Skyrmion, with $n = 2$, is equivalent to an $SU(2)$-Skyrmion with winding number $B = 1$ (see the discussion in Section 7.1.1 on page 60). For this reason, we expect our numerical results to agree in the appropriate limits with the results known in the literature.

Figure 8.1 shows numerical solutions obtained for $\eta \equiv G_N f^2 = 1/400\pi$ and $\mathrm{x_{def}} = 1$. The solutions for other values are qualitatively the same. We depict the (Komar) mass as a function of $\mathrm{x_{def}}$ in figure 8.2. First, notice that the mass approaches a finite value for vanishing $\mathrm{x_{def}}$. The reason for this finiteness is the same as in flat space. Recall that for $F(\mathrm{x_{def}}) = 2\pi$, the field Ω equals $\mathbb{1}$ at the defect. This is well

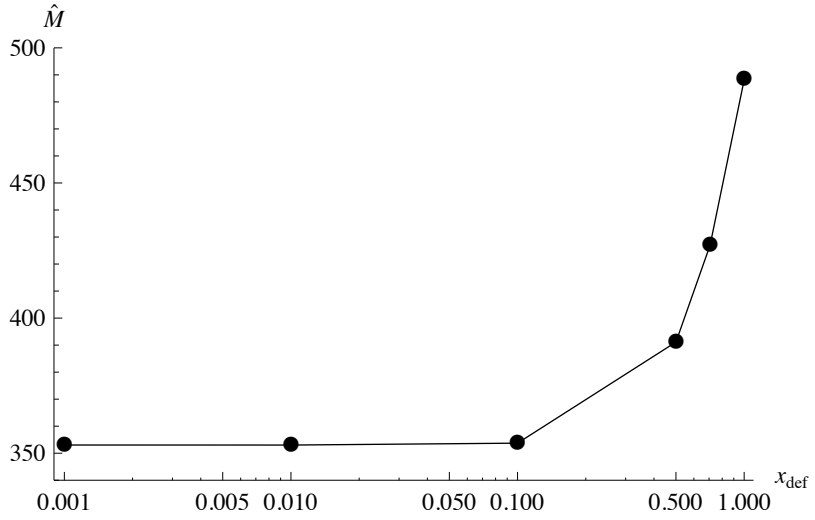

Figure 8.2.: Dependence of the dimensionless mass $\widehat{M} \equiv M_{\mathrm{Komar}}\, e/f$ on $\mathrm{x}_{\mathrm{def}} = ef\, b$ for $G_N f^2 = 1/400\pi$ and winding number $n = 2$. The limiting value is approximately 353. Lines are to guide the eye.

defined even when $\mathrm{x}_{\mathrm{def}} = 0$, and is independent of whether the base space is curved or not. Second, because with $n = 2$ our $SO(3)$-Skyrmion is equivalent to a $B = 1$ $SU(2)$-Skyrmion, we can compare our numerical result for the limiting value of the mass with that of a gravitating $SU(2)$-Skyrmion. To compare with the results of [39], we have to rescale our dimensionful quantities f and e as

$$f_3 \to f_2/2\,,$$
$$e_3 \to \sqrt{8} e_2\,.$$

Here, the indices '3' or '2' denote constants used in this thesis ($SO(3)$) or in [39] ($SU(2)$), respectively. Thus, our value of $\eta \equiv G_N f_2^2$ is equivalent to the factor $\alpha/16\pi$ used in [39], where $\alpha \equiv 4\pi G_N f_3^2$. To relate our mass M, in units of f_3/e_3, to their mass, in units of f_2/e_2, we have to divide $\widehat{M}$ by $\sqrt{32}$. Hence, our η of $1/400\pi$ corresponds to a value of $\alpha = 4 \times 10^{-2}$, and our mass of $\approx 353.04 f_3/e_3$ equals $\approx 62.41 f_2/e_2$. This is in agreement with the result of [39], as stated in their table 1.

Figure 8.3 shows how the mass depends on the relative strength $\eta \equiv G_N f^2$ between Newton's constant G_N and the Skyrme constant f. There exists a critical value $\eta_{\max} \approx 8.03 \times 10^{-4}$ above which no solutions can be found. Below $\eta_{\max}$ two branches of solutions exists which coalesce at $\eta_{\max}$. One such branch approaches the nongravitating Skyrmion as η approaches 0, whereas the energy of the other diverges.

To summarize: In this subsection we investigated our numerical results for the gravitating $SO(3)$-Skyrmion with winding number $n = 2$. When $\mathrm{x}_{\mathrm{def}} \to 0$ the mass approaches that of the gravitating $SU(2)$-Skyrmion with winding number one [39].

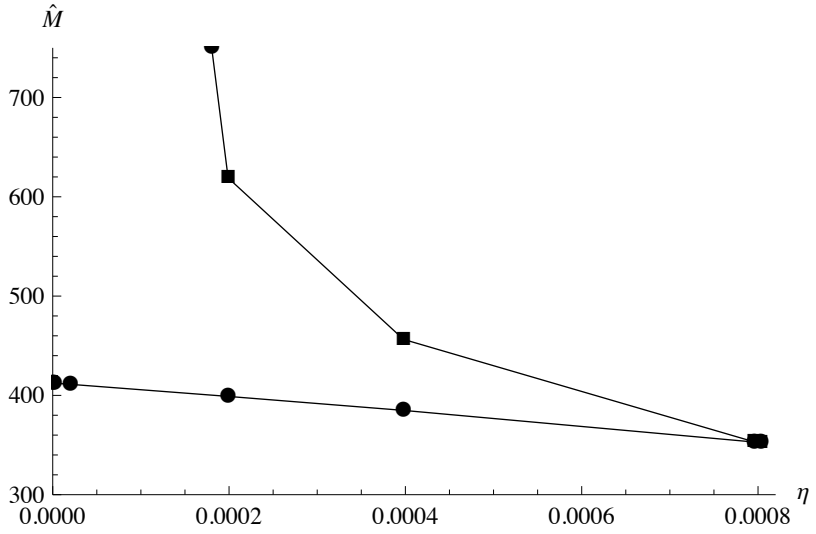

Figure 8.3.: Dependence of the dimensionless mass $\widehat{M} \equiv M_{\text{Komar}}\, e/f$ on $\eta \equiv G_N\, f^2$ for $\mathrm{x}_{\text{def}} = 10^{-2}$ and winding number $n = 2$. For the lower branch (circles) the mass continuously approaches that of the nongravitating $SO(3)$-Skyrmion. The energy of the upper branch (squares) diverges as $\eta \to 0$. Lines are to guide the eye.

We also reproduce the two "branches" of solutions. The two branches meet at a maximal value of η, above which no solutions exists. One branch approaches the nongravitating solution when $\eta \to 0$.

Since the (Komar) mass increases for increasing x_{def} but approaches a finite value when $\mathrm{x}_{\text{def}} \to 0$, we conclude that there is no finite defect parameter that minimizes the energy of the system in this case. Hence, as far as energy is concerned, there is nothing that would prevent the defect from collapsing.

8.3.2. Results for odd winding number

Having established in the last section that our model reproduces the well-studied gravitating $SU(2)$-Skyrmion in the appropriate limit, we now turn to the gravitating $SO(3)$-Skyrmion. To obtain results not already contained in the $SU(2)$ case, we consider Skyrme fields with odd winding number n. Specifically, we choose $n = 1$ and the boundary condition for the profile function reads

$$F(\mathrm{x}_{\text{def}}) = \pi\,.$$

Figure 8.4 shows numerical solutions of the profile function F and the two metric functions λ and ν obtained for $\eta \equiv G_N f^2 = 1/400\pi$ and $\mathrm{x}_{\text{def}} = 1/\sqrt{2}$. The solutions for other values are qualitatively the same. We depict the (Komar) mass as a function of x_{def} in figure 8.5 with η fixed at $1/16000\pi$. First, notice that there is a finite value of $\mathrm{x}_{\text{def}} \approx 1/\sqrt{2}$ that minimizes the mass. When compared at the same

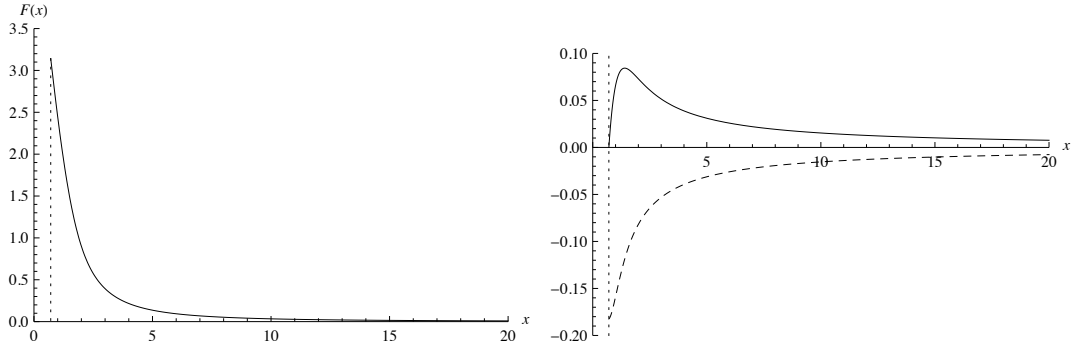

(a) (b)

Figure 8.4.: Numerical solutions of the Einstein-Skyrme equations as functions of the dimensionless parameter $x \equiv ef\,r$. (a) Profile function F. (b) Metric functions λ (continuous) and ν (dashed). The solutions were obtained with $G_N f^2 = 1/400\pi$ and $\mathrm{x_{def}} = 1/\sqrt{2}$ (dotted vertical line). The winding number of the Skyrme field was one.

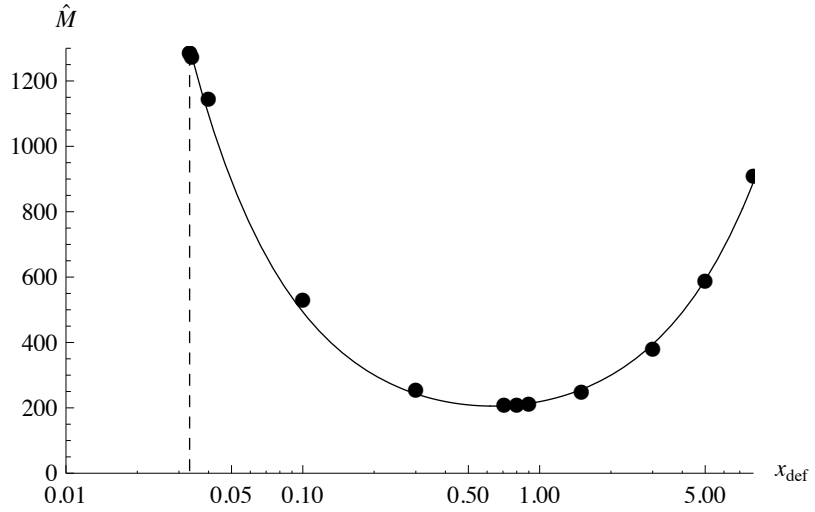

Figure 8.5.: Dependence of the dimensionless mass $\widehat{M} \equiv M_{\mathrm{Komar}}\, e/f$ on $\mathrm{x_{def}} = ef\,b$ for $G_N f^2 = 1/16000\pi \approx 2 \times 10^{-5}$ and winding number $n = 1$. Within the numerical uncertainty, the minimal value occurs at $x = 1/\sqrt{2}$. The vertical line at $\mathrm{x_{def}} = 0.03327048$ marks the critical value of $\mathrm{x_{def}}$, below which no solutions have been found. The curve $a/\mathrm{x_{def}} + b\mathrm{x_{def}} + c$ is fitted to the points with $a \approx 40.58$, $b \approx 101.12$, and $c \approx 77.31$.

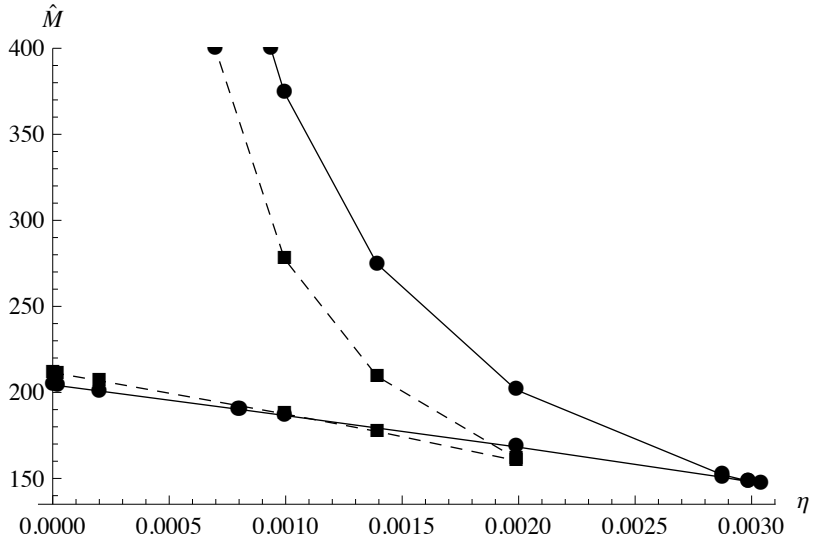

Figure 8.6.: Dependence of the dimensionless mass $\widehat{M} \equiv M_{\rm Komar}\, e/f$ of the $n = 1$ $SO(3)$-Skyrmion on $\eta \equiv G\, f^2$ for $\mathrm{x_{def}} = 1/\sqrt{2}$ (circles, joined by continuous lines) and $\mathrm{x_{def}} = 1/2$ (squares, joined by dashed lines). For each $\mathrm{x_{def}}$ two branches exist, which coalesce at a maximal value of η. This maximal value depends on $\mathrm{x_{def}}$. As $\eta \to 0$, the limiting masses of the two lower branches approach those of the nongravitating $n = 1$ $SO(3)$-Skyrmions. For small η, the masses obtained for $\mathrm{x_{def}} = 1/2$ are slightly larger than those for $\mathrm{x_{def}} = 1/\sqrt{2}$. However, for η close to the maximal value the masses for $\mathrm{x_{def}} = 1/2$ are slightly smaller. The masses of the upper branches diverge for $\eta \to 0$, with those for $\mathrm{x_{def}} = 1/2$ being smaller than those for $\mathrm{x_{def}} = 1/\sqrt{2}$.

value of η, the minimal mass of the $n = 1$ $SO(3)$-Skyrmion is about half that of the limiting value of the $n = 2$ $SO(3)$-Skyrmion. For $\eta = 1/16000\pi \approx 2 \times 10^{-5}$, we obtain masses of approximately $204 f/e$ and $411 f/e$ for the $SO(3)$- and $SU(2)$-Skyrmions, respectively (see also figures 8.5 and 8.3). A good fit to the data is given by a curve of the form $a/\mathrm{x_{def}} + b\mathrm{x_{def}} + c$. For the values of the parameters a, b, and c see the caption of figure 8.5. Hence, the mass increases linearly for $\mathrm{x_{def}} > 1/\sqrt{2}$ and diverges like $1/\mathrm{x_{def}}$ for smaller $\mathrm{x_{def}}$. However, unlike for the case of the nongravitating $n = 1$ $SO(3)$-Skyrmion, there exists a minimal value for $\mathrm{x_{def}}$ below which no solutions could be found.

Figure 8.6 shows the dependence of the mass on η for two values of $\mathrm{x_{def}}$. As for the $n = 2$ Skyrmion, two branches exist for each $\mathrm{x_{def}}$. The two branches coalesce at a maximal value of η that, now, depends on $\mathrm{x_{def}}$. As $\eta \to 0$, the limiting masses of the two lower branches approach those of the nongravitating $n = 1$ $SO(3)$-Skyrmions. In the lower branches the masses for $\mathrm{x_{def}} = 1/2$ exceed those for $\mathrm{x_{def}} = 1/\sqrt{2}$ if η is close to zero. However, when η approaches the maximal allowed value the masses for $\mathrm{x_{def}} = 1/2$ are smaller than those for $\mathrm{x_{def}} = 1/\sqrt{2}$. The masses of the upper branches diverge for $\eta \to 0$, with those for $\mathrm{x_{def}} = 1/2$ being smaller than those for $\mathrm{x_{def}} = 1/\sqrt{2}$.

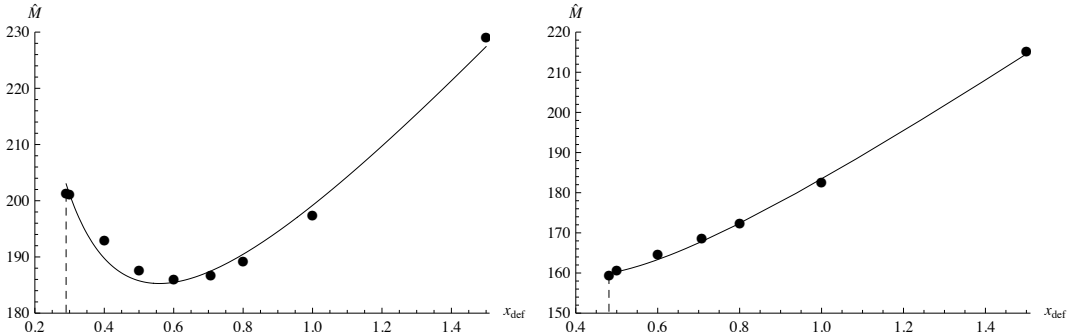

(a) (b)

Figure 8.7.: Dependence of the dimensionless mass $\widehat{M} \equiv M_{\rm Komar}\, e/f$ on the dimensionless defect parameter $\mathrm{x}_{\rm def} = ef\, b$ for (a) $\eta = 1/320\pi \approx 0.001$ and (b) $\eta = 1/160\pi \approx 0.002$. The smallest defect parameters, below which no solutions exists, occur at $\mathrm{x}_{\rm def} \approx \{0.29,\, 0.48\}$, respectively. The curve $a/\mathrm{x}_{\rm def} + b\mathrm{x}_{\rm def} + c$ is fitted to the points with $a \approx \{22.2526,\, 11.9909\}$, $b \approx \{71.3271,\, 70.2021\}$, and $c \approx \{105.595,\, 101.226\}$ for the $\{\text{left}, \text{right}\}$ figures, respectively. Notice that the would-be minimum of the right curve is at $\mathrm{x}_{\rm def} = \sqrt{a/b} \approx 0.41$, which is already smaller than the smallest attainable $\mathrm{x}_{\rm def}$.

Figure 8.7 depicts the dimensionless mass $\widehat{M}$ as a function of $\mathrm{x}_{\rm def}$ for two more values of η. The first value, $\eta = 1/320\pi \approx 0.001$, is the one where the two lower branches of figure 8.6 cross. As can be seen from figure 8.7(a) the masses are (almost) equal at these two defect parameters and the minimal value occurs at $\mathrm{x}_{\rm def} \approx 0.6$. The $\mathrm{x}_{\rm def}$ dependence of $\widehat{M}$ at the value $\eta = 1/320\pi \approx 0.001$ is shown in figure 8.7(b). This particular value of η is almost the maximum allowed value for which solutions with $\mathrm{x}_{\rm def} = 1/2$ exist. Here, no minimal value of the mass exists, and the mass increases monotonically with increasing $\mathrm{x}_{\rm def}$.

8.4. Discussion

We now discuss the various properties of the gravitating $SO(3)$-Skyrmions.

First, we consider how the dimensionless mass $\widehat{M}$ depends on the relative strength $\eta = G_N f^2$ between Newton's constant G_N and the Skyrme constant f. For either $n = 1$ or $n = 2$ Skyrmions two "branches" of solutions exist, see figures 8.3 and 8.6. One branch has a mass that is always smaller than that of the other branch and we will refer to them as the lower- and upper branch, respectively. The solutions in the lower branch converge to the nongravitating solutions as η approaches zero. Hence, $\widehat{M}$ approaches the energy of the nongravitating Skyrmions. However, the masses of the upper branch diverge in this limit. Furthermore, there exists a maximum value of η above which no solutions exist. When $n = 1$, this value depends on $\mathrm{x}_{\rm def}$.

As first noticed in [39], the occurrence of two branches can be understood by

noting that the limit $\eta \to 0$ can either mean $G \to 0$ or $f \to 0$. In the former case, the solutions approach the nongravitating Skyrmion and the mass remains finite. However, dimensionless quantities such as $x \equiv fer$ are not suitable for the purpose of investigating $f \to 0$. To analyze the limit $f \to 0$ new quantities are introduced [39]

$$\tilde{x} \equiv \frac{x}{\sqrt{32\pi\,\eta}} = \frac{e\,r}{\sqrt{32\pi\,G}}\,, \tag{8.21a}$$

$$w(\tilde{x}) \equiv \cos(F(x)/2)\,. \tag{8.21b}$$

When Eqs. (6.24)–(6.25) are expressed in these new variables and η is set to zero the equations remain well defined. Furthermore, they become equivalent to the spherically symmetric magnetic Einstein-Yang-Mills equations [40]. Their solutions interpolate between $w(0) = 1$ and $w(\infty) = -1$ and these boundary conditions are gauge equivalent [41] to $w(0) = -1$ and $w(\infty) = 1$. Our boundary conditions for F, when $n = 2$, translate into $w(\mathrm{x_{def}}) = \cos(\pi) = -1$ and $w(\infty) = \cos(0) = 1$. Since these are valid boundary conditions for the Einstein-Yang-Mills equations, we expect that the mass of the upper branch approaches that of the solution of the Einstein-Yang-Mills equations, once the appropriate units are used. To compare our value of $\widehat{M}$ to the value given in [39, 41], we have to multiply our value by $\sqrt{\eta/32\pi}$. Doing this, we find that the mass of the upper branch no longer diverges but approaches the value ≈ 0.856; which is approximately 3% larger than the value given in [39, 41] (≈ 0.83).

The situation is different when $n = 1$. Now, our boundary conditions for F translate into $w(\mathrm{x_{def}}) = \cos(\pi/2) = 0$ and $w(\infty) = \cos(0) = 1$. But it was shown in [41] that regular solutions of the Einstein-Yang-Mills equations must have $w(0) = \pm 1$. Therefore, our boundary condition $w(\mathrm{x_{def}}) = 0$ does not allow for a regular solution in the limit $f \to 0$. As a result, the masses of the upper branches diverge in the limit $\eta \to 0$. Even after rescaling the mass by a factor $\sqrt{\eta/32\pi}$, which produced the correct finite result in the previous paragraph, the rescaled mass diverges.

Next, we discuss the existence of the maximal value of η above which no solutions exist. This maximal value was first found by [30] for gravitating $SU(2)$-Skyrmions. It was then argued in [39] that at this value the Schwarzschild radius $R_{\mathrm{Schw}} \equiv 2G_N M$ becomes comparable to the "actual radius" of the Skyrmion and the configuration must collapse. To get a second length scale to compare to the Schwarzschild radius, we define r_H as the radius that minimizes $\exp(-2\lambda)$. By comparing our *Ansatz* for the metric with the Schwarzschild metric, we see that $\exp(-2\lambda)$ corresponds to $1 - 2M/r$. In the Schwarzschild metric the minimum would be a root, and r_H would equal R_{Schw}. Hence, if the ratio R_{Schw}/r_H equals one, we have a horizon. Figure 8.8 shows the ratio of R_{Schw} and r_H as a function of η for $n = 1$ (figure 8.8(a)) and $n = 2$ (figure 8.8(b)). From these figures we see that R_{Schw} indeed becomes equal to r_H as η approaches its maximal value.

Finally, we turn to the difference in the qualitative behavior of the mass between the $n = 1$ and $n = 2$ Skyrmions as the defect parameter $\mathrm{x_{def}}$ approaches zero. This difference can be seen by comparing figure 8.2 and figure 8.5. Namely, for $n = 2$ the

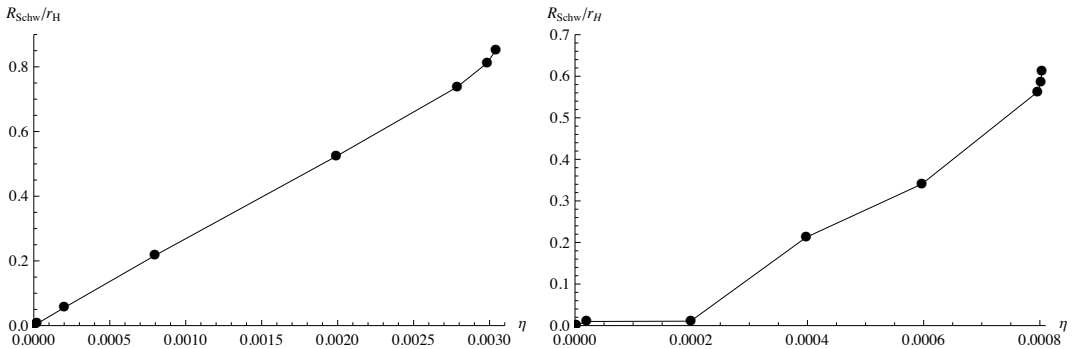

(a) (b)

Figure 8.8.: Ratios of the Schwarzschild radius $R_{\mathrm{Schw}} \equiv 2G_N M$ to r_H as a function of $\eta \equiv G_N f^2$ for $SO(3)$-Skyrmions with (a) $n = 1$ ($\mathrm{x}_{\mathrm{def}}$ fixed at $1/\sqrt{2}$) and (b) $n = 2$. Here, r_H is the radius that minimizes $\exp(-2\lambda)$. A ratio of one indicates that the extent of the Skyrmion becomes comparable to its Schwarzschild radius.

mass approaches a constant, figure 8.2, whereas for $n = 1$, figure 8.2, there exists a finite $\mathrm{x}_{\mathrm{def}}$ below which no solutions exist. As mentioned in Section 8.3.1, the boundary condition $n = 2$ implies $F(\mathrm{x}_{\mathrm{def}}) = 2\pi$, leading to $\Omega = \mathbb{1}$ at the defect. Since the field is constant at the defect, it is well defined even when $\mathrm{x}_{\mathrm{def}} = 0$, and the mass remains finite. However, the boundary condition $F(\mathrm{x}_{\mathrm{def}}) = \pi$ implies that $\Omega = -\mathbb{1} + 2\hat{n} \otimes \hat{n}$, where $\hat{n}$ is the ordinary unit normal vector. Now the field is *not* well defined at $\mathrm{x}_{\mathrm{def}} = 0$. In the (almost) flat case considered in Section 7.1, this resulted in a divergent energy as $\mathrm{x}_{\mathrm{def}}$ approached zero. Here, in the gravitating case, we find a minimal value for $\mathrm{x}_{\mathrm{def}}$ instead. Figure 8.9 shows the minimal value of $\exp(-2\lambda)$ as a function of $\mathrm{x}_{\mathrm{def}}$ for $\eta \approx 2 \times 10^{-5}$. A fit to the data yields that $\exp(-2\lambda)$ has a zero at $\mathrm{x}_{\mathrm{def}} \approx 0.0330546$. The physical significance of this is that the expansion θ of a family of null geodesics is proportional to $\exp(-\lambda)$ [42]. The surface where $\exp(-\lambda)$, and hence θ vanishes, is called an apparent horizon [22], and it can be shown [22] that it implies the existence of an event horizon. Therefore, we have found that an event horizon forms at the smallest possible value of $\mathrm{x}_{\mathrm{def}}$.

8.5. Summary

In this chapter we investigated gravitating $SO(3)$-Skyrmions. Two different methods were used to obtain the mass of a gravitating Skyrmion. The first was an application of Kepler's third law (Section 8.1) and the second used a mass definition due to Komar (Section 8.2). Both yield the same answer, but the latter definition allows us to investigate different contributions to the mass. Besides the contribution arising from the matter energy density and the gravitational self-energy we found a third contribution, M_{def}. Since M_{def} traces back to a δ-singularity in one of the components of the Ricci tensor that is not sourced by the matter field, we interpret it as the

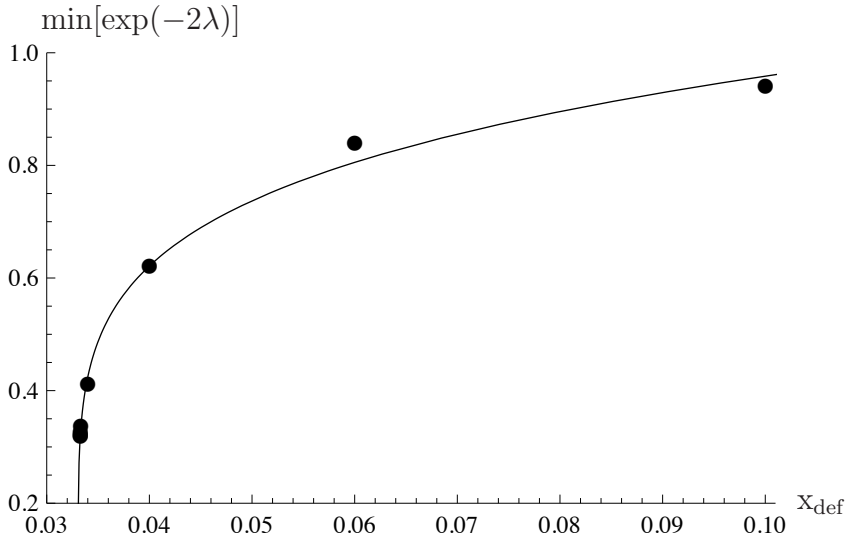

Figure 8.9.: Minimal value of $\exp(-2\lambda)$ as a function of $\mathrm{x}_{\mathrm{def}} \equiv feb$ for $\eta \equiv G_N f^2 \approx 2 \times 10^{-5}$. The curve $a(\mathrm{x}_{\mathrm{def}} - b)^c$ is fitted to the data with $a \approx 1.60775$, $b \approx 0.0330546$, and $c \approx 0.191296$. This shows the presence of an event horizon at $\mathrm{x}_{\mathrm{def}} \approx 0.0330546$ (for details see text).

energy needed to create a type I defect out of Minkowski spacetime.

Varying the parameter $\eta \equiv G_N f^2$, we found in Sections 8.3.1 and 8.3.2 that two "branches" of solutions exist, which coalesce at a maximal value of η. No solutions exist above this maximal value. The masses of the solutions in the so-called lower branch were always smaller than those in the upper branch. In the limit $\eta \to 0$, the lower branch approaches the nongravitating Skyrmion, whereas the mass of the upper branch diverges. We discussed how this upper branch is related to solutions of the Einstein-Yang-Mills equations. When the winding number n of the Skyrme field is even the upper branch approaches a regular solution of these equations as $\eta \to 0$. After using appropriate units, we found that the rescaled mass becomes finite in this limit. However, we showed that the boundary conditions for n odd do not allow for a regular solution of Einstein-Yang-Mills equations. As a result, even the rescaled mass diverges as $\eta \to 0$.

Ultimately, we were interested in the dependence of the mass (in the lower branch) on the defect parameter $\mathrm{x}_{\mathrm{def}} \equiv efb$. We found a dependence similar to the one for the nongravitating $SO(3)$-Skyrmions. Namely, the mass approaches a finite value when $\mathrm{x}_{\mathrm{def}} \to 0$ if $n = 2$. However, if $n = 1$, we found that a finite value of $\mathrm{x}_{\mathrm{def}}$ exists that minimizes the mass, provided that η is not too large. Unlike the mass of the nongravitating Skyrmion, it does not diverge as $\mathrm{x}_{\mathrm{def}} \to 0$. We found a minimal value of $\mathrm{x}_{\mathrm{def}}$, below which no solutions could be found. It turned out that an event horizon forms at this minimal value.

Thus, we find that a gravitating $SO(3)$-Skyrmion with odd winding number has the potential to energetically stabilize a spacetime with a type I defect. But besides

the δ-singularity in the Ricci tensor there is yet another singularity on which we comment in depth in the next chapter.

9. Nontrivial topology and singularity theorems

We presented numerical results of the Einstein-Skyrme equations in the previous chapter. Now, we show that these spacetimes are singular. First, in Section 9.1, we show that the Ricci scalar contains a δ-function centered at the defect. To find this δ-function we use the methods developed in Section 5.2.3. Recall that we showed there that the space M_{I} equipped with an (almost) flat metric has a diverging Ricci scalar. In fact, there exist theorems in general relativity that assert a singularity in a spacetime with nontrivial topology. We state these theorems in Section 9.2 (without proofs). In Section 9.3 we show that the spacetime containing a type I defect satisfies all the prerequisites of these theorems. Therefore, the divergence of the Ricci scalar is tied to the nontrivial topology of the spacetime. As the singularity theorems require matter with positive energy, a way to circumvent them is to allow for a negative energy density. For this reason we consider an additional term in the matter Lagrangian that gives a negative contribution to the energy. However, the search for smooth solutions of the Einstein-Skyrme equations has thus far yielded no results.

9.1. Singularity in the spacetime with a spherical defect

We have seen in Section 8.2 that components of the Ricci tensor are singular at the defect. We now show that the Ricci scalar also has a singularity at the defect. Since it is a property of a scalar, this divergence does not arise from a mere choice of bad coordinates. Again, we use coordinates (Y, Z, X) to discuss various quantities at the defect. They are defined in equation (5.30). Recall that, in these coordinates, points on the defect have $Y = 0$ and $Y \in (-\infty, \infty)$. In these coordinates the *Ansatz* for the metric we have been using thus far reads

$$ds^2 = -\mathrm{e}^{\nu(\mathrm{x}_{\mathrm{def}}+|Y|)}\mathrm{d}T^2 + \mathrm{e}^{\lambda(\mathrm{x}_{\mathrm{def}}+|Y|)}\mathrm{d}Y^2 + (\mathrm{x}_{\mathrm{def}} + |Y|)^2 \left[\mathrm{d}Z^2 + \sin^2 Z\, \mathrm{d}Y^2\right] .$$

Here, the defect parameter is defined by $\mathrm{x}_{\mathrm{def}} \equiv feb$ and all lengths are in units of $1/fe$. The Ricci scalar R of this metric is then seen to be

$$\begin{aligned} R = &- \frac{4\mathrm{e}^{-2\lambda(\mathrm{x}_{\mathrm{def}}+|Y|)}}{\mathrm{x}_{\mathrm{def}}+|Y|}\left[2+\mathrm{x}_{\mathrm{def}}\nu'(\mathrm{x}_{\mathrm{def}}+|Y|)\right]\delta(Y) \\ &+ \frac{2\mathrm{e}^{-2\lambda(\mathrm{x}_{\mathrm{def}}+|Y|)}}{(\mathrm{x}_{\mathrm{def}}+|Y|)^2}\left(\mathrm{e}^{2\lambda(\mathrm{x}_{\mathrm{def}}+|Y|)}+1+(\mathrm{x}_{\mathrm{def}}+|Y|)\left\{[\nu'(\mathrm{x}_{\mathrm{def}}+|Y|)-\lambda'(\mathrm{x}_{\mathrm{def}}+|Y|)]\right.\right. \\ &\left.\left.\times[2+(\mathrm{x}_{\mathrm{def}}+|Y|)\nu'(\mathrm{x}_{\mathrm{def}}+|Y|)]-(\mathrm{x}_{\mathrm{def}}+|Y|)\nu''(\mathrm{x}_{\mathrm{def}}+|Y|)\right\}\right). \end{aligned} \tag{9.1}$$

Notice that R contains a term proportional to a δ-function centered at $Y=0$. We encountered a similar problem in Section 5.2.3. There, we discussed two metrics for M_{I}. Both metrics led to a δ-function in the Ricci scalar, but for one the coefficient in front of the singularity turned out to be identically zero. Here, this coefficient in equation (9.1) would vanish if

$$\nu'(\mathrm{x}_{\mathrm{def}}) = -2/\mathrm{x}_{\mathrm{def}}\,. \tag{9.2}$$

But from the field equation for ν, equation (6.25) (with $F(\mathrm{x}_{\mathrm{def}})=n\pi$, $\lambda(\mathrm{x}_{\mathrm{def}})=0$, and $\gamma\equiv 0$), we get

$$\nu'(\mathrm{x}_{\mathrm{def}}) = \begin{cases} 2\pi\eta F'(\mathrm{x}_{\mathrm{def}})^2\mathrm{x}_{\mathrm{def}} & ,n \text{ even} \\ 2\pi\eta\left[(4+{\mathrm{x}_{\mathrm{def}}}^2)F'(\mathrm{x}_{\mathrm{def}})^2/\mathrm{x}_{\mathrm{def}} - 8(1+{\mathrm{x}_{\mathrm{def}}}^2)/{\mathrm{x}_{\mathrm{def}}}^3\right] & ,n \text{ odd} \end{cases}. \tag{9.3}$$

When the winding number n is even, equation (9.3) yields a *positive* derivative of ν whereas equation (9.2) requires a *negative* one. For n odd, the square bracket in equation (9.3) could at least become negative, but it turns out that this is not the case for the numerical solutions discussed in the last chapter. Hence, we conclude that it is not possible to make the coefficient of the δ-function vanish.

In fact, there exist several singularity theorems regarding spacetimes with a nontrivial topology. We will state these theorems in the next section, and use them to conclude that the diverging Ricci scalar is a consequence of the nontrivial topology. However, these theorem can be circumvented if the matter field has some "exotic" properties.

9.2. Singularity theorems

Several singularity theorems exist for general relativity, even though it is not possible to define a singularity of spacetime rigorously [17, 22].

Before we give the precise definitions needed for the singularity theorems, we develop an intuitive picture, capturing the ideas behind them. Naively, one could define a singularity of spacetime as a place where geometric quantities like the Ricci scalar diverge. But when geometric quantities are not defined at a place, a metric cannot be defined there either. And without a metric, there is no spacetime. Therefore, the singularity theorems of general relativity "only" prove the existence of the "holes" left behind by a spacetime singularity.

To do this, the theorems prove the existence of so-called incomplete geodesics. Loosely speaking, a geodesic is incomplete if it reaches the "edge" of spacetime in a finite amount of proper time. Thus the spatial infinity of Minkowski spacetime is not a singularity, because any particle needs an infinite amount of proper time to reach it. On the other hand, particles can reach the (nonexistent) value $r = 0$ of the Schwarzschild metric in a finite amount of proper time.

As with all theorems, the singularity theorems require some assumptions. Since the theorems concern the behavior of geodesics, some assumptions on the geometry of spacetime are required. In general relativity the geometry is linked to the matter content via Einstein's equations. It turns out that one of the assumptions for the occurrence of incomplete geodesics is that matter is not "exotic". Here, matter is considered exotic if, for example, it has negative energy density. Furthermore, the spacetime must not allow for "time travel". Since the energy condition is satisfied for the baryonic and dark matter in our universe, and there is not the slightest evidence that "time travel" is possible, the theorems prove that incomplete geodesics are present inside a black hole and at the big bang.

In particular, Gannon showed [5] that a spacetime with a nonsimply connected spatial hypersurface has incomplete geodesics. As with the other singularity theorems, Gannon's theorem requires matter not to be "exotic". Building upon this result, it was shown [6] that the "active probing" of the nontrivial topology is not allowed either. Roughly, this means that all geodesics that start at infinity in the past and arrive at infinity in the future lie in the topologically trivial part. Therefore, an experimenter at infinity cannot probe the topology by sending out test particles that pass through the nontrivial part of spacetime and which return afterwards. The view of the nontrivial topology is "censored" from the experimenter, and therefore the theorem is known as the topological censorship theorem. The *theorem* also gives support to Penrose's censorship *conjecture*. The latter conjectures that *all* singularities are hidden behind an event horizon (the possible exception being initial singularities like the big bang).

We now state the above mentioned theorems, together with all definitions required.

First of all, we say that a curve is *causal* if it is not spacelike. Thus, two events that can be connected by either a particle's or a photon's world line can influence each other. Following [17], we define a *future endpoint* p of a future directed causal curve λ in a spacetime M if for every neighborhood O of p there exists a parameter t_0 such that $\lambda(t) \in O$ for all $t > t_0$. The curve is said to be future *inextendible* if it has no future endpoint. A curve is *incomplete* if it is inextendible but only has a finite range of affine parameter. For example, the geodesic of a massive particle inside a Schwarzschild black hole is incomplete because the would-be endpoint $r = 0$ is not present in the spacetime, and as the particle approaches $r = 0$ its proper time remains finite.

The remaining definitions are given in [5]. A *partial Cauchy surface* S is a spacelike hypersurface without an edge, and is called a *Cauchy surface* if it also has the property that every causal curve in M intersects S. The importance of Cauchy

surfaces is that they serve as initial hypersurfaces. Given a three-metric (together with a lapse function and a shift vector) and all matter fields on a Cauchy surface it is possible to solve Einstein's equations with these initial conditions to yield a four-dimensional spacetime. A manifold S is said to be *nonsimply connected* if its first fundamental group is nontrivial. As mentioned in Sections 5.1.2 and 5.1.3, this statement means that nonsimply connected manifolds contain closed curves that cannot be continuously shrunk to a point.

Next, we define the convergence c of a congruence of geodesics. A family of geodesics is a *congruence* in S if through each point of S there passes precisely one geodesic. Here, we consider a congruence of timelike geodesics normal to S. This means that the tangent vectors ξ of each geodesic are timelike, normal to S and have unit length. Then the *convergence* c of the congruence is defined by

$$c \equiv -\nabla_a \xi^a \,.$$

Here, $a = 1, 2, 3$, because the condition of the ξ's being normal to S effectively reduces them to three-dimensional vectors. We mention in passing that the negative of c is called the expansion of the congruence [17]. The convergence c is a measure for how fast nearby geodesics approach or separate from each other if $c > 0$ or $c < 0$ respectively. It also plays a key role in many singularity theorems. For example, consider a sphere inside a Schwarzschild black hole. It turns out that the convergence of *both* in- and out-going geodesics emanating from this sphere is positive [22]. This clearly signals that something strange is going on, since normally one finds the negative and positive convergence for the in- and out-going geodesics, respectively.

Gannon introduced the notion of a spacelike hypersurface S that is regular at infinity. For S to be *regular at infinity*, it must satisfy the following three conditions [5]

1. $S = \bigcup_{i=1}^{\infty} W_i$, where each W_i is a compact-three manifold whose boundary ∂W_i is homeomorphic to a sphere.

2. S with the interior of any W_i removed is homeomorphic to $\partial W_i \times \mathbb{R}^+$, where $\mathbb{R}^+$ denotes the set of positive reals.

3. The inward directed null geodesics orthogonal to ∂W_i have positive convergence.

In essence, such an S allows the region with nontrivial topology to be surrounded by spheres that are "well-behaved", i.e. the inward directed geodesics are converging[1]. A spacetime that is asymptotically flat satisfies all these requirements (except for the compactness) [17].

[1]The example of a sphere in the interior of a Schwarzschild black hole shows that this need not always be the case.

The last definition needed for the singularity theorem is the weak energy condition. The matter energy momentum tensor is said to satisfy the *weak energy condition* if for every timelike vector ξ

$$T_{\mu\nu}\xi^\mu\xi^\nu \geq 0\,. \tag{9.4}$$

Since $T_{\mu\nu}\xi^\mu\xi^\nu$ is the energy density seen by an observer with four-velocity ξ, equation (9.4) states that the energy density must be positive (or zero) for all observers.

Finally, we have all ingredients to state Gannon's singularity theorem, a proof of which can be found in [5].

Theorem 9.1 *(*Gannon's theorem*) Let (M,g) satisfy the [weak] energy condition and have a partial Cauchy surface S nonsimply connected and regular near infinity. Then if $c > 0$ everywhere on S, (M,g) is not timelike geodesically complete.*

Here, the positive convergence refers to the inward directed geodesics. Essentially, theorem 9.1 states that a static, asymptotically flat manifold M containing a nonsimply connected three-manifold has a singularity. Notice that the theorem requires matter to satisfy the weak energy condition.

Before we show that our spacetime with a type I defect satisfies all the prerequisites of theorem 9.1, we state one more theorem concerning spacetimes with nontrivial topology.

Again, we have to introduce some definitions to state the topological censorship theorem [6]. First, a spacetime M is *globally hyperbolic* if it has a Cauchy surface S. So, a globally hyperbolic spacetime arises from the evolution of suitable initial conditions. Next, we introduce future and past null infinity together with the definition for asymptotic flatness. M is *asymptotically flat* if

1. There is a conformal completion $\tilde{M}$ of M such that $\tilde{M}$ is compact and with metric $\tilde{g} = \Omega g$, where g is the metric of M and Ω is positive.

2. The boundary $\mathcal{J} \equiv \tilde{M} - M$ is a disjoint union of *future* and *past null infinity* $\mathcal{J}^+$ and $\mathcal{J}^-$. Each null infinity has the topology $\mathbb{R} \times S^2$. The conformal factor Ω vanishes on $\mathcal{J}$ but has non vanishing null divergence.

This represents the intuitive notion of infinity as spheres with "large" r at each instant of time t. In a Minkowski spacetime all light rays (null geodesics) start at past null infinity $\mathcal{J}^-$ and end at $\mathcal{J}^+$. For a Schwarzschild black hole the event horizon prevents some light rays from reaching future null infinity.

Instead of the weak energy condition, the topological censorship theorem only requires matter to satisfy the *averaged null energy condition*. It states that the integral of the energy density along any null geodesic with tangent vector k and affine parameter λ must be positive

$$\int T_{\mu\nu}k^\mu k^\nu \,\mathrm{d}\lambda \geq 0\,. \tag{9.5}$$

The last ingredient for the topological censorship theorem is a timelike curve γ_0 from past to future null infinity, which lies in the simply connected part of $\mathcal{J}$. We

are now in the position to state the topological censorship theorem, a proof of which can be found in [6].

Theorem 9.2 *(*Topological censorship theorem*) If an asymptotically flat, globally hyperbolic spacetime (M,g) satisfies the averaged null energy condition, then every causal curve from $\mathcal{J}^-$ to $\mathcal{J}^+$ is deformable to γ_0 rel[ative to] $\mathcal{J}$.*

Thus, if an experimenter remaining at infinity tries to actively detect the nontrivial topology by sending out test particles she will find that all particles that return follow paths that can continuously be deformed to her own world line. Particles that traverse a topologically nontrivial portion of spacetime never return.

The two theorems can be summarized by saying that an asymptotically flat spacetime with nontrivial topology where matter has positive energy has a singularity (Gannon's theorem) and the view of the nontrivial topology is censored from an outside observer (topological censorship theorem). Next, we show how our spacetime with a type I defect fits into this picture.

First of all, we showed in Section 6.1 that the spacetime with a type I defect has the topology $\mathbb{R}\times\mathrm{SO}(3)-\{\text{point}\}$. Every spatial hypersurface has the topology of $SO(3)$ and we showed in Section 5.2.2 that $SO(3)$ is nonsimply connected. The main prerequisite of the singularity theorems, a nonsimply connected spatial hypersurface, is thus satisfied.

Our metric g approaches the flat Minkowski metric sufficiently fast as r approaches infinity. In fact, we showed in Section 6.4 that g_{tt} and g_{rr} are inverse to each other in this limit. Hence, far away from the defect the metric approaches a Schwarzschild metric, and the latter is known to be flat asymptotically. The compact sets W_i needed in the definition of regularity at infinity consist of all points with radius $b \leq r \leq r_i$. Once the interior of such a W_i is removed, the resulting space has a radial coordinate in the range $r_i \leq r < \infty$ and the sphere of radius r_i as a boundary. (Recall that this surgery corresponds to the first step in the construction of the type I defect.) Also, the convergence turns out to be positive for inward directed geodesics. Therefore, our spacetime is asymptotically flat and regular near infinity. From proposition 6.9.2 of [22] it follows that it is also globally hyperbolic.

Now we consider the weak energy condition. We gave the expression for the energy density seen by a static observer, where it equals T_{00}, in equation (6.27). Recall that we are still using $\gamma = 0$ and, then, T_{00} is seen to be positive. Using the explicit expressions for the remaining components, it is not difficult to show that $T_{\mu\nu}\xi^\mu\xi^\nu \geq 0$ for any timelike ξ. Therefore, the weak energy condition is satisfied by our matter field. The weak energy condition also implies the null energy condition, and hence the averaged null energy conditions is satisfied as well.

We have seen that a spacetime with a type I defect satisfies all assumptions of the two singularity theorems. Therefore, Gannon's theorem asserts the existence of incomplete timelike geodesics. This means that at least one particle can "end its existence" in a finite amount of proper time. The way the particle's existence ends is that it encounters the singularity of the Ricci scalar, given in equation (9.1). Given our matter with positive energy density and the spacetime with the topology

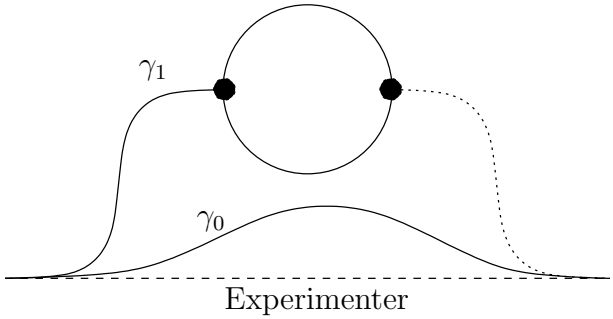

Figure 9.1.: Curves illustrating the topological censorship theorem. An experimenter at infinity sends out two test particles, which travel on paths γ_0 and γ_1. The particle following path γ_0 does not hit the defect and returns to the observer. Notice that γ_0 can be continuously deformed into the observer's world line. The other particle follows γ_1 and hits the defect, where it encounters the singularity in the Ricci scalar. Hence it does not return to the observer. Notice that if γ_1 were amended by the dotted path, it would be a path that is *not* deformable to the observer's world line. This illustrates that all particles that return to an observer at infinity lie in the topologically trivial part of the spacetime.

of $SO(3)$, the singularity *had* to occur. Gannon's theorem is thus seen to be the reason for the δ-function in equation (9.1).

The singularity also effectively censors the observation of the defect. Consider an experimenter far away from the defect who sends out two test particles (see figure 9.1). One particle does not pass through the defect and returns to the experimenter (curve γ_0 in figure 9.1). In agreement with the topological censorship theorem, this curve is deformable to the experimenter's world line. The other particle hits the defect, where it encounters the singularity (curve γ_1 in figure 9.1). Hence, it cannot continue its journey and does not return to the experimenter. Therefore, the experimenter cannot actively probe the nontrivial topology and the view of the defect is censored. Notice that if γ_1 were amended by the dotted curve in figure 9.1, the path would not be deformable to the experimenter's world line.

9.3. Circumventing the singularity theorems

We have seen that singularities always occur in spacetimes that have a nontrivial topology and where the energy density of matter is positive. Since the spacetime with a type I defect does have nontrivial topology, and the energy density of the $SO(3)$-Skyrme field is positive, the Ricci scalar contains a δ-function centered at the defect (see equation (9.1)). To make the coefficient in front of the δ-function vanish, the condition in equation (9.2) needs to be imposed. The spacetime would then be smooth. The singularity theorems then imply that the spacetime cannot be flat asymptotically. We conclude that we must have *negative* matter energy density

if we want a smooth, asymptotically flat spacetime with nontrivial topology.

In our model Lagrangian, equation (8.1), we have thus far only used the kinetic- and Skyrme term. This results in a positive energy density (see discussion at the end of Section 6.4). The inclusion of the additional fourth-order term to the Lagrangian yields terms that give a negative contribution to the energy density. With these additional terms we can in principle achieve a negative density, and circumvent the singularity theorems this way.

The task is now to solve Eqs .(6.24)–(6.25) with $\gamma > 0$. As before, the boundary conditions for the profile function F and the metric are

$$\begin{aligned} F(x_{\mathrm{def}}) = n\,\pi, \quad F(\infty) = 0\,, \\ \nu(\infty) = 0, \qquad \lambda(\infty) = 0\,. \end{aligned} \tag{9.6}$$

The first condition ensures that the matter field is compatible with the topology at the defect and the second gives a vanishing energy density at infinity. That spacetime is asymptotically flat is ensured by the remaining two conditions. Also, for the spacetime to be smooth at the defect, we must have

$$\nu'(\mathrm{x}_{\mathrm{def}}) = -2/\mathrm{x}_{\mathrm{def}}\,. \tag{9.7}$$

Now, $\nu'(\mathrm{x}_{\mathrm{def}})$ also needs to satisfy the field equation (6.25). Together, equations (9.7) and (6.25) yield a nontrivial relation. We use this relation to solve for $\lambda(\mathrm{x}_{\mathrm{def}})$ instead of simply setting $\lambda(\mathrm{x}_{\mathrm{def}})$ to zero. Therefore our initial condition for λ is

$$\lambda(\mathrm{x}_{\mathrm{def}}) = f(\mathrm{x}_{\mathrm{def}}, F'(\mathrm{x}_{\mathrm{def}}), \gamma, \eta)\,, \tag{9.8}$$

where f is a transcendental function of $\mathrm{x}_{\mathrm{def}}$, $F'(\mathrm{x}_{\mathrm{def}})$, γ, and η. Since f is essentially a logarithm of square roots, the requirement that the arguments be positive leads to further relations between the shooting parameter $F'(\mathrm{x}_{\mathrm{def}})$ and the model parameters $\mathrm{x}_{\mathrm{def}}$, γ, and η.

"All" that is left to do is to solve the field equations subject to the conditions of equations (9.6)–(9.8). Unfortunately, this is not as simple as it sounds. For one thing, we showed in Section 5.2.3 that even the "flat" Minkowski metric has a singularity at the defect. Therefore, we cannot start from a known flat space solution and then slowly increase η to obtain a gravitating $SO(3)$-Skyrmion. Instead, we expect some minimal η to exist, below which no solutions occur. Furthermore, with $\gamma > 0$, the coefficient in front of F'' in the field equation (6.24a) can become zero. Since the field equations for F and λ are coupled, such a zero leads to λ approaching $-\infty$. This could very well be a consequence of the topological censorship theorem. Namely, if there is no singularity at the defect, and the averaged null energy condition is still satisfied, then an event horizon must form around the defect. Otherwise, an experimenter could view the defect by sending particles through it and detecting them later. λ approaching $-\infty$ would then signal that we approach the event horizon from the inside. (Recall that we start at $\mathrm{x}_{\mathrm{def}}$ and evolve to ∞.)

We conclude with one remark. In Section 8.2 we found that the Ricci tensor contains a singular part that is not sourced by the matter field. Since this singularity

contributes to the mass via M_{def} we interpreted it as the energy needed to create a type I defect out of Minkowski spacetime. From equation (8.18) we see that the singular part is proportional to $\nu'(\mathrm{x}_{\text{def}})$. Thus, even if the spacetime were smooth at the defect, which is the case if $\nu'(\mathrm{x}_{\text{def}}) = -2/\mathrm{x}_{\text{def}}$, the Ricci tensor would still be singular and M_{def} would not vanish. This further supports our interpretation that M_{def} cannot be explained by the field equations of general relativity themselves, but requires a theory which describes dynamical changes in topology.

10. Summary of Part III

Part III investigated two types of spacetimes with nontrivial topology, and whether general relativity admits these kind of spacetimes as solutions of the field equations. We started by reviewing wormhole spacetimes and how they can arise as solutions to Einstein's equations. The focus in the remainder of Part III was on another class of spacetime: a spacetime containing a type I defect. Due to its topological properties we argued that an $SO(3)$-valued scalar field would be needed to obtain this spacetime as a solution of Einstein's equations.

We investigated wormholes in Chapter 4. A wormhole connects asymptotic regions of spacetime via a throat. In particular, we concentrated on inter-universe wormholes. These wormholes connect two different asymptotic regions of spacetime. One of the earliest wormhole solutions was found by Einstein and Rosen in 1935 [16] and is now known as the Einstein-Rosen bridge. A closer inspection revealed that no particle could actually cross the bridge. It was several decades later, in 1988, that Morris and Thorne [2] found a wormhole solution that is traversible. By this, it is meant that a particle can actually pass through the wormhole in a reasonable amount of time and without encountering a singularity. In general such traversible wormholes are unstable under small perturbations. It was for this reason that Sushkov and Kim [19] considered a wormhole supported by a scalar field. The potential of the field was chosen in such a way that the field had some properties of a kink. In particular, a kink-like solution is stable because of its topological properties. These properties do not change under small perturbations. Hence, the scalar field acts as a "crutch" for the wormhole.

In the remaining chapters of Part III we considered spacetimes with topological defects. Our main focus was a defect constructed by removing a ball from $\mathbb{R}^3$ and identifying antipodal points on the would-be boundary. The three-space resulting from this "surgery" is called M_{I} and the radius of the cut-out-ball the defect parameter. We proved in Chapter 5 that M_{I} is a three-dimensional manifold. Furthermore, we showed that it shares many topological properties with $SO(3)$, the group of rotations in $\mathbb{R}^3$. It turned out that it is not possible to equip M_{I} with a Minkowski metric, because of a singularity in the Ricci scalar curvature at the defect. We showed that a metric with constant curvature, however, does not have a singular curvature.

Since we want the defect to be an isolated system in a smooth spacetime, a curved metric at the defect must become flat at large distances. Therefore, we added a matter field to the spacetime in order to "iron out" the curvature at infinity via Einstein's equations. The field had to be compatible with the topology of the spacetime and, therefore, we introduced an $SO(3)$-valued scalar field in Chapter 6.

The field's Lagrangian was that of a Skyrme model. It turned out that the model allowed for field configurations that have an integer winding number. We refer to these configurations as $SO(3)$-Skyrmions, and the winding number is a topological invariant: it cannot change under small perturbations. Therefore, the hope was that the $SO(3)$-Skyrmion acts like a "crutch" for the defect in a similar fashion as the kink and the wormhole discussed in Chapter 4.

Since the Einstein-Skyrme equations constitute a coupled set of nonlinear equations, we first investigated the Skyrme model on a fixed background metric in Chapter 7. First, we considered the standard, flat, Minkowski background metric. We solved the field equations numerically in this case. It turned out that the field's energy depends on the winding number and the defect parameter. If the winding number is even, the energy approaches that of a standard $SU(2)$-Skyrmion in the limit of vanishing defect parameter. This is so because an $SO(3)$-valued field with even winding number is equivalent to an $SU(2)$-valued field with half that winding number. If the winding number is odd, however, the energy diverges for a vanishing defect parameter. In this case there exists a finite defect parameter that minimizes the energy. Since the Minkowski metric contains a singular Ricci scalar curvature, we also discussed a smooth metric with constant curvature. In this case, the field equations could be solved analytically. Again we found a finite defect parameter that minimizes the energy.

We considered gravitating $SO(3)$-Skyrmions in Chapter 8. For this, we solved the Einstein-Skyrme equations numerically. Again the mass depended on the winding number and the defect parameter. When the winding number is even, the model reproduces all known results for gravitating $SU(2)$-Skyrmions. The mass is again minimized for a finite defect parameter when the winding number is odd. In this way, the $SO(3)$-Skyrmion does indeed act as a "crutch" for the defect. However, unlike for the flat case, the mass does not diverge for vanishing defect parameters. Instead, an event horizon forms at a minimal defect parameter. A closer look at the different mass contributions revealed that not all of the mass is sourced by the matter field. We interpret this spurious mass as the energy needed to create such a defect (i.e. the energy needed to "drill" a hole in Minkowski spacetime).

The spacetimes constructed in Chapter 8 are all plagued by a singular Ricci scalar curvature. This is due to the singularity theorems discussed in Chapter 9. These theorems can be summarized as follows: an asymptotically flat spacetime with nontrivial topology where the energy density of matter is positive must develop a singularity. The only way to circumvent these theorems without giving up either asymptotic flatness or nontrivial topology is to add matter that yields a negative energy density. That the energy density does indeed become negative near the throat of a traversible wormhole was already found by Morris and Thorne. It is possible to add an additional term to the matter Lagrangian of the Skyrme model that always yields a negative contribution to the energy density. As a result the field equations become even more complicated and one more undetermined parameter is introduced. Therefore, the question of whether general relativity does admit a spacetime with a type I defect is still open.

Part IV.

Phenomenology of Classical Spacetime Foam Models

11. General defect construction and boundary conditions

The construction of the spacetime defects always follow the same cut-and-glue procedure. Following [7], the starting point is three-dimensional Euclidean space. The first step is to remove an open set from this Euclidean space. For the defects considered in this thesis these regions will be either balls or tubes. The geometrical quantities that describe these shapes, such as the radius of the ball, will be referred to as defect parameters. In the next step, points on the resulting boundary are identified. Thus, the resulting space Σ does not have a boundary, but can have nontrivial topological properties. Finally, Σ becomes a spatial hypersurface in the four-dimensional spacetime M which has the structure $\mathbb{R} \times \Sigma$. Furthermore, we will assume that the spacetime metric is simply given by the Minkowski metric.

After the first step of removing an open region, points on the boundary are identified according to

$$\boldsymbol{x} \sim I(\boldsymbol{x}) \equiv \boldsymbol{x}' \,, \tag{11.1}$$

where $I(\boldsymbol{x})$ is an involution. A function I is an involution if it is its own inverse, or $I(I(x)) = x$. Here, this property ensures that the identified point of $\boldsymbol{x}'$ is $\boldsymbol{x}$ again. Besides the removed region, the specific form of the involution determines all other properties of the resulting spacetime. For example, the defects of Chapters 13 and 14 are both constructed by removing an open ball, but because of the different identifications one spacetime is simply connected while the other is not.

The identification of the "boundary points" also induces an identification of the tangent spaces at $\boldsymbol{x}$ and $\boldsymbol{x}'$. To obtain the identification rule for vectors, we decompose a vector $\boldsymbol{v}$ at $\boldsymbol{x}$ into its normal and tangential parts with respect to the original surface

$$\boldsymbol{v}(\boldsymbol{x}) \equiv \boldsymbol{v}_{\text{norm}} + \boldsymbol{v}_{\text{tang}} \,.$$

Because the differential I_* of the identification I maps tangent vectors at $\boldsymbol{x}$ to tangent vectors at $\boldsymbol{x}'$ we use it to identify the tangential part of vectors at identified points. That is, the tangential part $\boldsymbol{v}_{\text{tang}}$ at $\boldsymbol{x}$ is identified with $\boldsymbol{v}'_{\text{tang}}$ at $\boldsymbol{x}'$ via

$$\boldsymbol{v}_{\text{tang}}(\boldsymbol{x}) \sim \boldsymbol{v}\,'_{\text{tang}}(\boldsymbol{x}') \equiv I_*(\boldsymbol{x})\boldsymbol{v}_{\text{tang}}(\boldsymbol{x}) \,. \tag{11.2}$$

Given two tangential basis vectors $\boldsymbol{e}_1$ and $\boldsymbol{e}_2$ (for example $\hat{\theta}$ and $\hat{\phi}$ in spherical coordinates) the outward pointing normal basis vector $\boldsymbol{n}$ at $\boldsymbol{x}$ given by $\boldsymbol{n} \equiv \boldsymbol{e}_1 \times \boldsymbol{e}_2$. Hence the normal part of $\boldsymbol{v}$ is given by

$$\boldsymbol{v}_{\text{norm}}(\boldsymbol{x}) \equiv v_n(\boldsymbol{x})\boldsymbol{n}(\boldsymbol{x}) \equiv \boldsymbol{v}(\boldsymbol{x}) \cdot \boldsymbol{n}(\boldsymbol{x})\, \boldsymbol{n}(\boldsymbol{x}) \,.$$

Since $\boldsymbol{e}_i$ $(i = 1, 2)$ is identified with $\boldsymbol{e}'_i$ we have the following identification of the normal basis vector at $\boldsymbol{x}$ and $\boldsymbol{x}'$

$$\boldsymbol{n}(\boldsymbol{x}) \equiv \boldsymbol{e}_1(\boldsymbol{x}) \times \boldsymbol{e}_2(\boldsymbol{x}) \sim \boldsymbol{e}'_1(\boldsymbol{x}') \times \boldsymbol{e}'_2(\boldsymbol{x}') \equiv \boldsymbol{n}'(\boldsymbol{x}')\,, \tag{11.3}$$

and equation (11.3) finally leads to the identification rule for $\boldsymbol{v}_{\text{norm}}$ at $\boldsymbol{x}$ and $\boldsymbol{x}'$

$$\boldsymbol{v}_{\text{norm}}(\boldsymbol{x}) \sim \boldsymbol{v}'_{\text{norm}}(\boldsymbol{x}') = \boldsymbol{v}(\boldsymbol{x}') \cdot \boldsymbol{n}'(\boldsymbol{x}')\, \boldsymbol{n}'(\boldsymbol{x}')\,. \tag{11.4}$$

Equations (11.2) and (11.4) must be satisfied by all vector fields at the defect and hence impose nontrivial boundary conditions. In particular, these conditions must be satisfied by the electric field. They apply to the magnetic field with a slight modification, due to its pseudo-vector character.

For a Dirac spinor $\psi(\boldsymbol{x}, t)$ we require that ψ at $\boldsymbol{x}$ is related to ψ at the identified point $\boldsymbol{x}'$ by

$$\psi(t, \boldsymbol{x}') = S(\boldsymbol{x})\psi(t, \boldsymbol{x})\,, \tag{11.5}$$

where S is a 4×4 matrix. To obtain some properties of S, we investigate the probability four-current (j^μ) of the Dirac spinor. Its components are defined by

$$j^\mu \equiv \bar{\psi}\gamma^\mu\psi \equiv \psi^\dagger(\mathbb{1}, \boldsymbol{\alpha})\psi\,,$$

where the three 4×4 matrices $\boldsymbol{\alpha}$ are given by

$$\boldsymbol{\alpha} = \begin{pmatrix} 0 & \boldsymbol{\sigma} \\ \boldsymbol{\sigma} & 0 \end{pmatrix}$$

in terms of the 2×2 Pauli matrices $\boldsymbol{\sigma}$.

First, we want the probability density j^0 at $\boldsymbol{x}$ to equal the probability density at $\boldsymbol{x}'$. Explicitly, this means

$$\begin{aligned} & j^0(\boldsymbol{x}) = j^0(\boldsymbol{x}') \\ \Leftrightarrow\ & \psi^\dagger(\boldsymbol{x})\, \psi(\boldsymbol{x}) = \psi^\dagger(\boldsymbol{x}')\, \psi(\boldsymbol{x}') \\ \Leftrightarrow\ & \psi^\dagger(\boldsymbol{x})\, \psi(\boldsymbol{x}) = \psi^\dagger(\boldsymbol{x})\, S^\dagger(\boldsymbol{x})S(\boldsymbol{x})\psi(t, \boldsymbol{x}) \end{aligned}$$

where we have used equation (11.5) to express $\psi(\boldsymbol{x}')$ in terms of $\psi(\boldsymbol{x})$ in the last line. But this means that S must be a unitary matrix

$$S^\dagger(\boldsymbol{x})S(\boldsymbol{x}) = \mathbb{1}\,. \tag{11.6}$$

Second, an important property of the probability four-current is that it is a vector and, hence, its spatial part $\boldsymbol{j}$ must satisfy equations (11.2) and (11.4) as well. Thus, S must satisfy three more constraints imposed by the identification. We will make these constraints more specific once we have given the identification maps in the following chapters.

Finally, we mention another nontrivial property of S. Of course, equation (11.5) must also hold, when it is evaluated at the point $\boldsymbol{x}'$:

$$\psi(t, \boldsymbol{x}) = S(\boldsymbol{x}')\psi(t, \boldsymbol{x}') \,. \tag{11.7}$$

Replacing $\psi(t, \boldsymbol{x}')$ above with the r.h.s of equation (11.5) yields

$$\psi(t, \boldsymbol{x}) = S(\boldsymbol{x}')S(\boldsymbol{x})\psi(t, \boldsymbol{x}) \,.$$

Therefore, $S(\boldsymbol{x}')S(\boldsymbol{x})$ must be the unit matrix and, because of the unitarity of S, we finally have that

$$S(\boldsymbol{x}') = S^\dagger(\boldsymbol{x}) \,. \tag{11.8}$$

To summarize the above findings: The tangential part of any vector field must satisfy equation (11.2), whereas the normal part must respect equation (11.4). These equations lead to three boundary conditions at the defect. For a Dirac spinor we require that the spinor at $\boldsymbol{x}$ is related to the spinor at the identified point $\boldsymbol{x}'$ by a unitary matrix S that must also satisfy equation (11.8). Finally, three more conditions on S are imposed by demanding that the spatial part of the probability current must satisfy equations (11.2) and (11.4).

12. From a single defect to classical spacetime foam

We discussed how to construct a single spacetime defect in the previous chapter. Now, we build a spacetime foam out of many such defects, based on the work by Bernadotte and Klinkhamer [7]. We explain the mechanism by which a classical spacetime foam leads to macroscopic dispersion relations for electromagnetic waves and Dirac spinors.

Recall that we assume spacetime to be flat Minkowski spacetime away from a single defect. After the creation of the first defect we can, therefore, create a second defect far away from the first. Here, "far" means that the separation l between the two defects is much larger than their individual defect parameters b. Next, we add a third defect far away from the other two. Finally, then, our model of a spacetime foam is obtained by adding many defects at positions $\boldsymbol{x}_i$. Furthermore, we assume that the defects are homogeneously distributed and that their separation l is always much larger than the defect parameter b. Since $b \ll l$ our foam is a dilute gas of defects.

We show in the following two sections how such a spacetime foam model leads to modifications of the dispersion relations for electromagnetic waves and Dirac fermions. In the limit where the wavelength is much larger than the defect parameter the spacetime foam acts like an ordinary medium with a wavelength-dependent index of refraction.

12.1. Dispersion relation for electromagnetic waves

Since spacetime is still Minkowski spacetime away from the defect, we know that plane waves with wave vector $\boldsymbol{k}$ are valid solutions to Maxwell's equations. Hence, the electric- and magnetic field will, respectively, be given by

$$\begin{aligned} \boldsymbol{E}_{\mathrm{pw}}(t, \boldsymbol{x}) &= \mathrm{Re}\, \boldsymbol{E}_0 \exp(\mathrm{i}\boldsymbol{k} \cdot \boldsymbol{x} - \mathrm{i}\omega t)\,, \\ \boldsymbol{B}_{\mathrm{pw}}(t, \boldsymbol{x}) &= \mathrm{Re}\, \boldsymbol{B}_0 \exp(\mathrm{i}\boldsymbol{k} \cdot \boldsymbol{x} - \mathrm{i}\omega t)\,. \end{aligned}$$

Here, $\boldsymbol{E}_0$ and $\boldsymbol{B}_0$ are constant vectors such that $(\boldsymbol{k}, \boldsymbol{E}_0, \boldsymbol{B}_0)$ are pairwise orthogonal.

However, when we discuss specific defect examples in Chapters 13–15, we will see that these plane waves do *not* satisfy the boundary conditions at the defects. Therefore, correction fields $\boldsymbol{E}_c$ and $\boldsymbol{B}_c$ have to be added to the plane wave solutions, such that the sum satisfies the boundary conditions.

We will find in Chapters 13 and 14 that the correction field for the electric field is approximately given by a dipole field $\boldsymbol{p}$. Phrased differently, a single defect responds to the incoming plane wave by emitting dipole radiation. Following Section 4.5 of [43] we define the polarizability α of a defect by

$$\boldsymbol{E}_c \sim \boldsymbol{p} = \alpha \boldsymbol{E}_{\text{pw}} \,, \tag{12.1}$$

where α can either be a scalar or tensor quantity. In this way, it is possible to assign a microscopic polarizability to a single defect. Since the spacetime foam was constructed using the dilute gas approximation, we can use the Clausius-Mossotti relation to obtain the electric permittivity ϵ. Namely, the microscopic quantity α is related to the macroscopic ϵ by

$$\frac{\epsilon - 1}{\epsilon + 2} = \frac{n\alpha}{3} \,,$$

where n denotes the number density of defects. Inverting this we obtain

$$\epsilon = \frac{1 + 2n\alpha/3}{1 - n\alpha/3} = 1 + n\alpha + \mathcal{O}\left((n\alpha)^2\right) \,, \tag{12.2}$$

where we have used the assumption that the defects are very dilute ($n \ll 1$) in the last step.

Since essentially the same reasoning applies to the magnetic field as well, we will see in Chapters 13–15 that the magnetic correction field is also given by a dipole field $\boldsymbol{p}$. Hence, we define the magnetic moment β of the defect by

$$\boldsymbol{B}_c \sim \boldsymbol{p} = \beta \boldsymbol{B}_{\text{pw}} \,.$$

Again using the dilute gas approximation, we find that the magnetic permeability μ is given by

$$\mu = 1 + n\beta + \mathcal{O}\left((n\alpha)^2\right) \,. \tag{12.3}$$

The two macroscopic quantities ϵ and μ then allow us to calculate the index of refraction $n(k)$ via

$$n(k) \equiv \sqrt{\epsilon(k)\mu(k)} \,, \tag{12.4}$$

where we have emphasized that the permittivity ϵ and permeability μ may both be functions of the wave number $k \equiv |\boldsymbol{k}|$. Equation (12.4) has the interpretation that a classical spacetime foam composed of microscopic defects acts like an ordinary medium with an index of refraction that depends on the wave number.

Finally, we obtain the dispersion relation via

$$\omega^2(\boldsymbol{k}) = \frac{c^2 k^2}{n^2(k)} = \frac{c^2 k^2}{\epsilon(k)\mu(k)} \,. \tag{12.5}$$

If ϵ and μ depend on the wave vector then equation (12.5) gives a dispersion relation that is modified compared to its form in empty Minkowski space.

12.2. Dispersion relation for Dirac spinors

As for the electromagnetic field, we find that a plane wave solution of the Dirac equation does not satisfy the boundary conditions at a single defect. We, therefore, add a correction spinor to the plane wave, such that the sum satisfies the boundary condition. Here, we are interested in a Dirac fermion of very high energy compared to its rest mass m. Its wavelength is also supposed to be much larger than the defect parameter b and defect separation l:

$$m \ll k \ll 1/l \ll 1/b\,.$$

An initial solution to the free Dirac equation

$$\mathrm{i}\partial_t \psi(t,\boldsymbol{x}) = (-\mathrm{i}\boldsymbol{\alpha}\cdot\nabla + m\,\beta)\,\psi(t,\boldsymbol{x})\,,$$

where the matrices $\boldsymbol{\alpha}$ and β are defined in Appendix B, is a plane wave traveling in the positive z direction:

$$\psi_{\mathrm{pw}}(t,\boldsymbol{x}) \sim \exp\left(ikz - i\omega t\right) \begin{pmatrix} 1 \\ 0 \\ 1 \\ 0 \end{pmatrix}\,, \tag{12.6}$$

which, however, will turn out not to satisfy the boundary condition

$$\psi(t,\boldsymbol{x}'_{\mathrm{def}}) = S(\boldsymbol{x}_{\mathrm{def}})\psi(t,\boldsymbol{x}_{\mathrm{def}})\,. \tag{12.7}$$

Here, $\boldsymbol{x}_{\mathrm{def}}$ denotes a point on the defect and $\boldsymbol{x}'_{\mathrm{def}}$ its identified point. Therefore, we have to add a correction spinor $\psi_c(t,\boldsymbol{x})$ such that the total spinor

$$\psi_{\mathrm{tot}}(t,\boldsymbol{x}) \equiv \psi_{\mathrm{pw}}(t,\boldsymbol{x}) + \psi_c(t,\boldsymbol{x})\,, \tag{12.8}$$

satisfies the boundary condition.

To find $\psi_c(t,\boldsymbol{x})$, let us first investigate $\psi(t,\boldsymbol{x})_{\mathrm{pw}}$ for a point on the defect. Provided that the typical extent of the defect is small compared to the particle's wavelength we have, to lowest order in $\boldsymbol{k}\cdot\boldsymbol{x}_{\mathrm{def}}$,

$$\psi_{\mathrm{pw}}(t,\boldsymbol{x}_{\mathrm{def}}) \sim \exp\left(-i\omega t\right) \begin{pmatrix} 1 \\ 0 \\ 1 \\ 0 \end{pmatrix}\,. \tag{12.9}$$

Thus, the plane wave at the defect is, to lowest order, constant in space. We then make the following *Ansatz* for the correction spinor

$$\psi_c(t,\boldsymbol{x}) = g(r)\,S^\dagger(\boldsymbol{x})\psi_{\mathrm{pw}}(t,\boldsymbol{x}_{\mathrm{def}})\,. \tag{12.10}$$

Here, $r \equiv |\boldsymbol{x}|$ and $g(|\boldsymbol{x}_{\rm def}|) = 1$. Provided that S satisfies

$$S^\dagger(\boldsymbol{x}') = S(\boldsymbol{x})\,, \tag{12.11}$$

the spinor in equation (12.8) satisfies the boundary condition in equation (12.7). Namely, the right hand side of equation (12.7) becomes

$$\begin{aligned} S(\boldsymbol{x}_{\rm def})\psi_{\rm tot}(t,\boldsymbol{x}_{\rm def}) &= S(\boldsymbol{x}_{\rm def})\psi_{\rm pw}(t,\boldsymbol{x}_{\rm def}) + S(\boldsymbol{x}_{\rm def})S^\dagger(\boldsymbol{x}_{\rm def})\psi_{\rm pw}(t,\boldsymbol{x}_{\rm def}) \\ &= \psi_{\rm pw}(t,\boldsymbol{x}_{\rm def}) + S(\boldsymbol{x}_{\rm def})\psi_{\rm pw}(t,\boldsymbol{x}_{\rm def})\,. \end{aligned} \tag{12.12}$$

By virtue of equation (12.11) the left hand side of equation (12.7) is given by

$$\psi_{\rm tot}(t,\boldsymbol{x}'_{\rm def}) = \psi_{\rm pw}(t,\boldsymbol{x}_{\rm def}) + S(\boldsymbol{x}_{\rm def})\psi_{\rm pw}(t,\boldsymbol{x}_{\rm def})\,, \tag{12.13}$$

where we have also used the fact that the plane wave spinor is, to lowest order, constant at the defect.

As was shown in the previous chapter, the explicit form of $S(\boldsymbol{x})$ needs to be determined such that the probability four-current has the correct transformation property at a single defect. Once we have determined $S(\boldsymbol{x})$ we immediately obtain the correction spinor from equation (12.10). In a spacetime foam we sum up the correction spinors of the individual defects. Given the explicit expressions for the correction spinors, we will see that this sum averages to zero. Therefore, only the plane wave contribution does not vanish on scales much larger than the defect separation. The result is that the dispersion relation of a Dirac fermion is not modified compared to its form in Minkowski spacetime.

13. Model I: sphere with antipodal points identified

13.1. Defect construction

Following the general procedure in Chapter 11 we start the construction by removing all interior points of a spatial ball of radius b. In the rest of this chapter we will use spherical polar coordinates (r, θ, ϕ) and let $(\hat{n}, \hat{\theta}, \hat{\phi})$ denote the usual right-handed set of normal basis vectors.

In the second step we identify antipodal points on the boundary – i.e. the general identification equation (11.1) now becomes

$$\boldsymbol{x}_{\text{def}} \sim I(\boldsymbol{x}\text{def}) \equiv \boldsymbol{x}'_{\text{def}} \equiv -\boldsymbol{x}_{\text{def}} \,. \tag{13.1}$$

Via this identification we have constructed a type I defect. For the topological properties of the resulting space see Section 5.2.3. This type of defect is also discussed in [7], where it is called a $\tau = 1$ defect. Unless stated otherwise, all points are supposed to be on the defect. Since $I(\boldsymbol{x}) = -\boldsymbol{x}$, its differential is $I_*(\boldsymbol{x}) = -\mathbb{1}$. Hence, the rule for the identification of tangential parts of a vector, equation (11.2), now takes on the following form

$$\boldsymbol{v}_{\text{tang}}(\boldsymbol{x}) \sim \boldsymbol{v}\,'_{\text{tang}}(-\boldsymbol{x}) \equiv -\boldsymbol{v}_{\text{tang}}(\boldsymbol{x}) \,.$$

In particular, we have

$$\hat{\theta}(\boldsymbol{x}) \sim \hat{\theta}'(-\boldsymbol{x}) \equiv -\hat{\theta}(\boldsymbol{x}) = -\hat{\theta}(-\boldsymbol{x}) \,, \tag{13.2a}$$

$$\hat{\phi}(\boldsymbol{x}) \sim \hat{\phi}'(-\boldsymbol{x}) \equiv -\hat{\phi}(\boldsymbol{x}) = \hat{\phi}(-\boldsymbol{x}) \,, \tag{13.2b}$$

for the tangential basis vectors $\hat{\theta}$ and $\hat{\phi}$. From equation (11.4) this implies

$$\hat{n}(\boldsymbol{x}) \sim \hat{n}'(\boldsymbol{x}') \equiv \hat{\theta}'(-\boldsymbol{x}) \times \hat{\phi}'(-\boldsymbol{x}) = \hat{n}(\boldsymbol{x}) = -\hat{n}(\boldsymbol{x}') \,. \tag{13.3}$$

Notice that the direction of the identified vectors is reversed with respect to to the original vectors in equations (13.2a) and (13.2b), whereas the *outward* pointing normal at $\boldsymbol{x}$ is identified with the *inward* pointing normal at $-\boldsymbol{x}$. The identifications (13.2a)–(13.3) are shown in figure 13.1. Notice that the normal part "goes through" the defect, while the tangential part changes direction. This also means that if the tangential part at $\boldsymbol{x}$ points to another point $\boldsymbol{y}$ on the defect, then its identified vector at $\boldsymbol{x}'$ points to $\boldsymbol{y}'$.

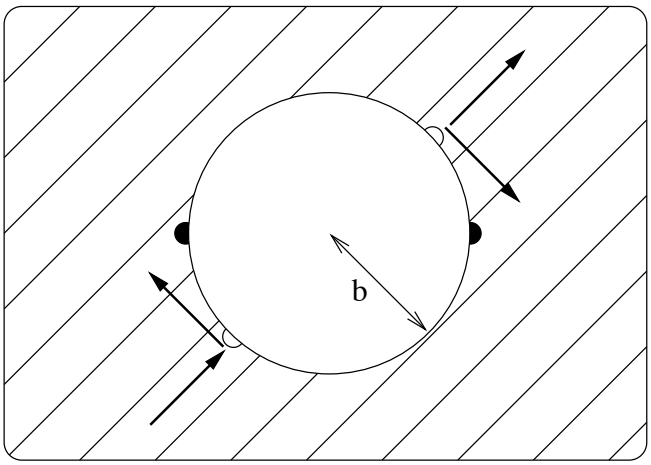

Figure 13.1.: Identification of the tangential and normal part of a vector at the defect with antipodal points identified. Notice that, in accord with equation (13.3), the normal part "goes through" the defect, while the tangential part, in agreement with equations (13.2a) and (13.2b), changes direction. This also means that if the tangential part at $\boldsymbol{x}$ points to another point $\boldsymbol{y}$ on the defect, then its identified vector at $\boldsymbol{x}'$ points to $\boldsymbol{y}'$.

It is useful to express the identifications (13.2a)–(13.3) in terms of components. To this goal we write

$$\boldsymbol{v}(\boldsymbol{x}) = \boldsymbol{v}_{\text{norm}}(\boldsymbol{x}) + \boldsymbol{v}_{\text{tang}}(\boldsymbol{x}) = v_n(\boldsymbol{x})\hat{n}(\boldsymbol{x}) + v_\theta(\boldsymbol{x})\hat{\theta}(\boldsymbol{x}) + v_\phi(\boldsymbol{x})\hat{\phi}(\boldsymbol{x})\,, \tag{13.4}$$

and

$$\begin{aligned}\boldsymbol{v}'(-\boldsymbol{x}) = \boldsymbol{v}'_{\text{norm}}(-\boldsymbol{x}) + \boldsymbol{v}'_{\text{tang}}(-\boldsymbol{x}) =& v'_n(-\boldsymbol{x})\hat{n}'(-\boldsymbol{x}) + v'_\theta(-\boldsymbol{x})\hat{\theta}(-\boldsymbol{x}) \\ &+ v'_\phi(-\boldsymbol{x})\hat{\phi}'(-\boldsymbol{x})\,.\end{aligned} \tag{13.5}$$

To be explicit, the components $v_n(\boldsymbol{x})$ and $v'_n(-\boldsymbol{x})$ are defined by $\hat{n}(\boldsymbol{x}) \cdot \boldsymbol{v}(\boldsymbol{x})$ and $\hat{n}'(-\boldsymbol{x}) \cdot \boldsymbol{v}(-\boldsymbol{x})$, respectively. Similar equations hold for the other components. But since the vectors in equations (13.4) and (13.5) are the same we must have

$$\begin{aligned} v_n(\boldsymbol{x}) &= v'_n(\boldsymbol{x}')\,, \\ v_\theta(\boldsymbol{x}) &= v'_\theta(\boldsymbol{x}')\,, \\ v_\phi(\boldsymbol{x}) &= v'_\phi(\boldsymbol{x}')\,. \end{aligned}$$

To rewrite the right hand side in terms of the *coordinate* basis at $\boldsymbol{x}'$ we use

$$\begin{aligned} \hat{n}'(-\boldsymbol{x}) &= -\hat{n}(-\boldsymbol{x}) \\ \hat{\theta}'(-\boldsymbol{x}) &= -\hat{\theta}(-\boldsymbol{x}) \\ \hat{\phi}'(-\boldsymbol{x}) &= \hat{\phi}(-\boldsymbol{x})\,. \end{aligned}$$

Thus we obtain the boundary conditions, to be satisfied by any vector field, expressed in terms of the *coordinate* basis as

$$v_n(\boldsymbol{x}) = -v_n(-\boldsymbol{x})\,, \tag{13.6a}$$
$$v_\theta(\boldsymbol{x}) = -v_\theta(-\boldsymbol{x})\,, \tag{13.6b}$$
$$v_\phi(\boldsymbol{x}) = +v_\phi(-\boldsymbol{x})\,. \tag{13.6c}$$

The meaning of equation (13.6a) is that if a vector points inwards at $\boldsymbol{x}$ it must point outwards at $\boldsymbol{x}'$, which is nothing but the meaning of equation (13.3) expressed in coordinates. Equations (13.6b) and (13.6c) express the property that if a vector at $\boldsymbol{x}$ points to to another point $\boldsymbol{y}$ on the defect, then its identified vector at $\boldsymbol{x}'$ points to $\boldsymbol{y}'$. Recall that equations (13.6a)–(13.6c) were also derived in Section 5.2.2.

13.2. Electromagnetic field

The boundary conditions in equations (13.6a)–(13.6c) apply for the electric field $\boldsymbol{E}(\boldsymbol{x})$ as well. Since the magnetic field $\boldsymbol{B}(\boldsymbol{x})$ is dual to the electric field, its boundary conditions are the negative of the conditions for $\boldsymbol{E}(\boldsymbol{x})$. Thus, we have

$$E_n(\boldsymbol{x}) = -E_n(-\boldsymbol{x})\,, \qquad B_n(\boldsymbol{x}) = +B_n(-\boldsymbol{x})\,, \tag{13.7a}$$
$$E_\theta(\boldsymbol{x}) = -E_\theta(-\boldsymbol{x})\,, \qquad B_\theta(\boldsymbol{x}) = +B_\theta(-\boldsymbol{x})\,, \tag{13.7b}$$
$$E_\phi(\boldsymbol{x}) = +E_\phi(-\boldsymbol{x})\,, \qquad B_\phi(\boldsymbol{x}) = -B_\phi(-\boldsymbol{x})\,. \tag{13.7c}$$

By construction, spacetime is simply Minkowski spacetime away from the defect, and plane waves are solutions to the Maxwell equations in vacuum. Here we choose a plane wave propagating in the positive z-direction with the electric field parallel to the x-axis:

$$\boldsymbol{E}_{\text{pw}}(t, \boldsymbol{x}) = \operatorname{Re} E_0 \exp(\mathrm{i}kz - \mathrm{i}\omega t)\hat{x}\,,$$
$$\boldsymbol{B}_{\text{pw}}(t, \boldsymbol{x}) = \operatorname{Re} E_0 \exp(\mathrm{i}kz - \mathrm{i}\omega t)\hat{y}\,.$$

However, a plane wave does not satisfy the boundary conditions in (13.7a)–(13.7c). As mentioned in the previous chapter, we introduce a correction field

$$\boldsymbol{E}_c(t, \boldsymbol{x}) \equiv -\exp(-\mathrm{i}\omega t)\nabla\Phi_c(\boldsymbol{x})$$

such that $\boldsymbol{E}_{\text{tot}} \equiv \boldsymbol{E}_{\text{pw}} + \boldsymbol{E}_c$ fulfills conditions (13.7a)–(13.7c). We now expand $\Phi_c(\boldsymbol{x})$ in spherical harmonics $Y_l^m(\theta, \phi)$ as

$$\Phi_c(r, \theta, \phi) = \sum_{l,m} \frac{A_l^m}{r^{l+1}} Y_l^m(\theta, \phi)\,.$$

To find the coefficients a_l^m, we expand the components of $\boldsymbol{E}_{\text{pw}}$ and $\boldsymbol{E}_c$ in spherical harmonics as well. We then choose them in such a way that $\boldsymbol{E}_{\text{tot}}$ satisfies conditions

(13.7a)–(13.7c). It turns out that the coefficients of $\Phi_c(\boldsymbol{x})$ must be given by

$$A_l^m = \begin{cases} \sqrt{\pi}\, m\, \mathrm{i}^{l+1}\, b^{l+2}\, E_0 \sqrt{\frac{l(l+1)}{2l+1}} (j_{l-1}(kb) + j_{l+1}(kb)) & l \text{ odd},\ m = \pm 1 \\ 0 & \text{otherwise} \end{cases} \tag{13.8}$$

Here, b denotes the defect parameter and $j_l(x)$ denotes the lth spherical Bessel function. We see from equation (13.8) that the correction field is, to lowest order in l, given by a dipole with $l = 1$. From equation (13.8) we find that the only nonvanishing dipole moment reads (see Section 4.1 of [43]):

$$p_x = 4\pi b^3 E_0 (j_0(kb) + j_2(kb))\,. \tag{13.9}$$

Note that it is aligned with the external electric field of the plane wave. There is no quadrupole moment because all coefficients with $l = 2$ are zero. Furthermore, higher multipoles will be suppressed because $j_l(kb) \sim (kb)^l$ and $kb \ll 1$. Comparing equation (13.9) with equation (12.1) we see that the polarizability of a single defect is given by

$$\alpha_{\mathrm{I}}(k) = 4\pi b^3 (j_0(kb) + j_2(kb))\,.$$

Via the inverted Clausius-Mossotti relation in equation (12.2) we then obtain the permittivity ϵ

$$\epsilon_{\mathrm{I}}(k) = 1 + 4\pi n b^3 (j_0(kb) + j_2(kb))\,. \tag{13.10}$$

Similarly, we find that the magnetic field of the plane wave does not satisfy the boundary conditions in (13.7a)–(13.7c). Again, we add a magnetic correction field

$$\boldsymbol{B}_c(t, \boldsymbol{x}) \equiv -\exp(-\mathrm{i}\omega t) \nabla \Phi_c(\boldsymbol{x})$$

such that the sum $\boldsymbol{B}_{\mathrm{tot}} \equiv \boldsymbol{B}_{\mathrm{pw}} + \boldsymbol{B}_c$ satisfies the boundary conditions. The potential Φ_c is expanded into spherical harmonics as

$$\Phi_c(r, \theta, \phi) = \sum_{l,m} \frac{B_l^m}{r^{l+1}} Y_l^m(\theta, \phi)\,.$$

Following the same procedure as for the electric field, we obtain for the coefficients

$$B_l^m = \begin{cases} -\sqrt{\pi} \mathrm{i}^l b^{l+2} E_0 \sqrt{\frac{l}{(l+1)(2l+1)}} (j_{l-1}(kb) + j_{l+1}(kb)) & l \text{ odd},\ m = \pm 1 \\ 0 & \text{otherwise} \end{cases}\,. \tag{13.11}$$

Using these coefficients, we find that the only nonvanishing component of the dipole field reads

$$p_y = -2\pi b^3 E_0 (j_0(kb) + j_2(kb))\,.$$

As for the electric field, the magnetic correction is aligned with the magnetic field of the incoming plane wave. No monopole or quadrupole radiation is present and higher multipoles are suppressed. Therefore, the magnetic moment of a single defect is given by

$$\beta_{\mathrm{I}}(k) = -2\pi b^3 (j_0(kb) + j_2(kb))\,,$$

which finally yields

$$\mu_{\mathrm{I}}(k) = 1 - 2\pi n b^3 (j_0(kb) + j_2(kb)) \,. \tag{13.12}$$

Now that we have determined the permittivity $\epsilon_{\mathrm{I}}(k)$ and the permeability $\mu_{\mathrm{I}}(k)$ we can use equation (12.5) to calculate the macroscopic dispersion relation for a spacetime foam composed of type I defects

$$\omega_{\mathrm{I}}^2(k) = \frac{c^2k^2}{\epsilon_{\mathrm{I}}(k)\mu_{\mathrm{I}}(k)} = \frac{c^2k^2}{\{1 + 4\pi n b^3[j_0(kb) + j_2(kb)]\}\{1 - 2\pi n b^3[j_0(kb) + j_2(kb)])\}} \,. \tag{13.13}$$

Keeping in mind that the number density of defects is $n \sim 1/l^3$ and that the spacetime foam is very dilute ($b \ll l$) we have $nb^3 \ll 1$. Since the wavelength $\lambda \sim 1/k$ of the plane wave is supposed to be much larger than the defect parameter b we have $kb \ll 1$ as well. We can, therefore, do a Taylor expansion in nb^3 and kb and equation (13.13) yields

$$\omega_{\mathrm{I}}^2(k) = c^2k^2 \left(1 - 2\pi n b^3\right) + \frac{\pi}{5} n b^5 c^2 k^4 + \mathcal{O}\left((nb^3)^2\right) + \mathcal{O}\left((kb)^3\right) \,, \tag{13.14}$$

which agrees with the result given in [7]. Notice that, because the first bracket is less than one, the speed of light is *reduced* compared to the free case. If it were not for the term $\propto k^4$ an experimenter, measuring only light, could not distinguish an empty spacetime from one containing a spacetime foam. Finally, we want to emphasize that equation (13.14) gives a direct link between the microscopic parameters n and b of the spacetime foam and the macroscopic dispersion relation.

13.3. Dirac spinor field

As mentioned in Chapter 11 the Dirac spinor must satisfy the boundary condition in equation (11.5). For the defect model discussed in this chapter it reads

$$\psi(t, -\boldsymbol{x}) = S_{\mathrm{I}}(\boldsymbol{x})\psi(t, \boldsymbol{x}) \,, \tag{13.15}$$

where S_{I} is the appropriate 4×4 matrix for a type I defect.

The boundary conditions in equations (13.6a)–(13.6c) lead to the following transformation properties the components of $\boldsymbol{j}$ in spherical coordinates (r, θ, ϕ):

$$j_n(\boldsymbol{x}) = -j_n(\boldsymbol{x}') \,, \tag{13.16a}$$
$$j_\theta(\boldsymbol{x}) = -j_\theta(\boldsymbol{x}') \,, \tag{13.16b}$$
$$j_\phi(\boldsymbol{x}) = j_\phi(\boldsymbol{x}') \,. \tag{13.16c}$$

With the use of equation (13.15) the four-current at $\boldsymbol{x}'$ is given by

$$j^\mu(t, \boldsymbol{x}') = \psi(t, \boldsymbol{x})^\dagger S(\boldsymbol{x})^\dagger (\mathbb{1}, \boldsymbol{\alpha}) S(\boldsymbol{x}) \psi(t, \boldsymbol{x}) \,. \tag{13.17}$$

In the following, we omit the $\psi^\dagger \dots \psi$ part for sake of brevity. With this convention, we obtain the following from equation (13.16a)

$$\begin{aligned} \hat{n}(\boldsymbol{x}) \cdot \boldsymbol{\alpha} &= -S^\dagger(\boldsymbol{x}) \hat{n}(\boldsymbol{x}\,') \cdot \boldsymbol{\alpha} S(\boldsymbol{x}) \\ \Leftrightarrow \hat{n}(\boldsymbol{x}) \cdot \boldsymbol{\alpha} &= S^\dagger(\boldsymbol{x}) \hat{n}(\boldsymbol{x}) \cdot \boldsymbol{\alpha} S(\boldsymbol{x}) \end{aligned} \tag{13.18}$$

where we have used the fact that $\hat{n}(\boldsymbol{x}') = -\hat{n}(\boldsymbol{x})$. Multiplying from the left with S and using the unitarity of S, equation (13.18) turns into

$$[S(\boldsymbol{x}), \hat{n}(\boldsymbol{x}) \cdot \boldsymbol{\alpha}] = 0\,. \tag{13.19}$$

In the same way we obtain

$$\left\{ S(\boldsymbol{x}), \hat{\theta}(\boldsymbol{x}) \cdot \boldsymbol{\alpha} \right\} = 0\,, \tag{13.20}$$

$$\left\{ S(\boldsymbol{x}), \hat{\phi}(\boldsymbol{x}) \cdot \boldsymbol{\alpha} \right\} = 0\,. \tag{13.21}$$

A unitary matrix satisfying equations (13.19)–(13.21) is

$$S_{\mathrm{I}}(\boldsymbol{x}) \equiv \mathrm{i} \hat{x} \cdot \boldsymbol{\alpha}\,, \tag{13.22}$$

with $\hat{x} \equiv \boldsymbol{x}/|\boldsymbol{x}| = \hat{n}$. The proof follows from equations (B.2a) and (B.2b) in Appendix B. Furthermore, using the fact that $\boldsymbol{\alpha}$ are hermitian matrices and that $\hat{n}(-\boldsymbol{x}) = -\hat{n}(\boldsymbol{x})$ we find that S_{I} satisfies

$$S_{\mathrm{I}}^\dagger(-\boldsymbol{x}) = S_{\mathrm{I}}(\boldsymbol{x})\,,$$

as well. Therefore, the matrix given in equation (13.22) satisfies all required properties. Notice that the parity transformation matrix $S_P = \beta$ does *not* satisfy equation (13.19). Hence, the transformed spinor cannot simply be a spinor reflected at the origin.

As was shown in Section 12.2, the following spinor satisfies the boundary condition in equation (13.15) at the defect

$$\psi_{\mathrm{tot}}(t, \boldsymbol{x}) = \psi_{\mathrm{pw}}(t, \boldsymbol{x}) + g(r)\, S_{\mathrm{I}}^\dagger(\boldsymbol{x}) \psi_{\mathrm{pw}}(t, \boldsymbol{x}_{\mathrm{def}})\,.$$

To satisfy the Dirac equation away from the defect, the function g must be given by

$$g(r) \equiv b^2/r^2\,.$$

All in all, the total spinor for a single defect reads

$$\psi_{\mathrm{tot}}(t, \boldsymbol{x}) \sim \exp\left(\mathrm{i}kz - \mathrm{i}\omega t\right) \begin{pmatrix} 1 \\ 0 \\ 1 \\ 0 \end{pmatrix} - \mathrm{i} \exp(-\mathrm{i}\omega t) \frac{b^2}{r_1^2} \begin{pmatrix} \cos\theta_1 \\ \sin\theta_1 \exp(\mathrm{i}\phi_1) \\ \cos\theta_1 \\ \sin\theta_1 \exp(\mathrm{i}\phi_1) \end{pmatrix}\,, \tag{13.23}$$

where (r_1, θ_1, ϕ_1) are the spherical coordinates of $\boldsymbol{x}$ with respect to the defect center. As for the electromagnetic case, discussed in the previous section, this result agrees with [7].

The next step is to sum over N defects with centers $\boldsymbol{x}_j$ for $j = 1, \cdots, N$:

$$\psi(t, \boldsymbol{x})_{tot} \sim \exp\left(\mathrm{i}kz - i\omega t\right) \begin{pmatrix} 1 \\ 0 \\ 1 \\ 0 \end{pmatrix} - \mathrm{i}\exp(-\mathrm{i}\omega t) \sum_{j=1}^{N} \frac{b^2}{|\boldsymbol{x} - \boldsymbol{x}_j|^2} \begin{pmatrix} \cos\theta_j \\ \sin\theta_j \exp(\mathrm{i}\phi_j) \\ \cos\theta_j \\ \sin\theta_j \exp(\mathrm{i}\phi_j) \end{pmatrix}. \tag{13.24}$$

Here, (θ_j, ϕ_j) are the spherical coordinates of $\hat{x}_j$ with respect to the jth defect center. For many randomly positioned defects ($N \gg 1$) the components of the correction spinors average to zero.

13.4. Summary

The type I spacetime defects discussed in this chapter were created by first removing an open spatial ball of radius b from empty Minkowski spacetime. Antipodal points on the boundary were then identified. Since the spacetime away from the defect is still flat Minkowski spacetime, a dilute spacetime foam was created by "punctuating" Minkowski spacetime by many well-separated defects.

In Section 13.1 we discussed the resulting boundary conditions for a vector field at a single defect. These conditions then have to apply for electric and magnetic fields as well. Since plane waves are solutions to Maxwell's equations between the defects but do not satisfy the boundary conditions, we introduced appropriate correction fields in Section 13.2. Furthermore, we calculated the polarizability and magnetic moment of a single defect. Via the Clausius-Mossotti relation we obtained the macroscopic permittivity and permeability. Finally, we calculated the dispersion relation for electromagnetic waves propagating through a spacetime foam composed of a dilute ensemble of defects. The dispersion relation was found to be different compared to its form in Minkowski spacetime. In particular, the speed of light is lower than in empty Minkowski spacetime and a quartic term exist.

We also calculated the correction spinor for a Dirac fermion in Section 13.3. This correction is necessary because the probability-current of a plane wave solution of the Dirac equation does not satisfy the boundary conditions at a single defect. However, when summed over many defects, these corrections average to zero. Thus, only the initial plane wave solution remains at distances which are large compared to the average defect separation. As a result, the dispersion relation of a Dirac fermion is not modified compared to its form in Minkowski spacetime.

Our results agree with [7], where the present defect type is referred to as a $\tau = 1$ defect.

14. Model II: sphere with mirrored points identified

14.1. Defect construction

The construction of this defect starts in the same way as that of the previous defect. That is, the interior of a sphere with radius b is cut out from $\mathbb{R}^3$. Now, however, a point $\boldsymbol{x}$ on the defect is identified with its mirror image, obtained by mirroring $\boldsymbol{x}$ at an equatorial plane with normal $\hat{a}$. Explicitly, we have

$$\boldsymbol{x}_{\text{def}} \sim \boldsymbol{x}'_{\text{def}} \equiv I(\boldsymbol{x}_{\text{def}}) \equiv (\mathbb{1} - 2\hat{a} \otimes \hat{a})\boldsymbol{x}_{\text{def}} \,. \tag{14.1}$$

For electromagnetic waves, this defect was also discussed in [7], where it is referred to as a $\tau = 2$ defect. In the following, all points are supposed to be on the defect, unless stated otherwise. For a two-dimensional illustration see figure 14.1. Vectors tangent to the sphere are identified via the differential I_* of the identification map. Therefore, we have the following relations between the basis tangent vectors and their identified counterparts

$$\hat{\theta}(\boldsymbol{x}) \sim \hat{\theta}'(\boldsymbol{x}') \equiv I_* \hat{\theta}(\boldsymbol{x}) = \hat{\theta}(\boldsymbol{x}) - 2a_\theta(\boldsymbol{x})\hat{a} \,, \tag{14.2a}$$

$$\hat{\phi}(\boldsymbol{x}) \sim \hat{\phi}'(\boldsymbol{x}') \equiv I_* \hat{\phi}(\boldsymbol{x}) = \hat{\phi}(\boldsymbol{x}) - 2a_\phi(\boldsymbol{x})\hat{a} \,, \tag{14.2b}$$

where $a_\theta(\boldsymbol{x}) \equiv \hat{\theta}(\boldsymbol{x}) \cdot \hat{a}$ and similarly for $a_\phi(\boldsymbol{x})$.

The normal vector $\hat{n}$ is identified with

$$\hat{n}(\boldsymbol{x}) \sim \hat{n}'(\boldsymbol{x}') \equiv \hat{\theta}'(\boldsymbol{x}') \times \hat{\phi}'(\boldsymbol{x}') \,. \tag{14.3}$$

Some algebra then gives the following relation between the identified normal vector $\hat{n}'(\boldsymbol{x}')$ and the normal vector $\hat{n}(\boldsymbol{x}')$

$$\hat{n}'(\boldsymbol{x}') = -\hat{n}(\boldsymbol{x}') \,. \tag{14.4}$$

The identification rules in equations (14.2) and (14.3) then imply the following conditions on the normal and tangential components of a vector field $\boldsymbol{v}(\boldsymbol{x})$.

$$v_n(\boldsymbol{x}) = v'_n(\boldsymbol{x}') \,, \tag{14.5a}$$

$$v_\theta(\boldsymbol{x}) = v'_\theta(\boldsymbol{x}') \,, \tag{14.5b}$$

$$v_\phi(\boldsymbol{x}) = v'_\phi(\boldsymbol{x}') \,, \tag{14.5c}$$

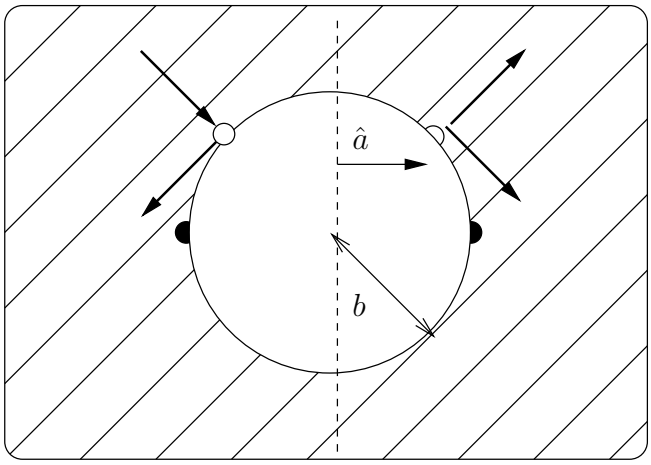

Figure 14.1.: Identification of the tangential and normal part of a vector at the defect with mirrored points identified. Notice that the normal part "goes through" the defect, while the tangential part changes direction. This also means that if the tangential part at $\boldsymbol{x}$ points to another point $\boldsymbol{y}$ on the defect, then its identified vector at $\boldsymbol{x}'$ points to $\boldsymbol{y}'$.

where $v'_n(\boldsymbol{x}') \equiv \hat{n}'(\boldsymbol{x}')\boldsymbol{v}(\boldsymbol{x}')$, etc. are the components of $\boldsymbol{v}(\boldsymbol{x}')$ with respect to the identified basis at $\boldsymbol{x}'$. Notice that, because of equation (14.4), a vector field that satisfies equation (14.5a) points away from the defect at $\boldsymbol{x}'$ if it points towards it at $\boldsymbol{x}$. This allows a particle to "go through" the defect. The last two equations have the interpretation that if a vector at $\boldsymbol{x}$ points to another point $\boldsymbol{y}$ on the defect, then the identified vector at $\boldsymbol{x}'$ points to the identified point $\boldsymbol{y}'$.

14.2. Electromagnetic field

As for the defect discussed in the previous chapter, the boundary conditions in equations (14.5a)–(14.5c) translate into the following conditions for the electric and magnetic field

$$E_n(\boldsymbol{x}) = E'_n(\boldsymbol{x}')\,, \qquad B_n(\boldsymbol{x}) = -B'_n(\boldsymbol{x}')\,, \tag{14.6a}$$
$$E_\theta(\boldsymbol{x}) = E'_\theta(\boldsymbol{x}')\,, \qquad B_\theta(\boldsymbol{x}) = -B'_\theta(\boldsymbol{x}')\,, \tag{14.6b}$$
$$E_\phi(\boldsymbol{x}) = E'_\phi(\boldsymbol{x}')\,, \qquad B_\phi(\boldsymbol{x}) = -B_\phi(\boldsymbol{x}')\,, \tag{14.6c}$$

where, again, the conditions for the magnetic field are dual to those of the electric field. The next steps follow the same pattern as in the previous chapter. That is, we choose the coordinates such that a plane electromagnetic wave vector is parallel to the z-axis, which means that $\boldsymbol{E}_{\mathrm{pw}}$ and $\boldsymbol{B}_{\mathrm{pw}}$ are given by

$$\boldsymbol{E}_{\mathrm{pw}}(t,\boldsymbol{x}) = \mathrm{Re}\, E_0 \exp(\mathrm{i}kz - \mathrm{i}\omega t)\hat{x}\,,$$
$$\boldsymbol{B}_{\mathrm{pw}}(t,\boldsymbol{x}) = \mathrm{Re}\, E_0 \exp(\mathrm{i}kz - \mathrm{i}\omega t)\hat{y}\,.$$

To satisfy the boundary conditions we introduce a correction field $\boldsymbol{E}_c(t,\boldsymbol{x})$, which is derived from the negative gradient of a scalar potential

$$\Phi_c(r,\theta,\phi) = \sum_{l,m} \frac{A_l^m}{r^{l+1}} Y_l^m(\theta,\phi)\,,$$

The coefficients A_l^m need to be determined such that the sum of $\boldsymbol{E}_{\rm pw}$ and $\boldsymbol{E}_c$ satisfies equations (14.6a)–(14.6c). We find for $l=1$

$$A_1^m = \sqrt{\frac{3\pi}{2}} b^3 \left[j_0(kb)+j_2(kb)\right] \begin{cases} -(a_x^2 - \frac{1}{3} - \mathrm{i}a_x a_y), & m=1 \\ \sqrt{2}a_x a_z, & m=0 \\ (a_x^2 - \frac{1}{3} + \mathrm{i}a_x a_y), & m=-1 \end{cases}.$$

Hence, the induced dipole reads

$$\begin{aligned} p_x &= 6\pi b^3 \left[j_0(kb)+j_2(kb)\right] \left(a_x^2 - \frac{1}{3}\right) E_0\,, \\ p_y &= 6\pi b^3 \left[j_0(kb)+j_2(kb)\right] a_x a_y E_0\,, \\ p_z &= 6\pi b^3 \left[j_0(kb)+j_2(kb)\right] a_x a_z E_0\,. \end{aligned}$$

Recalling that $\boldsymbol{p} = \alpha \boldsymbol{E}_{\rm pw}$ and that the electric field is parallel to the x-axis, we obtain for the polarizability α

$$\alpha = 2\pi b^3 \left[j_0(kb)+j_2(kb)\right] (3\hat{a}\otimes\hat{a} - \mathbb{1})\,. \tag{14.7}$$

Since the defect induces a preferred direction $\hat{a}$ the polarizability α is given by a tensor that depends on $\hat{a}$. We now make the assumption that the directions of the individual defects are not aligned[1]. In this case, the off-diagonal elements of α in equation (14.7) average to zero, whereas the diagonal elements yield

$$< a_x^2 >=< a_y^2 >=< a_z^2 >= 1/3\,,$$

and, hence, the polarizability vanishes for many randomly orientated defects. The (inverted) Clausius-Mossotti relation in equation (12.2) then yields a permittivity ϵ of

$$\epsilon_{\rm II} = 1\,,$$

which does not differ from its empty space value.

To satisfy the boundary conditions equations (14.6a)–(14.6c) the magnetic field $\boldsymbol{B}_{\rm pw}$ requires a correction field $\boldsymbol{B}_c$ as well. We again write

$$\boldsymbol{B}_c(t,\boldsymbol{x}) \equiv -\exp(-\mathrm{i}\omega t)\nabla\Phi_c(\boldsymbol{x})\,,$$

[1]For the case of aligned defects see [7]. In this case, the spacetime foam becomes a birefringent medium.

and expand the potential $\Phi_c(\boldsymbol{x})$ into spherical harmonics. The coefficients of this expansion with $l = 1$ read

$$B_1^m = \sqrt{\frac{3\pi}{2}} b^3 \left[j_0(kb) + j_2(kb)\right] \begin{cases} a_x a_y - \mathrm{i}\left(a_y^2 - 2/3\right), & m = 1 \\ -\sqrt{2} a_y a_z, & m = 0 \\ -a_x a_y + \mathrm{i}\left(a_y^2 - 2/3\right), & m = -1 \end{cases} .$$

With these coefficients, we obtain the induced dipole of a single defect as

$$\begin{aligned} p_x &= -6\pi \left(j_0(kb) + j_2(kb)\right) b^3 a_x a_y E_0 \,, \\ p_y &= -6\pi \left(j_0(kb) + j_2(kb)\right) b^3 \left(a_y^2 - 2/3\right) E_0 \,, \\ p_z &= -6\pi \left(j_0(kb) + j_2(kb)\right) b^3 a_z a_y E_0 \,. \end{aligned}$$

Since the magnetic field of the incoming plane wave is parallel to the y-axis we find that the magnetic moment β is given by

$$\beta = -2\pi b^3 \left[j_0(kb) + j_2(kb)\right] \left(3\hat{a} \otimes \hat{a} - 2\mathbb{1}\right) . \tag{14.8}$$

This is similar to the polarizability α in equation (14.7), but notice the factor 2 in front of the unit matrix. It is because of this factor that the averaged magnetic moment does not vanish but yields

$$< \beta >= 2\pi b^3 \left[j_0(kb) + j_2(kb)\right] \mathbb{1} \,.$$

Using equation (12.3) we find for the permeability μ

$$\mu_{\mathrm{II}}(k) = 1 + 2\pi n b^3 \left[j_0(kb) + j_2(kb)\right] \,,$$

which, unlike the permittivity, differs from its form in empty space. Therefore, the dispersion relation of electromagnetic waves propagating through a spacetime foam of nonaligned model II defects reads

$$\omega_{\mathrm{II}}^2(k) = \frac{c^2 k^2}{\epsilon_{\mathrm{II}}(k)\mu_{\mathrm{II}}(k)} = \frac{c^2 k^2}{1 \times \left\{1 + 2\pi n b^3 [j_0(kb) + j_2(kb)]\right\}} \,. \tag{14.9}$$

As in the previous chapter, the dilute gas approximation ($nb^3 \ll 1$) and the assumption that the wavelength is much larger than the defect parameter ($kb \ll 1$) allow us to make a Taylor expansion of equation (14.9). The result is

$$\omega_{\mathrm{II}}^2(k) = c^2 k^2 \left(1 - 2\pi n b^3\right) + \frac{\pi}{5} n b^5 c^2 k^4 + \mathcal{O}\left((nb^3)^2\right) + \mathcal{O}\left((kb)^3\right) \,. \tag{14.10}$$

To the order shown, this result coincides with the dispersion relation of the previous chapter, see equation (14.10) and also [7].

14.3. Dirac spinor field

A Dirac spinor ψ at $\boldsymbol{x}$ is related to the spinor at $\boldsymbol{x}'$ via

$$\psi(t, \boldsymbol{x}') = S(\boldsymbol{x})\psi(t, \boldsymbol{x})\,,$$

where $S(\boldsymbol{x})$ is a unitary 4×4 matrix. The spatial part of the probability four-current reads

$$\boldsymbol{j}(\boldsymbol{x}) \equiv \psi^\dagger(\boldsymbol{x})\boldsymbol{\alpha}\psi(\boldsymbol{x})\,,$$

where the matrices $\boldsymbol{\alpha}$ are defined in Appendix B. Since $\boldsymbol{j}(\boldsymbol{x})$ is also a vector field, its components must also satisfy the boundary conditions (14.5a)–(14.5c). Using equation (14.4) we obtain

$$j_n(\boldsymbol{x}) = -j_n(\boldsymbol{x}')\,, \tag{14.11a}$$
$$j_\theta(\boldsymbol{x}) = j'_\theta(\boldsymbol{x}')\,, \tag{14.11b}$$
$$j_\phi(\boldsymbol{x}) = j'_\phi(\boldsymbol{x}')\,. \tag{14.11c}$$

We rewrite $j(\boldsymbol{x}')$ by using equation (13.17) and drop the $\psi^\dagger \ldots \psi$ part in the following. With this convention, we obtain from equation (14.11a)

$$\begin{aligned} &\hat{n}(\boldsymbol{x}) \cdot \boldsymbol{\alpha} = -S(\boldsymbol{x})^\dagger \hat{n}(\boldsymbol{x}') \cdot \boldsymbol{\alpha} S(\boldsymbol{x}) \\ \Leftrightarrow\ &\hat{n}(\boldsymbol{x}) \cdot \boldsymbol{\alpha} = -S(\boldsymbol{x})^\dagger [\hat{n}(\boldsymbol{x}) - 2a_n(\boldsymbol{x})\hat{a}] \cdot \boldsymbol{\alpha} S(\boldsymbol{x}) \end{aligned} \tag{14.12}$$

where we have used $\hat{n}(\boldsymbol{x}') = \hat{n}(\boldsymbol{x}) - 2\hat{a}\cdot n(\boldsymbol{x})\,\hat{a}$. Multiplying from the left with $S(\boldsymbol{x})$ and using the unitarity of $S(\boldsymbol{x})$, equation (14.12) becomes

$$\{S(\boldsymbol{x}), \hat{n}(\boldsymbol{x}) \cdot \boldsymbol{\alpha}\} = 2a_n(\boldsymbol{x})\,\hat{a} \cdot \boldsymbol{\alpha}\, S(\boldsymbol{x})\,. \tag{14.13}$$

Along the previous lines, equations (14.11b) and (14.11c) yield

$$\left[S(\boldsymbol{x}), \hat{\theta}(\boldsymbol{x}) \cdot \boldsymbol{\alpha}\right] = -2a_\theta(\boldsymbol{x})\,\hat{a} \cdot \boldsymbol{\alpha} S(\boldsymbol{x})\,, \tag{14.14a}$$
$$\left[S(\boldsymbol{x}), \hat{\phi}(\boldsymbol{x}) \cdot \boldsymbol{\alpha}\right] = -2a_\phi(\boldsymbol{x})\,\hat{a} \cdot \boldsymbol{\alpha} S(\boldsymbol{x})\,. \tag{14.14b}$$

A unitary matrix satisfying equations (14.13)–(14.14) is given by

$$S_{\mathrm{II}}(\boldsymbol{x}) \equiv \mathrm{i}(\hat{a} \cdot \boldsymbol{\alpha})\,(\hat{x} \cdot \boldsymbol{\alpha})\,. \tag{14.15}$$

The proof is an application of the rules collected in Appendix B. Finally, we note that $S_{\mathrm{II}}(\boldsymbol{x})$ satisfies

$$S_{\mathrm{II}}^\dagger(\boldsymbol{x}') = S_{\mathrm{II}}(\boldsymbol{x})\,,$$

which follows from $\hat{n}(\boldsymbol{x}') = I_* \hat{n}(\boldsymbol{x})$ and the rules in Appendix B.

Now that we have the matrix S_{II} we can use it in equation (12.8) to obtain the total spinor.

$$\psi(t,\boldsymbol{x})_{tot} \sim \exp\left(\mathrm{i}kz - \mathrm{i}\omega t\right) \begin{pmatrix} 1 \\ 0 \\ 1 \\ 0 \end{pmatrix} - \mathrm{i}\exp(-\mathrm{i}\omega t)\frac{b^2}{r_1^2} \begin{pmatrix} \cos\theta_1\cos\vartheta_1 + \sin\theta_1\sin\vartheta_1\exp(\mathrm{i}(\varphi_1-\phi_1)) \\ \cos\vartheta_1\sin\theta_1\exp(\mathrm{i}\phi_1) - \sin\vartheta_1\cos\theta_1\exp(\mathrm{i}\varphi_1) \\ \cos\theta_1\cos\vartheta_1 + \sin\theta_1\sin\vartheta_1\exp(\mathrm{i}(\varphi_1-\phi_1)) \\ \cos\vartheta_1\sin\theta_1\exp(\mathrm{i}\phi_1) - \sin\vartheta_1\cos\theta_1\exp(\mathrm{i}\varphi_1) \end{pmatrix}. \tag{14.16}$$

Here, (θ_1,ϕ_1) and (ϑ_1,φ_1) are the spherical coordinates of $\hat{x}$ and $\hat{a}$ with respect to the defect center, respectively.

The next step consists of summing over N defects. Their individual mirror planes are given by the normal vectors $\hat{a}_j$, with $i = 1,\ldots,N$.

$$\psi(t,\boldsymbol{x})_{tot} \sim \exp\left(\mathrm{i}kz - \mathrm{i}\omega t\right) \begin{pmatrix} 1 \\ 0 \\ 1 \\ 0 \end{pmatrix} - \mathrm{i}\exp(-\mathrm{i}\omega t)\sum_{j=1}^{N}\frac{b^2}{|\boldsymbol{x}-\boldsymbol{x}_j|^2} \begin{pmatrix} \cos\theta_j\cos\vartheta_j + \sin\theta_j\sin\vartheta_j\mathrm{e}^{\mathrm{i}(\varphi_j-\phi_j)} \\ \cos\vartheta_j\sin\theta_j\mathrm{e}^{\mathrm{i}\phi_j} - \sin\vartheta_j\cos\theta_j\mathrm{e}^{\mathrm{i}\varphi_j} \\ \cos\theta_j\cos\vartheta_j + \sin\theta_j\sin\vartheta_j\mathrm{e}^{\mathrm{i}(\varphi_j-\phi_j)} \\ \cos\vartheta_j\sin\theta_j\mathrm{e}^{\mathrm{i}\phi_j} - \sin\vartheta_j\cos\theta_j\mathrm{e}^{\mathrm{i}\varphi_j} \end{pmatrix}. \tag{14.17}$$

Here, (θ_j,ϕ_j) and (ϑ_j,φ_j) are the spherical coordinates of $\hat{x}_j$ and $\hat{a}_j$ with respect to the jth defect center. As in the previous chapter, the components of the correction spinors average to zero for many randomly positioned defects ($N \gg 1$). Notice that this would happen even if the individual vectors $\hat{a}_j$ were aligned (i.e. if we had constant ϑ_j and φ_j for all defects).

14.4. Summary

The type II defects studied in this chapter were created by removing an open spatial ball from Minkowski spacetime. The identification of points proceeds by reflecting them at an equatorial plane with normal $\hat{a}$. The spacetime foam is then created by "punctuating" Minkowski spacetime with many such defects. We have assumed that the vectors $\hat{a}$ of the individual defects are randomly oriented. To obtain the dispersion relations for electromagnetic fields and Dirac fermions we followed the general procedure described in Chapter 12 and again outlined in the summary of the previous chapter (Section 13.4).

We discussed the electromagnetic field in Section 14.2. Since the defect has a preferred direction given by $\hat{a}$, its microscopic polarizability and magnetic moment turned out to be tensors depending on $\hat{a}$. Averaging over many defects, we found that the polarizability vanished whereas the magnetic moment did not. Hence, only the macroscopic permeability was changed compared to its value in Minkowski spacetime. The resulting dispersion relation was found to approximately equal the one found in Chapter 13. It is also the result found in [7], where the presently discussed defect type is called a $\tau = 2$ defect.

Section 14.3 discussed the correction spinor for a Dirac fermion. We calculated the correction spinor required such that the probability four-current satisfies the boundary conditions at the defect. When summing over many defects the correction spinors averaged to zero. Hence, only the original plane wave spinor remained on scales larger then the defect separation. The dispersion relation of a Dirac fermion is, therefore, not modified.

15. Model III: line defect

15.1. Defect construction

This defect is constructed by removing all interior points of a spatial tube of radius b and length L. We assume that the linear dimension L is much larger than the radius b, so that we can ignore the bottom and lid of the tube. Furthermore, the cylinder axis is denoted by $\hat{a}$. Next, antipodal points on the cylindrical boundary are identified, see figure 15.1. Rotating a point $\boldsymbol{x}_{\text{def}}$ on the cylinder around the cylinder axis $\hat{a}$ by 180° yields its antipodal point. Therefore, we have the following identification rule

$$\boldsymbol{x}_{\text{def}} \sim \boldsymbol{x}'_{\text{def}} \equiv R_{\hat{a}}(\pi)\boldsymbol{x}_{\text{def}} = 2\hat{a} \cdot x_{\text{def}}\, \hat{a} - \boldsymbol{x}_{\text{def}}\,,$$

where we have used equation (6.3) with $\omega = \pi$ and $\hat{n} = \hat{\alpha}$. The differential I_* used to identify vectors tangent to the cylinder is then given by

$$I_* = 2\hat{a} \otimes \hat{a} - \mathbb{1}\,. \tag{15.1}$$

For the electromagnetic waves discussed in Section 15.2 it will be convenient to let the cylinder axis coincide with the z-axis and let the wave vector $\boldsymbol{k}$ be arbitrary. However, when we discuss Dirac fermions in Section 15.3, we will choose the propagation to be along the z-axis and let the cylinder axis $\hat{a}$ be arbitrary. We will give the explicit form of the transformation properties of vectors implied by equation (15.1) in the respective sections. Here, we just mention that we choose them in such a way that they allow a particle to go through the defect, see figure 15.1.

Before we continue, we want to discuss the crucial difference between the defect of this chapter and the ones of the previous two chapters. Namely, by inspecting figure 15.1 we see that a left-handed dreibein entering the defect emerges right-handed. Therefore, the resulting spacetime is nonorientable. Another way to see this is the following. In a plane perpendicular to the cylinder axis the defect corresponds to the two-dimensional defect discussed in Section 5.1. In particular, we showed in Section 5.1.2 that this manifold is nonorientable.

15.2. Electromagnetic field

To obtain the explicit form of the boundary conditions on the electric and magnetic fields we choose the cylinder axis $\hat{a}$ to be parallel to the z-axis, that is $\hat{a} \equiv \hat{z}$. In cylindrical coordinates (ρ, ϕ, z), a point on the defect with coordinates (b, ϕ, z) is

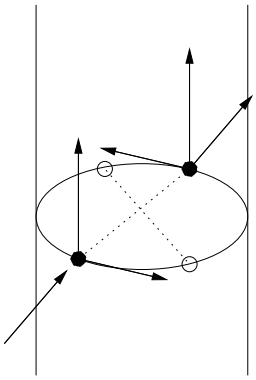

Figure 15.1.: To construct a line defect, a cylinder of radius b is removed from space and antipodal points on the resultant boundary are identified. The identification of vectors is also shown.

then identified with its antipodal point having coordinates $(b, \pi + \phi, z)$. Using I_* from equation (15.1) we obtain the following for the basis vectors $(\hat{\phi}, \hat{e}_z)$, which are tangent to the cylinder,

$$\hat{\phi}(\boldsymbol{x}) \sim \hat{\phi}'(\boldsymbol{x}') \equiv I_* \hat{\phi}(\boldsymbol{x}) = -\hat{\phi}(\boldsymbol{x}) = \hat{\phi}(\boldsymbol{x}')\,, \tag{15.2a}$$

$$\hat{z} \sim \hat{z}' \equiv I_* \hat{z} = \hat{z}\,. \tag{15.2b}$$

These two conditions mean that if a vector at $\boldsymbol{x}$ points to another point $\boldsymbol{y}$ on the defect, than the vector at $\boldsymbol{x}'$ points to $\boldsymbol{y}'$, see figure 15.1. For the normal basis vector $\hat{\rho}$ we have to make the following identification

$$\hat{\rho}(\boldsymbol{x}) \sim \hat{\rho}'(\boldsymbol{x}') \equiv -\hat{\phi}'(\boldsymbol{x}') \times \hat{z}' = -\hat{\rho}(\boldsymbol{x}') = \hat{\rho}(\boldsymbol{x})\,.$$

Notice that the additional minus sign ensures that the outward pointing normal vector $\hat{\rho}(\boldsymbol{x})$ at $\boldsymbol{x}$ is identified with the inward pointing normal $-\hat{\rho}(\boldsymbol{x}')$ at the identified point $\boldsymbol{x}'$. Therefore, we have the following boundary conditions for a vector field $\boldsymbol{v}(\boldsymbol{x})$

$$v_\rho(\boldsymbol{x}) = -v_\rho(\boldsymbol{x}')\,, \tag{15.3a}$$

$$v_\phi(\boldsymbol{x}) = +v_\phi(\boldsymbol{x}')\,, \tag{15.3b}$$

$$v_z(\boldsymbol{x}) = +v_z(\boldsymbol{x}')\,. \tag{15.3c}$$

where $v_\rho(\boldsymbol{x}) \equiv \boldsymbol{v}(\boldsymbol{x}) \cdot \hat{\rho}(\boldsymbol{x})$ and similarly for the other components.

The boundary conditions in equations (15.3a)–(15.3c) imply the following transformation properties of electromagnetic fields at the defect.

$$E_\rho(\boldsymbol{x}) = -E_\rho(\boldsymbol{x}'), \qquad B_\rho(\boldsymbol{x}) = +B_\rho(\boldsymbol{x}') \tag{15.4a}$$

$$E_\phi(\boldsymbol{x}) = +E_\phi(\boldsymbol{x}'), \qquad B_\phi(\boldsymbol{x}) = -B_\phi(\boldsymbol{x}') \tag{15.4b}$$

$$E_z(\boldsymbol{x}) = +E_z(\boldsymbol{x}'), \qquad B_z(\boldsymbol{x}) = -B_z(\boldsymbol{x}')\,, \tag{15.4c}$$

where, as for the other defects, the conditions on the magnetic field are dual to those of the electric field.

Away from the defect spacetime is just Minkowski spacetime. Therefore, plane waves are the solutions of Maxwell's equations. But these do not satisfy the boundary conditions at the defect, and hence correction fields $\boldsymbol{E}_c(\boldsymbol{x})$ and $\boldsymbol{B}_c(\boldsymbol{x})$ need to be introduced. The calculations to obtain these fields are quite involved and are given in Appendix C. The result, however, is quite simple

$$\boldsymbol{E}_c(t,\boldsymbol{x}) = -\boldsymbol{E}_{\mathrm{pw}}(t,\boldsymbol{x})\,, \tag{15.5a}$$

$$\boldsymbol{B}_c(t,\boldsymbol{x}) = -\boldsymbol{B}_{\mathrm{pw}}(t,\boldsymbol{x})\,. \tag{15.5b}$$

Notice that the correction fields are the negative of the plane wave fields, not only at the defect but for *all* points $\boldsymbol{x}$. Hence, the total electromagnetic field vanishes everywhere. This result disagrees with the one in [7], where the line defect is discussed briefly in footnote 20. The two different results trace back to a different identification of the electric and magnetic fields. In this thesis we impose nontrivial conditions on the components parallel to the cylinder (see equation (15.4c)). The conditions leading to the result in [7] are that only the perpendicular components transform nontrivially (see Chapter 6 of [44]).

One reason for the vanishing of the total field might be that the *Ansatz* for the correction fields is too restrictive. Due to the form of the boundary conditions we choose an *Ansatz* involving vector spherical harmonics. Furthermore, the electric and magnetic correction fields are coupled due to Maxwell's equations.

Another reason might be the nonorientability of the spacetime. It implies some restrictions on vector fields that are defined globally. For example, one cannot globally define a *unit* normal vector field on the Möbius strip. One can, however, define a normal vector field provided that is has at least one zero. Here, this could imply that the total electric field vanishes at some point. Via Maxwell's equations this could then lead to a vanishing magnetic field as well.

Certainly, the vanishing of the electromagnetic field on this nonorientable spacetime would be an interesting subject of future research.

15.3. Dirac spinor field

To obtain the correction fields for a Dirac spinor it is useful to let the plane wave propagate in the z-direction. The cylinder axis is given by a unit vector $\hat{a}$. Rotating a point $\boldsymbol{x}$ on the cylinder around the cylinder axis $\hat{a}$ by 180° yields its antipodal point. Therefore, we have the following identification rule

$$\boldsymbol{x} \sim \boldsymbol{x}' \equiv R_{\hat{a}}(\pi)\boldsymbol{x} = 2\hat{a}\cdot x\,\hat{a} - \boldsymbol{x}\,,$$

where we have used equation (6.3) with $\omega = \pi$ and $\hat{n} = \hat{\alpha}$. The differential I_* used to identify vectors tangent to the cylinder is then given by

$$I_* = 2\hat{a}\otimes\hat{a} - \mathbb{1}\,.$$

Since the basis vectors $\hat{\rho}$, $\hat{\phi}$, and $\hat{z}$ are neither strictly normal nor tangent to a cylinder with arbitrary orientation $\hat{a}$ we introduce a new set of normal and tangent basis vectors as follows. For a cylinder whose axis is parallel to the z-axis, the basis vectors $\hat{\phi}$, and $\hat{z}$ are tangent and $\hat{\rho}$ normal to the surface. Now, let $\hat{a}$ be obtained by rotating $\hat{z}$, that is, there exists some rotation matrix D such that

$$\hat{a} = D\hat{z}\,.$$

Acting with this D on the original basis vectors yields the following vectors

$$\hat{a}_\rho(\boldsymbol{x}) \equiv D\hat{\rho}\,, \tag{15.6a}$$
$$\hat{a}_\phi(\boldsymbol{x}) \equiv D\hat{\phi}\,, \tag{15.6b}$$
$$\hat{a} \equiv D\hat{z}\,. \tag{15.6c}$$

Since they are obtained by a rotation of a right-handed dreibein of basis vectors, the vectors defined in equations (15.6a)–(15.6c) also form a right-handed dreibein of basis vectors. Furthermore, $\hat{a}_\rho(\boldsymbol{x})$ is normal to the cylinder, whereas both $\hat{a}_\phi(\boldsymbol{x})$ and $\hat{a}$ are tangent to the cylinder. Now, the basis vectors are identified via

$$\begin{aligned}\hat{a}_\phi(\boldsymbol{x}) \sim \hat{a}'_\phi(\boldsymbol{x}') \equiv I_*\hat{a}_\phi(\boldsymbol{x}) = -\hat{a}_\phi(\boldsymbol{x}) = \hat{a}_\phi(\boldsymbol{x}')\,,\\ \hat{a} \sim \hat{a}'(\boldsymbol{x}') \equiv I_*\hat{a} = \hat{a}\,.\end{aligned}$$

In the last line $\hat{a}$ is identified with itself and this reflects the fact that only points in the plane perpendicular to the cylinder axis are identified. Finally, we have the following for the normal vector

$$\hat{a}_\rho(\boldsymbol{x}) \sim \hat{a}'_\rho(\boldsymbol{x}') \equiv -\hat{a}'_\phi(\boldsymbol{x}') \times \hat{a}'(\boldsymbol{x}') = -\hat{a}_\rho(\boldsymbol{x}') = \hat{a}_\rho(\boldsymbol{x})\,. \tag{15.7}$$

The minus sign is again needed to ensure that the outward pointing normal at $\boldsymbol{x}$ is identified with the inward pointing normal at $\boldsymbol{x}'$. It is a peculiarity of the cylindrical defect because in all the other types of defects the outward pointing normal at $\boldsymbol{x}$ is identified with the inward pointing normal at $\boldsymbol{x}'$. The boundary conditions on the spatial components of the probability current then read

$$j_\rho(\boldsymbol{x}) = j'_\rho(\boldsymbol{x}') = -j_\rho(\boldsymbol{x}')\,, \tag{15.8a}$$
$$j_\phi(\boldsymbol{x}) = j'_\phi(\boldsymbol{x}') = j_\phi(\boldsymbol{x}')\,, \tag{15.8b}$$
$$j_a(\boldsymbol{x}) = j'_a(\boldsymbol{x}') = j_a(\boldsymbol{x}')\,. \tag{15.8c}$$

The first equations express the boundary conditions in terms of the identified basis and the second in terms of the coordinate basis at $\boldsymbol{x}'$. Here, in a slight misuse of notation, the components of the vector field are defined by

$$\boldsymbol{j}(\boldsymbol{x}) = j_\rho(\boldsymbol{x})\hat{a}_\rho(\boldsymbol{x}) + j_\phi(\boldsymbol{x})\hat{a}_\phi(\boldsymbol{x}) + j_a(\boldsymbol{x})\hat{a}\,.$$

As mentioned, the minus sign in equation (15.8a) ensures that a particle really goes through the defect.

Again, the Dirac spinors at $\boldsymbol{x}$ and $\boldsymbol{x}'$ are related by a 4×4 matrix S as

$$\psi(t, \boldsymbol{x}\,') = S(\boldsymbol{x})\psi(t, \boldsymbol{x})\,, \tag{15.9}$$

and the probability four-current is given by

$$j^{\mu}(t, \boldsymbol{x}) = \psi(t, \boldsymbol{x})^{\dagger}(\mathbb{1}, \boldsymbol{\alpha})\psi(t, \boldsymbol{x})\,.$$

The boundary conditions (15.8a)–(15.8c) then translate into

$$[S, \hat{a}_{\rho} \cdot \boldsymbol{\alpha}] = 0\,, \tag{15.10a}$$

$$\{S, \hat{a}_{\phi} \cdot \boldsymbol{\alpha}\} = 0\,, \tag{15.10b}$$

$$[S, \hat{a} \cdot \boldsymbol{\alpha}] = 0\,, \tag{15.10c}$$

where all quantities are evaluated at $\boldsymbol{x}$. A unitary matrix satisfying equations (15.10a)–(15.10c) is

$$S_{\mathrm{III}}(\boldsymbol{x}) = [p\hat{a}_{\phi}(\boldsymbol{x}) \cdot \boldsymbol{\alpha} - q\hat{a} \cdot \boldsymbol{\alpha}\, \hat{a}_{\rho}(\boldsymbol{x}) \cdot \boldsymbol{\alpha}]\beta\,, \tag{15.11}$$

where p and q are any real numbers that satisfy

$$p^2 + q^2 = 1\,.$$

The proof consists of an application of equations (B.3) and (B.4) in Appendix B. Notice the occurrence of β in the definition of equation (15.11). Since β is the representation of the parity operator in spin space (see for instance [45]), we see that equation (15.9) implies that the Dirac spinor receives a reflection in spin space when it passes through the defect. Furthermore, we find that $S_{\mathrm{III}}(\boldsymbol{x})$ satisfies

$$S_{\mathrm{III}}^{\dagger}(\boldsymbol{x}') = S_{\mathrm{III}}(\boldsymbol{x})\,. \tag{15.12}$$

If we now assume that the defect's radius b and linear dimension L is small compared to the wavelength we can approximate the plane wave spinor by the constant spinor in equation (12.9). We then obtain the following for the correction spinor

$$\psi_c(t, \boldsymbol{x}) \sim S_{\mathrm{III}}^{\dagger}(\boldsymbol{x})\psi_{\mathrm{pw}}(t, \boldsymbol{x}_{\mathrm{def}}) \sim (p - \mathrm{i}q) \begin{pmatrix} (\hat{a}_{\phi})_z \\ (\hat{a}_{\phi})_x + \mathrm{i}\,(\hat{a}_{\phi})_y \\ -(\hat{a}_{\phi})_z \\ -(\hat{a}_{\phi})_x - \mathrm{i}\,(\hat{a}_{\phi})_y \end{pmatrix}\,, \tag{15.13}$$

where $(\hat{a}_{\phi})_x$ is the x-coordinate of $\hat{a}_{\phi}$ defined in equation (15.6b), and similarly for the other two components. For the total spinor we thus obtain

$$\begin{aligned} \psi_{\mathrm{tot}}(t, \boldsymbol{x}) \sim & \exp\left(\mathrm{i}\boldsymbol{k} \cdot \boldsymbol{x} - \mathrm{i}\omega t\right) \begin{pmatrix} \begin{pmatrix} 1 \\ 0 \end{pmatrix} \\ \boldsymbol{\sigma} \cdot \boldsymbol{k} \begin{pmatrix} 1 \\ 0 \end{pmatrix} \end{pmatrix} \\ & + \mathrm{i}(p - \mathrm{i}q) \exp(-\mathrm{i}\omega t) \frac{b}{\rho_1} \begin{pmatrix} 0 \\ \exp(\mathrm{i}\phi_1) \\ 0 \\ -\exp(\mathrm{i}\phi_1) \end{pmatrix}\,, \end{aligned} \tag{15.14}$$

where (ρ_1, ϕ_1, z_1) are the cylindrical polar coordinates with respect to the defect's center. Here, we have again used coordinates where the cylinder axis corresponds to the z-axis.

For many randomly oriented line defects, we see from equation (15.13) that the correction spinors of the individual defects average to zero. Even when the defects "conspire" to align themselves, so that defects have the same cylinder axis $\hat{a}$, equation (15.14) implies that the correction spinors average to zero.

We conclude this section by discussing the effect of the parity operator in equation (15.11). Recall that the parity operation transforms the left- and right-handed components of a Dirac spinor into each other (see, for instance, II.3 of [46]). Now, assume that we had discussed a *massless* Dirac fermion. The Dirac equation would then have decoupled into two equations for two Weyl spinors; one for the left-handed Weyl spinor and the other for the right-handed spinor. When passing through the line defect, the parity operator acts on the (massless) Dirac spinor and exchanges the left- and right-handed Weyl spinors. Phrased differently, the defect induces an interaction between the two Weyl spinors. Such an interaction can be described by an effective Lagrangian with a mass term. Hence, the nonorientable defect would induce an effective mass for chiral fermions. This was also the result of an explicit calculation performed in [47], where the defect was a nonorientable wormhole.

15.4. Summary

In this chapter the spacetime defect is created by removing the interior of a tube and then identifying antipodal points on the cylindrical boundary. Unlike the previous two types of defects, the resulting space is nonorientable.

We found the peculiar result that only a vanishing electromagnetic field could satisfy the electromagnetic boundary conditions. As discussed at the end of Section 15.2, this could either be due to a too restrictive *Ansatz* for the correction fields, or be a result of the nonorientable nature of the spacetime. That this result is different from the one obtained in footnote 20 of [7] traces back to different identification rules for the electromagnetic field.

Contrasting with the result for the electromagnetic field, a well defined correction spinor for a Dirac fermion was found. Intuitively, the reason is that the Dirac spinor can make an additional "twist" in spin space to compensate for the "flip" in three-space.

16. Summary of Part IV

Building on the work by Bernadotte and Klinkhamer [7], we showed in Part IV how a foam of spacetime defects affects the propagation properties of electromagnetic waves and Dirac fermions. The spacetime foam was supposed to be a dilute gas of spacetime defects. The wavelength of the electromagnetic waves and fermions was assumed to be much larger then the average defect separation.

Chapter 11 described the general procedure used to construct a single spacetime defect and the resulting boundary conditions on vector and spinor fields. The idea is to start with empty Minkowski spacetime and, then, remove an open spatial region from it. In the next step, points on the resulting boundary are identified. The geometric shape of the cut-out region and the identification rule determine the type of spacetime defect. Spacetimes obtained by this surgery do not have a boundary but have a different topology than the original Minkowski spacetime. We also give the relation between the identification of points and the transformation properties for vector fields on the defect. Furthermore, we state the boundary condition a Dirac spinor field has to satisfy at identified points.

Having discussed the effects of a single defect, Chapter 12 investigates how a spacetime foam of many such defects affects the propagation of electromagnetic waves and Dirac spinors. Such a foam can be created by "punctuating" Minkowski spacetime by many well-separated defects. Since spacetime is assumed to be flat between the defects, plane waves are solutions to Maxwell's and Dirac's equations. As a plane wave does not satisfy the boundary conditions, correction fields were introduced. For the electromagnetic field these correction fields turned out to be given by approximate dipole fields. Hence, a microscopic polarizability and magnetic moment could be assigned to a single defect. Via the Clausius-Mossotti relation the macroscopic permittivity and permeability could be calculated, which yield an index of refraction that depends on the wave vector. In this way, a spacetime foam corresponds to an ordinary medium. To obtain the macroscopic spinor we averaged over the spinorial correction fields of many defects.

Chapters 13–15 then discuss three explicit examples of spacetime defects. The first two defects, discussed in Chapters 13 and 14, are created by removing an open ball. For the defect in Chapter 13 we identify antipodal points on the boundary. The electromagnetic correction fields then yielded a dispersion relation that is different than in empty Minkowski spacetime. The speed of light is reduced compared to its value in Minkowski spacetime and quartic terms exist as well. However, the spinorial correction fields average to zero and, hence, only the plane wave solution exists on macroscopic scales. The dispersion relation for a Dirac spinor is not modified.

For the defect discussed in Chapter 14 the identification rule identified points

that were mirrored at an equatorial plane. The normal to this equatorial plane then defined a preferred direction. However, when the planes of the individual defects are not aligned, the dispersion relation for electromagnetic waves equals the one of Chapter 13. Similarly, we found that the spinorial correction fields averaged to zero, even when the defects were aligned.

Finally, we discussed a line defect in Chapter 15. Unlike the other two defect models, the line defect yields a nonorientable spacetime. We again found that the spinorial correction fields averaged to zero and that only the plane wave spinor "survives" on large scales. However, we found that the electromagnetic field vanishes on this spacetime, which would rule out the existence of such a defect in nature. If this peculiar behavior is indeed due to the non-orientability of this space this would provide evidence for the conjecture of Wheeler [1] that nonorientable spaces do not occur in a spacetime foam.

Part V.

Summary

In this thesis we investigated relations between nontrivial spacetime topologies and modified dispersion relations.

In Part II, we reviewed Wheeler's argument for the existence of a foam-like nature of spacetime at distances comparable to the Planck length. The idea is that quantum mechanical fluctuations in the curvature allow spacetime to change its topology. Spacetime would then constantly tunnel from one topology to another at these length scales. As a result, spacetime would become foam-like. Since a theory to describe such tunneling of spacetime is lacking, we investigated if and how spacetimes with nontrivial topology arise as solutions to Einstein's field equations of general relativity.

We investigated two types of classical spacetimes with nontrivial topology in Part III. First, we reviewed known results of spacetimes that contain wormholes in Chapter 4. As was discovered by Morris and Thorne, general relativity admits traversible wormholes. These are wormholes that can, at least in principle, be crossed by a particle. To stabilize a wormhole Sushkov and Kim introduced a scalar matter field. The field's potential was chosen so that the field acquired kink-like properties. In particular, the field has a topological charge that cannot change under smooth deformations. Therefore, the field acts like a "crutch" for the wormhole.

The second type of spacetimes we considered were spacetimes with a topological defect. A spacetime defect is created with a "surgery" procedure, in which a spatial region is cut out of spacetime, and then points on the boundary are identified. From this point of view, a spacetime defect resembles a dislocation of a single atom in an otherwise regular crystal. We focused on one particular kind of defect in Part III. This type I defect is created by first removing from space an open ball of radius b. In the second step, antipodal points on the boundary are identified. As was shown in Chapter 5, the resulting space M_{I} is still a manifold. Furthermore, we showed that it has the same topological properties as $SO(3)$, the group of rotations in three dimensions. In particular, M_{I} contains noncontractible loops, making it topologically nontrivial. Moreover, we showed that if M_{I} is equipped with the Euclidean metric, the Ricci scalar curvature is singular at the defect. A metric with constant curvature turned out to be smooth instead. Since we wanted the defect to be an isolated system, the spacetime containing it must become flat far away from the defect. The idea was to add a matter field to the spacetime. Via Einstein's equations a matter field could "iron out" the curvature, at least asymptotically.

This matter field should also respect the topology of the spacetime. For this reason, we discussed an $SO(3)$-valued scalar field in Chapter 6. The field's Lagrangian was taken to be that of a Skyrme model. We concluded Chapter 6 with the Einstein-Skyrme equations that describe the evolution of the spacetime metric and the matter field. We first solved the matter field equation in Chapter 7, with the background metric held fixed. For example, we took the background metric to be flat. The energy of the field then depended on the winding number and the defect parameter b. If the winding number is two, then the energy decreases with decreasing defect parameter but remains finite in the limit of vanishing defect parameter. This limiting energy equals that of an $SU(2)$-Skyrmion with winding number one.

However, if the winding number equals one, the field's energy diverges for vanishing defect parameter. Furthermore, we found a finite defect parameter that minimized the energy.

The findings of the nongravitating case essentially carried over to the gravitating case discussed in Chapter 8. Besides the winding number and the defect parameter, the mass also depends on the relative strength of Newton's constant and the Skyrme constant appearing in the matter Lagrangian. For even winding number, our results are the same as those of the gravitating $SU(2)$-Skyrmion discussed in the literature. In particular, the mass approaches a finite value for vanishing defect parameter. When the winding number is one, we found that the mass is again minimized for a finite defect parameter. Now, however, there exists a minimal defect parameter, at which an event horizon forms. Therefore, no solutions with smaller defect parameter exist.

The Ricci tensor, governing the geometry of the spacetime, contains a singular part that has no analogue on the matter side. We showed in Chapter 8 that this singularity contributes to the mass of the system even though it is not caused by the matter field. We interpret this spurious mass as the energy needed to create this specific kind of defect. Clearly, this issue deserves further research.

The Ricci scalar curvature is also singular at the defect. This singularity can be explained by the singularity theorems presented in Chapter 9. Briefly, these theorems assert that an asymptotically flat spacetime with nontrivial topology must have a singularity, provided that the matter energy density is positive. To circumvent these theorems we discussed an additional term in the matter Lagrangian, which always gives a negative contribution to the energy density. The resulting field equations, however, could not be solved thus far. It is, therefore, still open whether general relativity admits this particular kind of spacetime defect as a solution.

Part IV investigates how microscopic spacetime defects influence the macroscopic dispersion relations of electromagnetic waves and Dirac fermions. The three types of defects considered are created by first removing an open region from three-dimensional space and then identifying points on the boundary. Away from the defect spacetime remains flat. The spacetime foam is then modeled by many such well-separated defects.

As shown in Chapter 11, these identifications imply nontrivial boundary conditions on vector and spinor fields. Physically, they ensure that a particle can "pass through" the defect. Since spacetime is still flat away from the defect, plane waves are solutions to Maxwell's equations and the Dirac equation. However, they do not satisfy the boundary conditions at the defect. Therefore, correction fields have to be added, such that the total field satisfies the boundary conditions. How to obtain the modified dispersion relations from these correction fields was the subject of Chapter 12. In the electromagnetic case, the correction fields are, to lowest order, dipole fields. In this way it is possible to assign a microscopic polarizability to a spacetime defect. The Clausius-Mossotti relation can then be used to obtain the macroscopic dielectric constant. The same reasoning leads to a magnetic permeability, and together the two yield the index of refraction. Since this index of refraction generally

depends on the wave vector, the result is a dispersion relation for electromagnetic waves that is different from the one in empty spacetime. In the case of a Dirac fermion the contributions from each individual defect average to zero. The result is an unmodified dispersion relation for a Dirac fermion.

As explicit examples, we discussed two types of defects that were created by first removing an open ball. For the defect discussed in Chapter 13 antipodal points on the boundary were identified. In Chapter 14 points mirrored at an equatorial plane were identified instead. We obtained modified dispersion relations for electromagnetic waves by using the method discussed above. The corrections for the Dirac spinor averaged to zero for many defects.

Finally, Chapter 15 discussed a defect created by removing the interior of a tube and then identifying antipodal points on the cylindrical boundary. As with the previous defect types, we obtained the correction spinor for a Dirac fermion. But we found that the total electromagnetic field vanishes on this spacetime. If this effect is due to the nonorientable nature of this defect, it would provide evidence for Wheeler's conjecture that nonorientable topologies do not occur in a spacetime foam. The origin of this "super-selection rule" might be an interesting subject for future research.

A. Further properties of the $SO(3)$-Skyrme field

In this appendix to Chapter 6 we prove two properties of the $SO(3)$-valued scalar field Ω. The first, proven in Section A.1, is that the gradient of the hedgehog *Ansatz* satisfies the boundary conditions for a vector field at the defect. The second proof, presented in Section A.2, shows that the integer occurring in the boundary of the profile function equals the winding number.

A.1. Gradient of the Skyrme field at the spherical defect

We now show that the gradient $\nabla\Omega$ automatically satisfies the boundary conditions for a vector at the defect, provided Ω is given by the hedgehog *Ansatz*

$$\Omega(\boldsymbol{x}) \equiv R_{\hat{x}}(F(r))$$

and the profile function F satisfies equation (6.8), which we repeat here for convenience

$$F(b) = n\,\pi,\ n \in \mathbb{Z}\,. \tag{A.1}$$

The components of the gradient are given by

$$(\nabla\Omega)^i = g^{ij}\partial_j\Omega\,.$$

Provided that the (inverse) metric is diagonal and continuous at the defect, that is $g^{ij}(\boldsymbol{x}\big|_{r=b}) = g^{ij}(-\boldsymbol{x}\big|_{r=b})$, it suffices to show (see equation (5.38))

$$\partial_r\Omega(\boldsymbol{x}\big|_{r=b}) = -\partial_r\Omega(-\boldsymbol{x}\big|_{r=b})\,, \tag{A.2a}$$
$$\partial_\theta\Omega(\boldsymbol{x}\big|_{r=b}) = -\partial_\theta\Omega(-\boldsymbol{x}\big|_{r=b})\ , \tag{A.2b}$$
$$\partial_\phi\Omega(\boldsymbol{x}\big|_{r=b}) = \partial_\phi\Omega(-\boldsymbol{x}\big|_{r=b})\,. \tag{A.2c}$$

From equation (6.5) we obtain

$$\begin{aligned}
\partial_r\Omega &= F'(r)\left[\sin F(r)(\hat{x}\otimes\hat{x} - \mathbb{1}) + \cos F(r)\hat{x}\cdot\boldsymbol{X}\right]\,,\\
\partial_\theta\Omega &= \sin F(r)\hat{\theta}\cdot\boldsymbol{X} + (1-\cos F(r))(\hat{\theta}\otimes\hat{x} + \hat{x}\otimes\hat{\theta})\,,\\
\partial_\phi\Omega &= \sin F(r)\hat{\phi}\cdot\boldsymbol{X} + (1-\cos F(r))(\hat{\phi}\otimes\hat{x} + \hat{x}\otimes\hat{\phi})\,.
\end{aligned}$$

Using the boundary condition in equation (A.1) for the profile function at the defect, these equations turn into

$$\partial_r \Omega = (-1)^n F'(b) \hat{x} \cdot \boldsymbol{X} \,, \tag{A.3a}$$
$$\partial_\theta \Omega = [1-(-1)^n](\hat{\theta} \otimes \hat{x} + \hat{x} \otimes \hat{\theta}) \,, \tag{A.3b}$$
$$\partial_\phi \Omega = [1-(-1)^n](\hat{\phi} \otimes \hat{x} + \hat{x} \otimes \hat{\phi}) \,. \tag{A.3c}$$

The basis vectors at $\boldsymbol{x}$ and $-\boldsymbol{x}$, however, are related by

$$\begin{aligned} \hat{x}(\boldsymbol{x}) &= -\hat{x}(-\boldsymbol{x}) \,, \\ \hat{\theta}(\boldsymbol{x}) &= \hat{\theta}(-\boldsymbol{x}) \,, \\ \hat{\phi}(\boldsymbol{x}) &= -\hat{\phi}(-\boldsymbol{x}) \,, \end{aligned}$$

from which we see that equations (A.3a) and (A.3b), evaluated at $-\boldsymbol{x}$, gain one minus sign whereas equation (A.3c) remains the same. These are exactly the relative signs required in Eqs. (A.2a)–(A.2c). Hence, when a hedgehog *Ansatz* is used for Ω, its gradient $\nabla\Omega$ automatically satisfies the boundary conditions for a vector field.

A.2. Calculation of the winding number

In calculating the winding number of Ω we follow [20]. First, we need the normalized volume form $\widehat{\mathrm{vol}}$ of $SO(3)$. As mentioned on page 48 we parametrize $SO(3)$ by three angles $(\vartheta, \alpha, \beta)$. In these coordinates the metric H of $SO(3)$ reads

$$H = \mathrm{d}\vartheta^2 + 4\sin^2(\vartheta/2)\mathrm{d}\alpha^2 + 4\sin^2(\vartheta/2)\sin^2\alpha\mathrm{d}\beta^2 \,. \tag{A.4}$$

From equation (A.4) we find the corresponding normalized volume as

$$\widehat{\mathrm{vol}} = \frac{1}{8\pi^2}\sqrt{H}\mathrm{d}\vartheta \wedge \mathrm{d}\alpha \wedge \mathrm{d}\beta = \frac{\sin^2(\vartheta/2)\sin\alpha}{2\pi^2}\mathrm{d}\vartheta \wedge \mathrm{d}\alpha \wedge \mathrm{d}\beta \,,$$

where $\sqrt{H}$ denotes the square root of the determinant of H. The factor $8\pi^2$ is the invariant volume of $SO(3)$ [48]. The topological degree of Ω is then given by the integral of the pull-back of $\widehat{\mathrm{vol}}$:

$$\begin{aligned} \deg\Omega &= -\int_{M_\mathrm{I}} \Omega^* \left(\widehat{\mathrm{vol}}\right) \\ &= -\int_{M_\mathrm{I}} \frac{\sqrt{H(\vartheta(\boldsymbol{x}),\alpha(\boldsymbol{x}),\beta(\boldsymbol{x}))}}{8\pi^2} \det\left(\frac{\partial\theta^I}{\partial x^i}\right) \mathrm{d}x^1 \wedge \mathrm{d}x^2 \wedge \mathrm{d}x^3 \,. \end{aligned} \tag{A.5}$$

Here (θ^I) and (x^i) are the coordinates of $SO(3)$ and M_I respectively, and $\det\left(\frac{\partial\theta^I}{\partial x^i}\right)$ denotes the determinant of the Jacobian of the map Ω. Strictly speaking, the degree is only defined for maps between manifolds of the same dimension and we have a

(3+1) dimensional theory. Since we only consider time-independent fields, however, Ω is effectively a map between three-dimensional manifolds. The minus sign arises because we "suppress" the time dimension. For time-dependent fields we would instead have to integrate the time-component of the topological current instead [49]. Explicitly using the hedgehog *Ansatz*

$$\begin{aligned}\vartheta(\boldsymbol{x}) &= F(r)\,,\\ \alpha(\boldsymbol{x}) &= \theta\,,\\ \beta(\boldsymbol{x}) &= \phi\,,\end{aligned}$$

then yields $\sqrt{H(\boldsymbol{x})} = 4\sin^2(F(r)/2)\sin\theta$ and $\det\left(\frac{\partial\theta^I}{\partial x^i}\right) = F'(r)$. Finally, equation (A.5) turns out to be

$$\begin{aligned}\deg\Omega &= -\int_0^{2\pi}\int_0^{\pi}\int_b^{\infty}\frac{4\sin^2(F(r)/2)\sin\theta}{8\pi^2}F'(r)\mathrm{d}r\,\mathrm{d}\theta\,\mathrm{d}\phi = -\frac{2}{\pi}\int_{n\,\pi}^{0}\sin^2(F/2)\mathrm{d}F\\ &= n\,.\end{aligned} \tag{A.6}$$

In the second integral we used the boundary condition in equation (6.11a). Equation (A.6) is the final result, the winding number of the field Ω is given by the integer n occurring in the boundary condition at the defect. Alternatively, the degree of Ω could have been obtained by counting the number of preimages of a generic point in $SO(3)$ (here n) multiplied with the sign of Jacobian of the map Ω (here, -1 since F decreases from π to 0) and the additional factor -1 [20].

B. Properties of α matrices

This appendix summarizes some relations between α-matrices. These relations are used to find the correction spinors in Sections 13.3, 14.3, and 15.3.

The three 4×4 matrices $\boldsymbol{\alpha}$ are defined by

$$\boldsymbol{\alpha} \equiv \begin{pmatrix} 0 & \boldsymbol{\sigma} \\ \boldsymbol{\sigma} & 0 \end{pmatrix} .$$

Here, $\boldsymbol{\sigma}$ denote the three 2×2 Pauli matrices, which read explicitly

$$\sigma_x \equiv \begin{pmatrix} 0 & 1 \\ 1 & 0 \end{pmatrix} , \quad \sigma_y \equiv \begin{pmatrix} 0 & -\mathrm{i} \\ \mathrm{i} & 0 \end{pmatrix} , \quad \sigma_z \equiv \begin{pmatrix} 1 & 0 \\ 0 & -1 \end{pmatrix} .$$

For two three-vectors $\boldsymbol{v}$ and $\boldsymbol{w}$ the following relation holds

$$\boldsymbol{v} \cdot \boldsymbol{\sigma} \boldsymbol{w} \cdot \boldsymbol{\sigma} = \boldsymbol{v} \cdot \boldsymbol{w} \mathbb{1}_2 + \mathrm{i} \boldsymbol{\sigma} \cdot (\boldsymbol{v} \times \boldsymbol{w}) ,$$

where $\mathbb{1}_2$ denotes the two-dimensional unit matrix. Using this relation we obtain

$$\boldsymbol{v} \cdot \boldsymbol{\alpha} \boldsymbol{w} \cdot \boldsymbol{\alpha} = [\boldsymbol{v} \cdot \boldsymbol{w} \mathbb{1}_2 + \mathrm{i} \boldsymbol{\sigma} \cdot (\boldsymbol{v} \times \boldsymbol{w})] \otimes \mathbb{1}_2 . \tag{B.1}$$

In particular, we have for any unit vector $\hat{a}$

$$(\hat{a} \cdot \boldsymbol{\alpha})^2 = \mathbb{1}_4 .$$

In case of the standard normalized basis vectors in spherical polar coordinates $(\hat{n}, \hat{\theta}, \hat{\phi})$ we have

$$\hat{n} \cdot \boldsymbol{\alpha} \hat{\theta} \cdot \boldsymbol{\alpha} = \mathrm{i} \boldsymbol{\sigma} \cdot \hat{\phi} \otimes \mathbb{1}_2 ,$$

where we have used $\hat{n} \times \hat{\theta} = \hat{\phi}$. Similar relations are obtained through cyclical permutation of the basis vectors.

For the commutator and anti-commutator the following relations hold

$$[\boldsymbol{v} \cdot \boldsymbol{\alpha}, \boldsymbol{w} \cdot \boldsymbol{\alpha}] = [2\mathrm{i} \boldsymbol{\sigma} (\boldsymbol{v} \times \boldsymbol{w})] \otimes \mathbb{1}_2 , \tag{B.2a}$$

$$\{\boldsymbol{v} \cdot \boldsymbol{\alpha}, \boldsymbol{w} \cdot \boldsymbol{\alpha}\} = 2 \boldsymbol{v} \cdot \boldsymbol{w} \mathbb{1}_4 . \tag{B.2b}$$

From the last relation we obtain

$$\boldsymbol{v} \cdot \boldsymbol{\alpha} \boldsymbol{w} \cdot \boldsymbol{\alpha} = 2 \boldsymbol{v} \cdot \boldsymbol{w} \mathbb{1}_4 - \boldsymbol{w} \cdot \boldsymbol{\alpha} \boldsymbol{v} \cdot \boldsymbol{\alpha} .$$

The product for two *orthogonal* vectors therefore anti-commutes

$$\boldsymbol{v} \cdot \boldsymbol{\alpha} \boldsymbol{w} \cdot \boldsymbol{\alpha} = -\boldsymbol{w} \cdot \boldsymbol{\alpha} \boldsymbol{v} \cdot \boldsymbol{\alpha} , \text{ if } \boldsymbol{v} \perp \boldsymbol{w} . \tag{B.3}$$

Finally, we define the hermitian matrix β as

$$\beta \equiv \begin{pmatrix} \mathbb{1}_2 & 0 \\ 0 & -\mathbb{1}_2 \end{pmatrix} .$$

This matrix anti-commutes with each of the α-matrices and we have

$$\boldsymbol{v} \cdot \alpha\beta = -\beta\boldsymbol{v} \cdot \alpha \, . \tag{B.4}$$

C. Electromagnetic correction fields for a line defect

In this appendix we calculate the electromagnetic correction fields for the line defect discussed in Chapter 15. The cylinder has radius b and its axis is parallel to the z-axis. In polar coordinates (ρ, ϕ, z) the boundary conditions for the electric and magnetic field read

$$E_\rho(\boldsymbol{x}) = -E_\rho(\boldsymbol{x}'), \qquad B_\rho(\boldsymbol{x}) = +B_\rho(\boldsymbol{x}')\,, \tag{C.1a}$$
$$E_\phi(\boldsymbol{x}) = +E_\phi(\boldsymbol{x}'), \qquad B_\phi(\boldsymbol{x}) = -B_\phi(\boldsymbol{x}')\,, \tag{C.1b}$$
$$E_z(\boldsymbol{x}) = +E_z(\boldsymbol{x}'), \qquad B_z(\boldsymbol{x}) = -B_z(\boldsymbol{x}')\,. \tag{C.1c}$$

Here, $\boldsymbol{x}'$ is a point on the cylinder with coordinates $(b, \phi', z') = (b, \pi + \phi, z)$. It is convenient to switch to spherical polar coordinates (r, θ, ϕ) at this point. Hence the point (b, θ, ϕ) is identified with $(b, \theta', \phi') = (b, \theta, \phi + \pi)$. The transformation of polar basis vectors to spherical basis vectors is given by

$$\begin{aligned}
\rho(\boldsymbol{x}) &= \sin\theta\hat{n}(\boldsymbol{x}) + \cos\theta\hat{\theta}(\boldsymbol{x})\,,\\
\hat{z} &= \cos\theta\hat{n}(\boldsymbol{x}) - \sin\theta\hat{\theta}(\boldsymbol{x})\,,\\
\hat{\phi}(\boldsymbol{x}) &= \hat{\phi}(\boldsymbol{x})\,.
\end{aligned}$$

Therefore, the boundary conditions for the electric and magnetic field become

$$\begin{aligned}
E_n(\boldsymbol{x}) &= (\cos^2\theta' - \sin^2\theta')\,E_n(\boldsymbol{x}') - 2\cos\theta'\,\sin\theta'\,E_\theta(\boldsymbol{x}')\,,\\
E_\theta(\boldsymbol{x}) &= -(\cos^2\theta' - \sin^2\theta')\,E_\theta(\boldsymbol{x}') - 2\cos\theta'\,\sin\theta'\,E_n(\boldsymbol{x}')\,,\\
E_\phi(\boldsymbol{x}) &= E_\phi(\boldsymbol{x}')\,,\\
B_n(\boldsymbol{x}) &= -(\cos^2\theta' - \sin^2\theta')\,B_n(\boldsymbol{x}') + 2\cos\theta'\,\sin\theta'\,B_\theta(\boldsymbol{x}')\,,\\
B_\theta(\boldsymbol{x}) &= -(\cos^2\theta' - \sin^2\theta')\,B_\theta(\boldsymbol{x}') + 2\cos\theta'\,\sin\theta'\,B_n(\boldsymbol{x}')\,,\\
B_\phi(\boldsymbol{x}) &= -B_\phi(\boldsymbol{x}')\,.
\end{aligned}$$

Since we want to perform an expansion in vector spherical harmonics we multiply the equations for the spherical components by $\sin\theta$ and obtain

$$E_n(\boldsymbol{x}) = (\cos^2\theta - \sin^2\theta)\,E_n(\boldsymbol{x}') - 2\cos\theta'\,\sin\theta'\,E_\theta(\boldsymbol{x}')\,, \tag{C.2a}$$
$$\sin\theta\,E_\theta(\boldsymbol{x}) = -(\cos^2\theta' - \sin^2\theta')\,\sin\theta\,E_\theta(\boldsymbol{x}') - 2\cos\theta'\,\sin^2\theta'\,E_n(\boldsymbol{x}')\,, \tag{C.2b}$$
$$\sin\theta\,E_\phi(\boldsymbol{x}) = \sin\theta' E_\phi(\boldsymbol{x}')\,, \tag{C.2c}$$
$$B_n(\boldsymbol{x}) = -(\cos^2\theta - \sin^2\theta)\,B_n(\boldsymbol{x}') + 2\cos\theta'\,\sin\theta'\,B_\theta(\boldsymbol{x}')\,, \tag{C.2d}$$
$$\sin\theta\,B_\theta(\boldsymbol{x}) = (\cos^2\theta' - \sin^2\theta')\,\sin\theta\,B_\theta(\boldsymbol{x}') + 2\cos\theta'\,\sin^2\theta'\,B_n(\boldsymbol{x}')\,, \tag{C.2e}$$
$$\sin\theta\,B_\phi(\boldsymbol{x}) = -\sin\theta' B_\phi(\boldsymbol{x}')\,. \tag{C.2f}$$

In this step we also used the fact that $\theta = \theta'$. To expand the fields we use the following definition for the vector spherical harmonics [50, 51]

$$\boldsymbol{Y}_l^m(\theta,\phi) \equiv Y_l^m \hat{n}, \quad \boldsymbol{\Psi}_l^m(\theta,\phi) \equiv r\nabla Y_l^m, \quad \boldsymbol{\Phi}_l^m(\theta,\phi) \equiv \hat{n} \times \boldsymbol{\Psi}(\theta,\phi)\,.$$

Here, $\hat{n} \equiv \hat{n}(\theta,\phi)$ is the radial unit vector and $Y_l^m \equiv Y_l^m(\theta,\phi)$ denotes a spherical harmonic function. In terms of this basis the correction fields read

$$\begin{aligned}
\boldsymbol{E}^c &= \sum_{l,m} \frac{1}{\mathrm{i}k\,r}\alpha_l^m \left[l(l+1) f_l(k\,r)\boldsymbol{Y}_l^m + \frac{d}{dr}\left(r\, f_l(k\,r)\right)\boldsymbol{\Psi}_l^m \right] + \beta_l^m\, g_l(k\,r)\boldsymbol{\Phi}_l^m\,, \\
\boldsymbol{B}^c &= \sum_{l,m} \alpha_l^m\, f_l(k\,r)\boldsymbol{\Phi} + \frac{i}{k\,r}\beta_l^m \left[l(l+1) g_l(k\,r)\boldsymbol{Y}_l^m + \frac{d}{dr}\left(r\, g_l(k\,r)\right)\boldsymbol{\Psi}_l^m \right],
\end{aligned}$$

where α_l^m and β_l^m are the coefficients which need to be determined such that $\boldsymbol{E}^{\mathrm{tot}}$ and $\boldsymbol{B}^{\mathrm{tot}}$ satisfy the boundary conditions (C.2a) to (C.2f). The two radial functions $f_l(kr)$ and $g_l(kr)$ are linear combinations of spherical Bessel functions [43], whose precise form will be determined later. Our aim is to expand all components of the correction fields, and the expressions on the right hand side of the boundary conditions, into spherical harmonics. Matching the coefficients gives a inhomogeneous linear system of equations for the coefficients α_l^m and β_l^m. This system turns out to have a unique solution.

To obtain the components of $\boldsymbol{E}^{\mathrm{c}}$ and $\boldsymbol{B}^{\mathrm{c}}$ in spherical coordinates we use

$$\begin{aligned}
\boldsymbol{Y}_l^m &= Y_l^m\, \hat{n}\,, \\
\sin\theta\, \boldsymbol{\Psi}_l^m &= \sin\theta \partial_\theta Y_l^m\, \hat{\theta} + \partial_\phi Y_l^m\, \hat{\phi}\,, \\
\sin\theta\, \boldsymbol{\Phi}_l^m &= \sin\theta \partial_\theta Y_l^m\, \hat{\phi} - \partial_\phi Y_l^m\, \hat{\theta}\,.
\end{aligned}$$

The derivative with respect to θ can be written as a sum of two spherical harmonics

$$\sin\theta\, \partial_\theta Y_l^m = -(l+1)\sqrt{\frac{(l-m)(l+m)}{(2l+1)(2l-1)}} Y_{l-1}^m + l\sqrt{\frac{(l+1-m)(l+1+m)}{(2l+1)(2l+3)}} Y_{l+1}^m\,.$$

By using these equations we can now express the coefficients of $\boldsymbol{E}^{\mathrm{c}}$ as a sum of spherical harmonics. Explicitly, we obtain

$$\begin{aligned}
E_n^c &= \hat{n} \cdot \boldsymbol{E}^c = \sum_{l,m} E_{n\,l}^{c\,m} Y_l^m\,, \\
\sin\theta E_\theta^c &= \sin\theta \hat{\theta} \cdot \boldsymbol{E}^c = \sum_{l,m} E_{\theta\,l}^{c\,m} Y_l^m\,, \\
\sin\theta E_\phi^c &= \sin\theta \hat{\phi} \cdot \boldsymbol{E}^c = \sum_{l,m} E_{\phi\,l}^{c\,m} Y_l^m\,,
\end{aligned}$$

with

$$
\begin{aligned}
E^{c\,m}_{n\,l} \equiv& \frac{l(l+1)}{\mathrm{i}k\,r}\, f_l(k\,r)\, \alpha^m_l\,, \\
E^{c\,m}_{\theta\,l} \equiv& \frac{\mathrm{i}(l+2)}{kr}\sqrt{\frac{(l+1-m)(l+1+m)}{(2l+1)(2l+3)}}\partial_r[r f_{l+1}(kr)]\alpha^m_{l+1} - \mathrm{i}m g_l(kr)\beta^m_l \\
&- \frac{\mathrm{i}(l-1)}{kr}\sqrt{\frac{(l-m)(l+m)}{(2l-1)(2l+1)}}\partial_r[r f_{l-1}(kr)]\alpha^m_{l-1}\,, \\
E^{c\,m}_{\phi\,l} \equiv& -(l+2)\sqrt{\frac{(l+1-m)(l+1+m)}{(2l+1)(2l+3)}} g_{l+1}(kr)\beta^m_{l+1} + \frac{m}{kr}\partial_r[r f_l(kr)]\alpha^m_l \\
&+ (l-1)\sqrt{\frac{(l-m)(l+m)}{(2l-1)(2l+1)}} g_{l-1}(kr)\beta^m_{l-1}\,.
\end{aligned}
$$

Similarly, the coefficients of the magnetic field are defined by

$$
\begin{aligned}
B^c_n = \hat{n}\cdot\boldsymbol{B}^c &= \sum_{l,m} B^{c\,m}_{n\,l} Y^m_l\,, \\
\sin\theta B^c_\theta = \sin\theta\hat{\theta}\cdot\boldsymbol{B}^c &= \sum_{l,m} B^{c\,m}_{\theta\,l} Y^m_l\,, \\
\sin\theta B^c_\phi = \sin\theta\hat{\phi}\cdot\boldsymbol{B}^c &= \sum_{l,m} B^{c\,m}_{\phi\,l} Y^m_l\,,
\end{aligned}
$$

and read

$$
\begin{aligned}
B^{c\,m}_{n\,l} \equiv& \frac{\mathrm{i}l(l+1)}{k\,r}\, g_l(k\,r)\, \beta^m_l\,, \\
B^{c\,m}_{\theta\,l} \equiv& \frac{l+2}{\mathrm{i}kr}\sqrt{\frac{(l+1-m)(l+1+m)}{(2l+1)(2l+3)}}\partial_r[r g_{l+1}(kr)]\beta^m_{l+1} - \mathrm{i}m f_l(kr)\alpha^m_l \\
&+ \frac{\mathrm{i}(l-1)}{kr}\sqrt{\frac{(l-m)(l+m)}{(2l-1)(2l+1)}}\partial_r[r g_{l-1}(kr)]\beta^m_{l-1}\,, \\
B^{c\,m}_{\phi\,l} \equiv& -(l+2)\sqrt{\frac{(l+1-m)(l+1+m)}{(2l+1)(2l+3)}} f_{l+1}(kr)\alpha^m_{l+1} - \frac{m}{kr}\partial_r[r g_l(kr)]\beta^m_l \\
&+ (l-1)\sqrt{\frac{(l-m)(l+m)}{(2l-1)(2l+1)}} f_{l-1}(kr)\alpha^m_{l-1}\,.
\end{aligned}
$$

The electric and magnetic field of a plane wave with wave vector $\boldsymbol{k} = (k, \vartheta, \varphi)$ are given by

$$
\begin{aligned}
\boldsymbol{E}^{\mathrm{pw}}(\boldsymbol{x}) &= \mathrm{e}^{\mathrm{i}\boldsymbol{k}\cdot\boldsymbol{x}}\,\boldsymbol{E}_0\,, \\
\boldsymbol{B}^{\mathrm{pw}}(\boldsymbol{x}) &= \mathrm{e}^{\mathrm{i}\boldsymbol{k}\cdot\boldsymbol{x}}\,\boldsymbol{B}_0\,.
\end{aligned}
$$

Here, $\boldsymbol{E}_0$ and $\boldsymbol{B}_0$ are constant vectors. Of course, $\boldsymbol{k}$, $\boldsymbol{E}_0$, and $\boldsymbol{B}_0$ are pairwise orthogonal but the dreibein $(\boldsymbol{k}, \boldsymbol{E}_0, \boldsymbol{B}_0)$ can have an arbitrary orientation. To expand the plane wave vectors into spherical harmonics we use the well known relation [43]

$$\exp(\mathrm{i}\boldsymbol{k}\cdot\boldsymbol{x}) = \sum_{l,m} 4\pi\,\mathrm{i}^l\, Y_l^{m\,*}(\vartheta,\varphi)\, j_l(k\,r)\, Y_l^m \equiv \sum_{l,m} c_l^m Y_l^m\,,$$

where the c_l^m's are functions of r that depend on k, ϑ, and φ. We then have

$$\begin{aligned}
E_n^{\mathrm{pw}} &= \mathrm{e}^{\mathrm{i}\boldsymbol{k}\cdot\boldsymbol{x}}\,(E_{0\,x}\sin\theta\,\cos\phi + E_{0\,y}\sin\theta\,\sin\phi + E_{0\,z}\cos\theta) \equiv \sum_{l,m} E_{n\,l}^{\mathrm{pw}\,m}\, Y_l^m\,,\\
\sin\theta E_\theta^{\mathrm{pw}} &= \sin\theta \mathrm{e}^{\mathrm{i}\boldsymbol{k}\cdot\boldsymbol{x}}\,(E_{0\,x}\cos\theta\,\cos\phi + E_{0\,y}\cos\theta\,\sin\phi - E_{0\,z}\sin\theta)\\
&\equiv \sum_{l,m} E_{\theta\,l}^{\mathrm{pw}\,m}\, Y_l^m\,,\\
\sin\theta E_\phi^{\mathrm{pw}} &= \mathrm{e}^{\mathrm{i}\boldsymbol{k}\cdot\boldsymbol{x}}\,(E_{0\,y}\sin\theta\,\cos\phi - E_{0\,x}\sin\theta\,\sin\phi) \equiv \sum_{l,m} E_{\phi\,l}^{\mathrm{pw}\,m}\, Y_l^m\,.
\end{aligned}$$

To obtain these coefficients explicitly, we note that the trigonometric factors can be decomposed into spherical harmonics as

$$\begin{aligned}
\cos\theta &= \sqrt{\frac{4\pi}{3}}\, Y_1^0\,, & \sin^2\theta &= \frac{4}{3}\sqrt{\frac{\pi}{5}}\left(\sqrt{5}Y_0^0 - Y_2^0\right)\,,\\
\sin\theta\cos\phi &= -\sqrt{\frac{2\pi}{3}}\left(Y_1^1 - Y_1^{-1}\right)\,, & \sin\theta\sin\phi &= \mathrm{i}\sqrt{\frac{2\pi}{3}}\left(Y_1^1 + Y_1^{-1}\right)\,,\\
\cos\theta\sin\theta\cos\phi &= -\sqrt{\frac{2\pi}{15}}\left(Y_2^1 - Y_2^{-1}\right)\,, & \cos\theta\sin\theta\sin\phi &= \mathrm{i}\sqrt{\frac{2\pi}{15}}\left(Y_2^1 + Y_2^{-1}\right)\,.
\end{aligned}$$

Next, we use the following equation to rewrite a product of spherical harmonics into a sum of spherical harmonics

$$Y_m^l\, Y_M^L = \sum_{\lambda=|l-L|}^{l+L} \sqrt{\frac{(2l+1)(2L+1)}{4\pi(2\lambda+1)}} \left(\begin{array}{cc|c} l & L & \lambda \\ 0 & 0 & 0 \end{array}\right) \left(\begin{array}{cc|c} l & L & \lambda \\ m & M & m+M \end{array}\right) Y_\lambda^{m+M}\,,$$

with $\left(\begin{array}{cc|c} l & L & \lambda \\ m & M & \mu \end{array}\right)$ denoting the Clebsch-Gordan coefficients. This procedure fi-

nally yields for $E_{n\,l}^{\mathrm{pw}\,m}$

$$
\begin{aligned}
E_{n\,l}^{\mathrm{pw}\,m} = \Bigg(& -\sqrt{\frac{(l+m+1)(l+m+2)}{(2l+1)(2l+3)}}\, c_{l+1}^{m+1} \\
& + \sqrt{\frac{(l-m-1)(l-m)}{(2l-1)(2l+1)}}\, c_{l-1}^{m+1} \Bigg) \frac{E_{0\,x} + \mathrm{i} E_{0\,y}}{2} \\
& + \left(\sqrt{\frac{(l-m+1)(l+m+1)}{(2l+1)(2l+3)}} c_{l+1}^{m} + \sqrt{\frac{(l-m)(l+m)}{(2l-1)(2l+1)}} c_{l-1}^{m} \right) E_{0\,z} \\
& + \Bigg(\sqrt{\frac{(l-m+1)(l-m+2)}{(2l+1)(2l+3)}}\, c_{l+1}^{m-1} \\
& - \sqrt{\frac{(l+m)(l+m-1)}{(2l-1)(2l+1)}}\, c_{l-1}^{m-1} \Bigg) \frac{E_{0\,x} - \mathrm{i} E_{0\,y}}{2} \,.
\end{aligned}
$$

Similar lengthy expressions follow for $E_{\theta\,l}^{\mathrm{pw}\,m}$ and $E_{\phi\,l}^{\mathrm{pw}\,m}$. The coefficients $B_{n\,l}^{\mathrm{pw}\,m}$, $B_{\theta\,l}^{\mathrm{pw}\,m}$, and $B_{\phi\,l}^{\mathrm{pw}\,m}$ are obtained by replacing $E_{0\,i}$ with $B_{0\,i}$ in the coefficients of the electric field.

Finally, note that the trigonometric factors on the right hand sides of equations (C.2a)–(C.2f) can readily be written as a sum of spherical harmonics

$$
\begin{aligned}
\cos^2\theta - \sin^2\theta &= -\frac{2\sqrt{\pi}}{3} Y_0^0 + \frac{8}{3}\sqrt{\frac{\pi}{5}} Y_2^0 \,, \\
\sin^2\theta\, \cos\theta &= \frac{4}{5}\left(\sqrt{\frac{\pi}{3}}\, Y_1^0 - \sqrt{\frac{\pi}{7}}\, Y_3^0 \right) .
\end{aligned}
$$

After we have expanded the prefactors in equations (C.2a)–(C.2f) into spherical harmonics as well as the components of the plane wave and the correction fields, we can write the right hand sides of equations (C.2a)–(C.2f) as a sum of spherical harmonics. Finally, we use $Y_l^m(\theta', \phi') = (-1)^m Y_l^m(\theta, \phi)$. For example, equation (C.2a) yields

$$
\begin{aligned}
\frac{E_{n\,l}^{\mathrm{tot}\,m}}{2(-1)^m} = & \sqrt{\frac{(l+1-m)(l+2-m)(l+2+m)(l+1+m)}{(2l+1)(2l+3)^2(2l+5)}} E_{n\,l+2}^{\mathrm{tot}\,m} \\
& + \frac{(1-2m)(1+2m)}{2(2l-1)(2l+3)} E_{n\,l}^{\mathrm{tot}\,m} \\
& + \sqrt{\frac{(l-1-m)(l-m)(l+m)(l-1+m)}{(2l-3)(2l-1)^2(2l+1)}} E_{n\,l-2}^{\mathrm{tot}\,m} \\
& - \sqrt{\frac{(l-m+1)(l+m+1)}{(2l+1)(2l+3)}} E_{\theta\,l+1}^{\mathrm{tot}\,m} - \sqrt{\frac{(l-m)(l+m)}{(2l-1)(2l+1)}} E_{\theta\,l-1}^{\mathrm{tot}\,m} \,.
\end{aligned}
$$

We now have all ingredients necessary to transform equations (C.2a)–(C.2f) into an inhomogeneous linear system of equations for the unknown coefficients α_l^m and β_l^m. Due to equations (C.2b) and (C.2e), the general system involves the 14 unknowns $\alpha_{l-3}^m, \alpha_{l-2}^m, \ldots, \alpha_{l+3}^m, \beta_{l-3}^m, \ldots \beta_{l-3}^m$ and is not easy to solve. But we are mainly interested in the coefficients with $l = 1$ and the system for these can be solved. Considering the prefactors of Y_0^0 in equations (C.2a)–(C.2f) gives only five equations for six coefficients $\alpha_1^0, \alpha_2^0, \alpha_3^0, \beta_1^0, \beta_2^0, \beta_3^0$ (the equation arising from equation (C.2c) is satisfied identically). Including, however, the prefactors of Y_1^0 gives five additional equations also involving α_4^0 and β_4^0. Hence, we have ten equations for eight unknowns. Two of these equations are actually linear combinations of the other eight, once we set the unknown radial functions $f_l(kr)$ and $g_l(kr)$ to

$$f_l(kr) \equiv j_l(kr)\,,$$
$$g_l(kr) \equiv g_l(kr)\,.$$

Thus, we arrive at the following system

$$\begin{pmatrix} 0 & A_{1,2} & 0 & 0 & 0 & 0 & 0 & 0 \\ A_{2,1} & 0 & A_{2,3} & 0 & 0 & 0 & 0 & 0 \\ 0 & 0 & 0 & 0 & 0 & B_{3,2} & 0 & 0 \\ 0 & 0 & 0 & 0 & B_{4,1} & 0 & B_{4,3} & 0 \\ A_{5,1} & 0 & 0 & 0 & 0 & 0 & 0 & 0 \\ A_{6,1} & 0 & A_{6,3} & 0 & 0 & 0 & 0 & 0 \\ 0 & A_{7,2} & 0 & A_{7,4} & 0 & 0 & 0 & 0 \\ 0 & 0 & 0 & 0 & B_{8,1} & 0 & B_{8,3} & 0 \\ 0 & 0 & 0 & 0 & 0 & B_{9,2} & 0 & B_{9,4} \\ 0 & A_{10,2} & 0 & 0 & 0 & 0 & 0 & 0 \end{pmatrix} \cdot \begin{pmatrix} \alpha_1^0 \\ \alpha_2^0 \\ \alpha_3^0 \\ \alpha_4^0 \\ \beta_1^0 \\ \beta_2^0 \\ \beta_3^0 \\ \beta_4^0 \end{pmatrix} = \begin{pmatrix} c_1 \\ c_2 \\ c_3 \\ c_4 \\ c_5 \\ c_6 \\ c_7 \\ c_8 \\ c_9 \\ c_{10} \end{pmatrix} . \quad \text{(C.3)}$$

Explicitly, the matrix elements read

$$A_{1,2} \equiv \frac{4\mathrm{i}}{\sqrt{5}} j_1, \qquad A_{2,1} \equiv -\frac{4\mathrm{i}}{5\sqrt{3}} j_2, \qquad A_{2,3} \equiv \frac{16\mathrm{i}}{5\sqrt{7}} j_2, \qquad A_{5,1} \equiv \frac{-4}{\sqrt{3}} j_1,$$
$$A_{6,1} \equiv -\frac{4\mathrm{i}}{5} j_2, \qquad A_{6,3} \equiv \frac{16\sqrt{3}\mathrm{i}}{5\sqrt{7}} j_2, \qquad A_{10,2} \equiv -4\sqrt{\frac{3}{5}} j_2, \qquad A_{7,4} \equiv \frac{16\mathrm{i}}{7\sqrt{3}} j_3$$
$$B_{3,2} \equiv A_{1,2}, \qquad B_{4,3} \equiv \frac{16\mathrm{i}}{5\sqrt{7}} j_2, \qquad B_{8,3} \equiv A_{6,3}, \qquad B_{9,4} \equiv A_{7,4}\,,$$

where all spherical Bessel functions j_n depend on kr. The remaining matrix elements are

$$A_{7,2} \equiv 4\sqrt{\frac{3}{5}}\mathrm{i} \left(\frac{j_2(kr)}{kr} - \frac{3}{7} j_3(kr) \right), \qquad B_{4,1} \equiv \frac{8\mathrm{i}}{15\sqrt{3}} \left(j_2(kr) - 5 j_0(kr) \right),$$
$$B_{8,1} \equiv \frac{4\mathrm{i}}{5} \left(j_0(kr) + 2\frac{j_1(kr)}{kr} \right), \qquad B_{9,2} \equiv -\frac{8\sqrt{3}\mathrm{i}}{7\sqrt{5}} \left(2 j_1(kr) - 3\frac{j_2(kr)}{kr} \right).$$

The coefficients on the right hand side are given by

$$
\begin{aligned}
c_1 &\equiv -4\sqrt{\pi}\mathrm{i}\left(E_{0x}k_x + E_{0y}k_y\right) j_1(kr)/k\,,\\
c_2 &\equiv 4\sqrt{\pi}\left(E_{0x}k_x + E_{0y}k_y\right) k_z j_2(kr)/k^2\,,\\
c_3 &\equiv -4\sqrt{\pi}\mathrm{i}B_{0z}k_z j_1(kr)/k\,,\\
c_4 &\equiv \frac{4\sqrt{\pi}}{3}B_{0z}\left(2j_0(kr) - j_2(kr) + 3kz^2 j_2(kr)/k^2\right)\,,\\
c_5 &\equiv 4\sqrt{\pi}\mathrm{i}E_{0z}j_1(kr)\,,\\
c_6 &\equiv 4\sqrt{3\pi}\left(E_{0x}k_x + E_{0y}k_y\right) kz j_1(kr)/k^2\,,\\
c_7 &\equiv \frac{4\sqrt{3\pi}}{\mathrm{i}k}\left(E_{0x}k_x + E_{0y}k_y\right)\left(\frac{j_2(kr)}{kr} - j_3(kr)\right)\,,\\
c_8 &\equiv -4\sqrt{\frac{\pi}{3}}B_z\left(\frac{2j_1(kr)}{kr} - 3\frac{kz^2}{k^2}j_2(kr)\right)\,,\\
c_9 &\equiv 4\sqrt{3\pi}\mathrm{i}B_{0z}\left(j_2'(kr) + k_z^2 j_3(kr)/k^2\right)/k\,,\\
c_{10} &\equiv -4\sqrt{3\pi}E_{0z}k_z j_2(kr)/k\,.
\end{aligned}
$$

We find the coefficients α_l^0 and β_l^0 by solving equation (C.3). In the same way, we can obtain a linear system of equations for the coefficients with $m = -1$ and $m = 1$. For $m = -1, 0, 1$ and l up to 3 we obtain

$$
\begin{aligned}
E_{n\,l}^{c\,m} &= -E_{n\,l}^{\mathrm{pw}\,m}\,, & B_{n\,l}^{c\,m} &= -B_{n\,l}^{\mathrm{pw}\,m}\,,\\
E_{\theta\,l}^{c\,m} &= -E_{\theta\,l}^{\mathrm{pw}\,m}\,, & B_{\theta\,l}^{c\,m} &= -B_{\theta\,l}^{\mathrm{pw}\,m}\,,\\
E_{\phi\,l}^{c\,m} &= -E_{\phi\,l}^{\mathrm{pw}\,m}\,, & B_{\phi\,l}^{c\,m} &= -B_{\phi\,l}^{\mathrm{pw}\,m}\,.
\end{aligned}
$$

This means that the correction fields for a line defect are the negative of the incoming plane wave. Hence, the two fields sum to zero, and the total electromagnetic field vanishes.

Bibliography

[1] J. A. Wheeler, Superspace and quantum geometrodynamics, in *Battelle Rencontres*, edited by C. M. DeWitt and J. A. Wheeler, W.A. Benjamin, Inc., 1968.

[2] M. S. Morris and K. S. Thorne, Wormholes in spacetime and their use for interstellar travel: A tool for teaching general relativity, Am. J. Phys. **56**, 395 (1988).

[3] T. H. R. Skyrme, A nonlinear field theory, Proc. R. Soc. Lond. A **260**, 127 (1961).

[4] T. H. R. Skyrme, A unified field theory of mesons and baryons, Nucl. Phys. **31**, 556 (1962).

[5] D. Gannon, Singularities in nonsimply connected space-times, J. Math. Phys. **16**, 2364 (1975).

[6] J. L. Friedman, K. Schleich, and D. M. Witt, Topological censorship, Phys. Rev. Let. **71**, 1486 (1993), gr-qc/9305017.

[7] S. Bernadotte and F. R. Klinkhamer, Bounds on length scales of classical spacetime foam models, Phys. Rev. D **75**, 024018 (2007), hep-ph/0610216.

[8] F. R. Klinkhamer and C. Rupp, Spacetime foam and high-energy photons, (2005), astro-ph/0511267.

[9] R. Arnowitt, S. Deser, and C. W. Misner, The dynamics of general relativity, in *Gravitation: An Introduction to Current Research*, edited by L. Witten, Wiley, 1962.

[10] G. Amelino-Camelia, J. Ellis, N. E. Mavromatos, D. V. Nanopoulos, and S. Sarkar, Tests of quantum gravity from observations of gamma-ray bursts, Nature **393**, 763 (1998), astro-ph/9712103.

[11] E. F. Beall, Measuring the gravitational interaction of elementary particles, Phys. Rev. D **1**, 961 (1970).

[12] S. Coleman and S. L. Glashow, Cosmic ray and neutrino tests of special relativity, Phys. Lett. B **405**, 249 (1997), hep-ph/9703240.

[13] Pierre Auger Collaboration, e. a. J. Abraham, Correlation of the highest-energy cosmic rays with the positions of nearby active galactic nuclei, Astropart. Phys. **29**, 188 (2008), arXiv:0712.2843 [astro-ph].

[14] F. R. Klinkhamer and M. Risse, Ultrahigh-energy cosmics-ray bounds on nonbirefringent modified-maxwell theory, Phys. Rev. D **77**, 016002 (2008), arXiv:0709.2502 [hep-ph], Addendum ibid. 77, 117901 (2008).

[15] F. R. Klinkhamer and M. Schreck, New two-sided bounds on the isotropic lorentz-violating parameter of modified maxwell theory, Phys. Rev. D **78**, 085026 (2008), arXiv:0809.3217 [hep-ph].

[16] A. Einstein and N. Rosen, The particle problem in the general theory of relativity, Phys. Rev. **48**, 73 (1935).

[17] R. M. Wald, *General Relativity* (The University of Chicago Press, 1984).

[18] K. Thorne, *Black Holes and Time Warps: Einstein's Outrageous Legacy* (WW Norton & Co, 1994).

[19] S. V. Sushkov and S.-W. Kim, Wormholes supported by a kink-like configuration of a scalar field, Class. Quant. Grav. **19**, 4909 (2002), gr-qc/0208069.

[20] N. Manton and P. Sutcliffe, *Topological Solitons* (Cambridge University Press, 2004).

[21] M. Nakahara, *Geometry, Topology and Physics*, 2nd ed. (IOP Publishing Ltd, 2005).

[22] S. W. Hawking and G. F. R. Ellis, *The large scale structure of space-time* (Cambridge University Press, 1973).

[23] M. Visser, *Lorentzian wormholes: from Einstein to Hawking* (Springer-Verlag New York, 1996).

[24] R. Kusner, Conformal geometry and complete minimal surfaces, Bulletin (New Series) of the American Mathematical Society **17**, 291 (1987).

[25] T. Frankel, *The Geometry of Physics*, 2nd ed. (Cambridge University Press, 2004).

[26] A. M. Polyakov, Particle spectrum in quantum field theory, JETP Lett. **20**, 194 (1974).

[27] D. E. L. Pottinger and E. Rathske, Metastability of solitons in a generalized skyrme model, Phys. Rev. D **33**, 2448 (1986).

[28] E. Witten, Global aspects of current algebra, Nucl. Phys. B **223**, 422 (1983).

[29] O. V. Manko, N. S. Manton, and S. W. Wood, Light nuclei as quantized skyrmions, Phys. Rev. C **76**, 055203 (2007), arXiv:0707.0868 [hep-th].

[30] S. Droz, M. Heusler, and N. Straumann, New black hole solutions with hair, Phys. Lett. B **268**, 371 (1991).

[31] J. Mickelsson, Geometry of spin and statistics in classical and quantum mechanics, Phys. Rev. D **30**, 1843 (1984).

[32] E. Bogomol'nyi, The stability of classical solutions, Sov. J. Nucl. Phys. **24**, 449 (1976).

[33] N. S. Manton, Geometry of skyrmions, Commun. Math. Phys. **111**, 469 (1987).

[34] S. Gillessen *et al.*, Monitoring stellar orbits around the massive black hole in the galactic center, Astrophys. J. **692**, 1075 (2009), arXiv:0810.4674 [astro-ph].

[35] A. Komar, Covariant conservation laws in general relativity, Phys. Rev. **113**, 934 (1959).

[36] C. W. Misner, K. S. Thorne, and J. A. Wheeler, *Gravitation* (W. H. Freeman and Company, 1973).

[37] C. Møller, On the localization of the energy of a physical system in the general theory of relativity, Ann. Phys., N.Y. **4**, 347 (1958).

[38] F. H. J. Cornish, Møller's energy momentum pseudo-tensor and its application to the born-infeld model of a charged particle, Proc. Phys. Soc. **82**, 807 (1963).

[39] P. Bizon and T. Chamaj, Gravitating skyrmions, Phys. Rev. Lett. B **297**, 55 (1992).

[40] R. Bartnik and J. McKinnon, Particlelike solutions of the Einstein-Yang-Mills equations, Phys. Rev. Lett. **61**, 141 (1988).

[41] P. Breitenlohner, P. Forgás, and D. Maison, Static spherically symmetric solutions of the Einstein-Yang-Mills equations, Commun. Math. Phys. **163**, 141 (1994).

[42] E. Poisson, *A relativist's toolkit: the mathematics of black hole mechanics* (Cambridge University Press, 2004).

[43] J. D. Jackson, *Classical Electrodynamics*, 2nd ed. (John Wiley & Sons, 1975).

[44] S. Bernadotte, Einfache Raumzeitschaummodelle und Propagation elektromagnetischer Wellen, Diplomarbeit, Universität Karlsruhe, 2006.

[45] J. J. Sakurai, *Advanced quantum mechanics* (Addison-Wesley Publishing Company, 1967).

[46] A. Zee, *Quantum field theory in a nutshell* (Princeton University Press, 2003).

[47] J. L. Friedman, N. Papastamatiou, L. Parker, and H. Zhang, Non-orientable foam and an effective planck mass for point-like fermions, Nucl. Phys. B **309**, 533 (1988).

[48] I. M. Gel'fand, R. A. Minlos, and Z. Y. Shapiro, *Representations of the rotation and Lorentz groups and their applications* (Pergamon Press, 1963).

[49] V. G. Machankov, J. P. Rybakov, and V. I. Sanjuk, *The Skyrme model : fundamentals, methods, applications* (Springer, Berlin, 1993).

[50] R. G. Barrera, G. A. Estevez, and J. Giraldo, Vector spherical harmonics and their application to magnetostatics, Eur. J. Phys. **6**, 287 (1985).

[51] B. Carrascal, G. A. Estevez, P. Lee, and V. Lorenzo, Vector spherical harmonics and their application to classical electrodynamics, Eur. J. Phys. **12**, 184 (1991).

Acknowledgments

First of all, I would like to thank Professor Klinkhamer who introduced me to the subject of nontrivial spacetime topology. In particular, I want to thank him for the many discussions, from which I learned a lot.

Next, I want to thank Professor Polónyi for accepting to be the *Korreferent* of my thesis.

I thank the *Graduiertenkolleg Hochenergiephysik und Teilchenastrophysik* for financial support over the last three years.

I also want to acknowledge the many discussions with my fellow PhD students about physics and life in general. In particular, I want to thank Maher Succar, Christian Kaufhold, Marco Schreck, Elisabeth Kant and Mareike Haberichter. These last two I also have to thank, together with Ralf Hofmann and Sophy Palmer, for proof reading my thesis. Finally, I want to thank Hanno Sahlmann for the many helpful discussions on the finer aspects of topologically nontrivial spacetimes and dispersion relations.

Orandum est, ut sit mens sana in corpore sano[1]. For helping me with this I want to thank my friends at *Katholische Hochschulgruppe Karlsruhe*, *Amnesty International Hochschulgruppe Karlsruhe*, and *Karlsruher Rheinklub Alemannia*, respectively.

Last, but certainly not least, I want to thank my parents for their continuous love and support over nearly three decades.

[1]Pray for a healthy mind in a healthy body.